The copyright of this thesis vests in the author. No quotation from it or information derived from it is to be published without full acknowledgement of the source. The thesis is to be used for private study or non-commercial research purposes only.

Published by the University of Cape Town (UCT) in terms of the non-exclusive license granted to UCT by the author.

University of Cape Town

Real-time motion and main magnetic field correction in MR spectroscopy using an EPI volumetric navigator

University of Cape Town

Aaron T. Hess

Department of Human Biology

University of Cape Town

Thesis presented for the degree of

Doctor of Philosophy

February 2011

Abstract

In population groups where subjects do not lie still during Magnetic Resonance Spectroscopy (MRS) scans, real-time volume of interest (VOI), frequency, and main magnetic field (B0) shim correction may be necessary. This work demonstrates firstly that head movement causes significant B0 disruption in both single voxel spectroscopy and spectroscopic imaging. A novel 3D echo planar imaging (EPI) volumetric navigator (vNav) is presented that enables prospective correction of the subject's head position, orientation, and resulting B0 disruption. The vNav rapidly acquires successive image volumes that cover all or most of the brain. Head position and orientation is measured by co-registering each volume to the first. The B0 field is measured by acquiring a second vNav contrast, interleaved with the first, to compute a 3D field map. The 3D field map is used to calculate frequency, first-order, and second-order B0 changes in the VOI.

The vNav has been incorporated into single voxel spectroscopy (SVS) and magnetic resonance spectroscopic imaging (MRSI) sequences. The navigated SVS and MRSI sequences have been validated in healthy volunteers. It was shown that spectral linewidth and SNR are maintained in the presence of motion and that the vNav has no observable effect on the spectral signal to noise ratio compared to standard sequences. The vNav did not increase the scan time in the MRSI sequence and only increased the minimum SVS scan time by 0.5 s per measurement.

In SVS residual frequency and phase errors were corrected using a novel pre-processing technique. The frequency correction is found by cross-correlating a portion of the spectrum with a simulated spectrum.

University of Cape Town

Phase correction is performed using singular value decomposition for the same section of the spectrum.

52 paediatric vNav SVS scans were acquired in ten-year old children as part of a one year follow up study. Results from the follow up study demonstrated a reduced variance in concentrations, reduced linewidths, and an increased signal to noise ratio. A further 47 vNav SVS scans acquired in five-year old children demonstrated significant movement in 15% of the scans. Despite this motion 46 of the 47 scans produced high quality spectra.

University of Cape Town

Contents

University of Cape Town

University of Cape Town

University of Cape Town

University of Cape Town

List of Figures

University of Cape Town

University of Cape Town

University of Cape Town

University of Cape Town

University of Cape Town

University of Cape Town

List of Tables

University of Cape Town

Preface

This thesis presents and evaluates a novel method to improve the efficacy of *in vivo* spectroscopic studies at the Cape Universities Brain Imaging Centre (CUBIC). The rationale for this work was the large number of failed paediatric neuro spectroscopic scans performed at CUBIC that were believed to result from subject movement.

This thesis includes three independent articles. These articles are to be found in chapters two, three and four. Each chapter documents and evaluates various aspects of the methodology, research, and findings. A comprehensive introduction provides the necessary background and context to the work. This style facilitates direct access and concise evaluation of the different methodologies and follows the logical progression of the work. However, as a complete document it contains necessary repetition due to the fact that each core chapter is being presented as an independent article. For the purpose of thesis examination the contributions from co-authors is given below.

Chapter one describes the principles of Nuclear Magnetic Resonance (NMR) spectroscopy and spectroscopic imaging. It details the artifacts and errors generated by subject movement and the current techniques available to address them. It provides the necessary background theory relevant to the body of the thesis.

Chapter two is an article that at the time of writing is in press in Magnetic Resonance in Medicine. The chapter presents the implementation of a novel echo planar imaging volumetric navigator to correct motion and resulting magnetic field changes in single voxel spectroscopy (SVS). It also demonstrates the effect of movement on the main magnetic field in single voxel spectroscopy.

I am the primary author of this chapter, but was assisted by five co-authors. One of my supervisors for this work was André van der Kouwe who conceptu-

University of Cape Town

alised the EPI navigator. My local supervisor, Ernesta Meintjes, identified the problem of motion in single voxel spectroscopy and assisted with overall project supervision. Ovidiu Andronesi provided phantoms used in the initial testing and helped to optimise methods for spectroscopic data acquisition. M. Dylan Tisdall and I together developed the initial proof of concept for an EPI based motion correction navigator. While the novel idea to extend the navigator to perform real-time B0 shim calculations and apply them in real time came about through discussions, it was primarily mine and proved to be crucial to the success of the method. I implemented and developed the EPI based navigator for motion and B0 shim correction in SVS for the scanner at CUBIC. Furthermore, I acquired the data, developed the algorithms and methods for the validation, and performed the data processing. The article was drafted by me and given to the co-authors for editorial and scientific input.

Chapter three is a manuscript that has been reviewed by a journal and was recently resubmitted with minor revisions. At the time of writing the article is under review. The chapter firstly demonstrates the relationship between movement and magnetic field perturbation in magnetic resonance spectroscopic imaging (MRSI). The effects of movement on the magnetic field provide the rationale for performing motion and main magnetic field navigation in spectroscopic imaging. The results of scans acquired in eight healthy volunteers using motion and main magnetic field navigation in MRSI are presented.

I was the primary author of this article, with insights and assistance added by six co-authors. Firstly, I together with Ovidiu Andronesi identified the need to implement motion correction in MRSI. I also identified the added benefits of B0 shim correction. Ovidiu Andronesi and Gregory Sorensen provided the LASER MRSI sequence used in the experiments. I adapted this sequence to perform real-time motion and main magnetic field (shim) correction. I additionally wrote and formulated the article and gave it to the co-authors for comment, programmed the sequence, performed the experiments described, and performed data analyses.

Chapter four is also a prepared manuscript that will be submitted for publication. It documents the use of the navigated single voxel spectroscopy sequence in two studies with five- and ten-year old children, respectively. The chapter further presents a method for offline residual frequency and phase correction, together

University of Cape Town

with a method for offline registration of the scanned VOI to an anatomical image. The contributions from various people to this work are as follows: Ernesta Meintjes (my supervisor) arranged for the navigated MRS sequence to be used in the two paediatric studies and is the principal investigator (PI) responsible for imaging aspects for each of the studies. Sandra Jacobson, Joseph Jacobson, Christopher C. Molteno, and Barbara Laughton are the clinical PIs of the studies and were responsible for recruitment and characterisation of the children. André van der Kouwe (my supervisor) is a co-PI responsible for imaging aspects of one of the studies, gave expert guidance, and helped with setting up and optimizing imaging protocols. I set up the scan parameters, developed the pre-processing methods presented, performed all the pre-processing and data analyses, formulated the appropriate quality measures of the data, and wrote the article.

Chapter five is a comprehensive discussion that summarises the main findings, highlights limitations and strengths of the methods and studies presented, and discusses possible future work. An appendix includes results of a phantom experiment that was performed to validate the mathematics used in the implementation of the navigator.

University of Cape Town

Acknowledgements

Ernesta Meintjies and André van der Kouwe supervised the work. They provided the context, expert ideas, advice, support, and numerous resources required for the implementation of this work. I would like to thank them for their significant contributions, as without them this would not have been possible. M. Dylan Tisdall provided ideas, discussion, and jointly developed the initial prototype, which is now the Martinos center version of the EPI navigator. Ovidiu Andronesi provided advice on spectroscopic imaging and analysis, support, the LASER spectroscopic imaging sequence, and the initial spectroscopy phantoms used in this work. Marjanska Malgorzata compiled the LCModel LASER basis set. Charles Harris constructed the moving phantom jigs. Thomas Benner, Michael Hamm (Siemens), and Bruce Spottiswoode (CUBIC) provided advice and resources necessary to this project. The paediatric studies were possible thanks to Mark F Cotton, Shabir A Madhi, Barbara Laughton, Sandy and Joseph Jacobson, and Christopher Molteno. I also wish to thank research assistants Nicolette Hamman, Mariska Pienaar, Maggie September, Emma Makin, and Lungiswa Rosy Khethelo, and radiographers Marie-Louise de Villiers and Nailah Maroof for assistance with data collection.

The following organisations have provided the resources used in this work: The University of Cape Town, Cape Universities Brain Imaging Centre, and the Athinoula A. Martinos Center for Biomedical Imaging.

Funding was provided by the South African Research Chairs Initiative of the Department of Science and Technology and the National Research Foundation of South Africa, Medical Research Council of South Africa, NIH grants R21AA017410, R01AA016781, R21EB008547, R21DA026104, R33DA026104, R01NS055754, P41RR014075, and U19A153217, the Ellison Medical Foundation, the Harry

University of Cape Town

Crossley Foundation, and the University of Cape Town.

Funding through the following scholarships: South African Research Chairs Initiative doctoral scholarship, the JW de Jager scholarship for international students, University of Cape Town Doctoral Research Scholarship, the Harry Crossley scholarship, Marcus Rubin scholarship, and the University of Cape Town International travel scholarship.

University of Cape Town

Chapter 1

Introduction

University of Cape Town

This thesis presents a novel method to correct errors and artifacts caused by motion in Single Voxel Spectroscopy (SVS) and Magnetic Resonance Spectroscopic Imaging (MRSI). In this chapter the relevant background theory, effects of motion in SVS and MRSI, and the current mechanisms for addressing them are presented. Chapters 2 and 3 describe the implementation of an EPI volumetric navigator (vNav) to correct these errors in real time in SVS and MRSI, respectively. The method prospectively corrects motion induced changes to the subject's head pose (position and orientation) and to the scanner's main magnetic field (B0). Chapter 4 presents results from the application of this method to two separate paediatric SVS studies. Chapter 5 is a comprehensive discussion, summarising the main findings of chapters 2, 3, and 4. The final chapter presents the conclusions.

1.1 Background and motivation

Magnetic Resonance Spectroscopy (MRS) is a non invasive technique that can be used to determine the concentrations of certain metabolites (molecules) *in vivo*. It shows physiological variations that are not evident in anatomical examinations. MRS scans are prone to signal loss, line broadening, and reduced specificity as a result of subject movement. Subjects are instructed to lie still for several minutes during the scan. For some, this may not be possible. Subjects move for reasons

including, but not limited to, swallowing, breathing, coughing, discomfort, talking, and/or restlessness. Resultant signal degradation range from unnoticeable errors to a completely destroyed spectrum.

A number of ongoing paediatric studies are being performed at the Cape Universities Brain Imaging Centre (CUBIC) located adjacent to Tygerberg hospital. It became evident that a large number of both Magnetic Resonance Imaging (MRI) and MRS scans are corrupted, possibly as a result of subject motion. The aim of this project was to develop a practical solution that would improve the research outcome of spectroscopy scans performed at CUBIC. The development was, therefore, done on a Siemens 3T Allegra scanner (Erlangen, Germany), with prototype development on a Siemens 3T Tim Trio scanner located at the Martinos Center for Biomedical Imaging (Boston, MA, USA).

University of Cape Town

1.2 Magnetic resonance spectroscopy

1.2.1 Principles of nuclear magnetic resonance

Core to nuclear magnetic resonance (NMR) is the concept of the nuclear spin. This spin can be described as the precession of an atomic nucleus in the presence of a static magnetic field. The classical description of NMR is based on the interactions between an external magnetic field and a resultant macroscopic nuclear magnetic field resulting from these precessing spins. Precession of the nuclei occurs about the main magnetic field, B0, with an angular frequency (ω) given by the Larmor equation

$$\omega_0 = \gamma \mathbf{B}_0, \tag{1.1}$$

where γ is the gyromagnetic ratio for a particular nucleus and the magnitude of $\mathbf{B}_0$ is B0. This precession gives rise to a net magnetization vector, $\mathbf{M}$, initially parallel to $\mathbf{B}_0$, where $\mathbf{B}_0$ also defines the Z axis. Hydrogen (^{1}H) is abundant in living organisms and possesses excellent NMR properties. As such hydrogen is typically imaged in *in vivo* NMR. For ^{1}H the gyromagnetic ratio (γ) is 267.5 rad/s/T, so that on a "3T" scanner with B0 = 2.89 T, the ^{1}H ω_0 = 774.1 x 10^6

rad/s or $f_0 = 123.2$ MHz.

An externally applied radiofrequency (RF) electromagnetic field, with its frequency set equal to the Larmor frequency (resonance condition) and in the presence of an external static magnetic field $\mathbf{B}_0$, will flip the magnetisation $\mathbf{M}$ (initially parallel to Z) to the transverse or X-Y plane (M_{xy}). This is referred to as an excitation RF pulse. The M_{xy} magnetisation persists after the RF pulse is removed, and continues to precess about Z. As a result an RF electromagnetic field is generated, producing a Free Induction Decay (FID) signal that can be detected by a receiving RF antenna or coil. The magnitude of magnetisation transferred from Z to X-Y depends on the flip angle, θ, and the strength of the radiofrequency electromagnetic field. In this description, X' and Y' represent a rotating reference frame with respect to which an ideal 1H nucleus is stationary. For $\theta = 90°$, and applied about X', the entire Z magnetisation will be rotated into the Y' plane. Alternatively, for $\theta = 180°$ about X', the magnetisation will be rotated from Z to -Z. An RF pulse that produces -Z magnetisation is called an inversion RF pulse.

This mechanism of excitation is described by the Bloch equation, given by

$$\frac{\delta \mathbf{M}(t)}{\delta t} = \mathbf{M}(t) \times \gamma \mathbf{B}(t), \tag{1.2}$$

and accounting for the manner in which the signal decays and relaxes after excitation expands to

$$\begin{aligned} \frac{\delta M_x(t)}{\delta t} &= (\mathbf{M}(t) \times \gamma \mathbf{B}(t))_x - \frac{M_x(t)}{\mathrm{T2}^*}, \\ \frac{\delta M_y(t)}{\delta t} &= (\mathbf{M}(t) \times \gamma \mathbf{B}(t))_y - \frac{M_y(t)}{\mathrm{T2}^*}, \\ \frac{\delta M_z(t)}{\delta t} &= (\mathbf{M}(t) \times \gamma \mathbf{B}(t))_z - \frac{M_z(t) - M_0}{\mathrm{T1}}, \end{aligned} \tag{1.3}$$

where $\mathbf{B}(t)$ is the sum of the static main magnetic field ($\mathbf{B}_0$) and the alternating transverse magnetic field resulting from the RF pulse ($\mathbf{B}_1$) and T1 and T2* determine the rate of longitudinal and transverse relaxation respectively. To understand the mechanisms by which $\mathbf{M}(t)$ relaxes back to its equilibrium state parallel to Z, we should consider the Bloch equation where $\mathbf{B}(t) = \mathbf{B}_0$, i.e.

University of Cape Town

with no external RF magnetic field. The tranverse component of the magnetisation (M_{xy}), generated following an excitation pulse of $\theta°$, decays in the following exponential manner

$$M_{xy}(t) = sin(\theta)M_0 e^{(-t/\mathrm{T2}^*)}. \tag{1.4}$$

T2* is defined as the time at which M_{xy} has decayed to 37% of its maximum value. This decay results from both dephasing in the presence of local $\mathbf{B}_0$ field inhomogeneities and unrecoverable spin - spin relaxation (T2). T1 recovery refers to the relaxation (regrowth) of the longitudinal component of the magnetisation (M_Z) and following an excitation pulse of $\theta°$ is given by

$$M_Z(t) = cos(\theta)M_0 + sin(\theta)M_0(1 - e^{(-t/\mathrm{T1})}). \tag{1.5}$$

Spatial localisation of the signal is required in order to produce an image. This localisation is achieved with a set of electromagnetic fields known as gradients. The gradients induce linearly varying magnetic fields in different directions across the subject at different times during the image acquisition. Arbitrary orientations of the linear gradients can be achieved through the simultaneous application of fixed-orientation gradients in three axes, X, Y, and Z. The basis of spatial localisation is the fact that the nuclear precession frequency is directly proportional to the magnetic field (eq. 1.1), so that the precession frequency can be varied linearly in a specific direction across a subject by applying a field gradient. By applying the gradient during excitation, only spins from specific locations (slices) will be excited, as only spins that meet the resonance condition will be flipped. Similarly, by applying the gradient during readout, the location from which signal with a specific frequency originated can be determined, yielding a 'profile' image. In order to produce a tomographic image, it is necessary to acquire multiple profile images, so that signal excitation needs to be repeated many times with time allowed for relaxation between excitations. The time between repeated excitations is known as the repetition time (TR).

An FID that has decayed as a result of T2* can be refocused using an RF pulse with a 180° flip angle. This mechanism is called a spin echo. The maximum of the new FID will occur at a time TE (Time to Echo) after the initial excitation

University of Cape Town

and equal to twice the time between the excitation and the refocusing pulse. Only signal loss resulting from B0 inhomogeneities are rephased using this mechanism, so that the magnitude of the echo is given by $M_{xy}exp$(-TE/T2). In a gradient echo sequence, a pair of bipolar gradients are used to first cause spins to dephase and to then rephase them. As in the case of the spin echo, the time at which the echo occurs after excitation is defined as the time to echo (TE).

1.2.2 ^{1}H spectroscopy and the chemical shift

Magnetic Resonance Spectroscopy (MRS) exploits the fact that the local magnetic field experienced by an individual hydrogen nucleus depends on its chemical environment and neighbouring atoms. The chemical environment can shield the nucleus of interest from the external magnetic field and cause a shift in its Larmor frequency (eq. 1.1) known as a chemical shift. The chemical shift δ of a nucleus is quantified in parts per million (ppm) and calculated as follows:

$$\delta = \frac{f - f_{ref}}{f_{ref}} \times 10^6, \tag{1.6}$$

where f is the resonance frequency of the nucleus and f_{ref} is the resonance frequency of a chosen reference compound, usually tetra-methylsilane which is typically located at 4.26 ppm above water. Metabolites of ^{1}H that are found in the human brain and that exhibit different chemical shifts include choline (Cho), creatine (Cr), phosphocreatine (PCr), phosphocholine (PCh), GABA, glutamate (Glu), glutamine (Gln), myo-inositol (Ino), N-acetylaspartate (NAA), and N-acetylaspartylglutamate (NAAG). Each metabolite will have a unique NMR signature. MRS is therefore the process of acquiring a spectrum that contains various metabolite signatures. Standard MRS techniques require a three stage MR acquisition process. The first stage, water suppression, minimises the dominant signal generated by ^{1}H in water. This signal occurs around 4.7 ppm. If the water is not suppressed the spectrum will be dominated by the water signal and strong spectral sidebands will be generated that are comparable to metabolite concentrations. Water suppression techniques are discussed in section 1.2.3.

The second step of an MRS acquisition is known as inner volume excitation. The goal of this step is to localise the region from which the signal will origi-

University of Cape Town

nate. This mechanism can limit the source of the signal to a single voxel, as in Single Voxel Spectroscopy (SVS), or to a volume of interest (VOI), as in MR Spectroscopic Imaging (MRSI). In MRSI this step excludes signal from unwanted tissue, such as subcutaneous fat, and prevents its large spectral magnitude from interfering with the metabolite signatures. Inner volume excitation techniques are presented in section 1.2.4.

The final step of the acquisition is FID readout and quantisation using an analogue to digital converter (ADC). In the spectral domain the exponential envelope of the FID, quantified by T2*, forms a Lorentzian line shape. A typical Lorentzian line shape is shown in fig. 1.1. The real component of the Lorentzian line shape is known as the absorption component, while the imaginary component is known as the dispersion component. When analysing a spectrum, one would ideally only use the absorption component as it has a narrower Full Width at Half Maximum (FWHM) linewidth than the dispersion spectrum. The FWHM linewidth (fig. 1.1) of the absorption spectrum equals $1/(\pi T2^*)$.

University of Cape Town

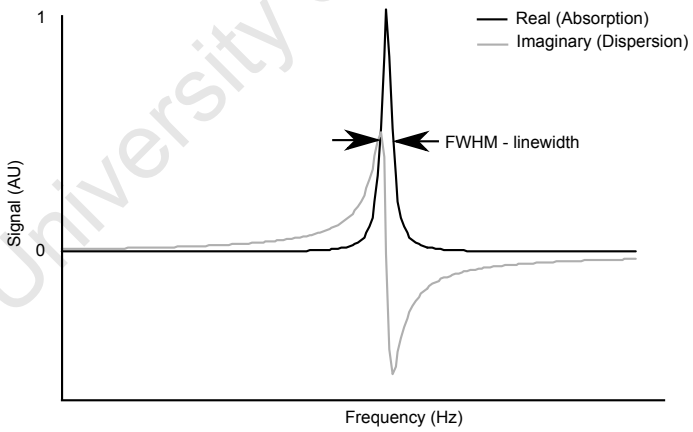

Figure 1.1: Lorentzian line shape. The real term describes the absorption component of the Lorentzian, while the imaginary describes the dispersion component. The Full Width at Half Maximum (FWHM) is depicted on the Absorbtion component of the Lorentzian.

Narrow linewidths are crucial to successful MRS as it improves the ability

to resolve multiple resonances at similar frequencies. In addition, a long T2* (inverse linewidth) provides greater signal in the FID and thus an optimal Signal to Noise Ratio (SNR). Both of these factors will affect the accuracy of metabolite quantification, as discussed in section 1.2.5.

1.2.3 Water suppression

Although water suppression can be achieved through several mechanisms, the most widely used approach is to presaturate the water signal prior to spectral excitation. A narrow band 90° excitation pulse is first applied to bring the water signal into the transverse plane, followed by a strong dephasing gradient. Techniques such as Water suppression Enhanced through T1 effects (WET, Ogg et al., 1994) and CHEmical Shift Selective (CHESS, Haase et al., 1985) water suppression operate in this manner. The effectiveness is often improved by applying multiple excitation and dephasing gradients. A limitation of this method is that T1 relaxation occurs between presaturation and spectral excitation.

Spectral excitation methods, such as binomial RF pulses (Morris and Freeman, 1978), do not suffer from T1 relaxation but have non-uniform excitation across the spectral range. Frequency selective refocusing applies water selective 180° RF pulses during the inner volume excitation, which serves to invert the water signal while leaving the metabolites unaffected. MEGA (Mescher et al., 1996) and WATERGATE (Piotto et al., 1992) are two examples of frequency selective refocusing. Frequency selective refocusing is, however, not suited for short echo times.

University of Cape Town

1.2.4 Inner volume excitation

Inner volume excitation has three purposes in an MRS scan. The first is to exclude unwanted signal, such as subcutaneous fat. The second is to localise the source of the signal. Finally, inner volume excitation enables improved optimisation of the B0 and B1 magnetic fields due to the reduced volume. Three inner volume excitation techniques are described in this section: Point RESolved Spectroscopy (PRESS, Bottomley, 1987), Stimulated Echo Acquisition Mode

(STEAM, Frahm et al., 1989), and Localization by Adiabatic Selective Refocusing (LASER, Garwood and DelaBarre, 2001).

PRESS uses a double spin echo for inner volume localisation. It consists of a slice selective 90° excitation, followed by two orthogonal slice selective 180° RF pulses. The slice selective 90° pulse excites only spins within a single slice. The first slice selective 180° RF pulse refocuses the spins contained in a pencil beam where the two planes intersect to produce a spin echo signal and inverts the magnetisation in the remainder of the plane. Gradients are used to dephase the non-refocused magnetisation in the remainder of the slice. The third slice selective 180° RF pulse is applied in a third orthogonal plane causing spins in the region where all three planes intersect to be refocused, while all magnetisation outside of the intersection of the pencil beam and this third plane are dephased by gradients. In this manner only spins within a single rectangular volume of interest are excited. The echo time (TE) is given by $2t_2$ ($t_2 > t_1$), where t_1 is the duration between the 90° and the first 180° RF pulse and t_2 the duration between the two 180° RF pulses. These RF pulses are not perfect square pulses and will always generate signal from outside the intended VOI (signal bleeding). In addition, the narrow bandwidth required for slice selection generates a spectral dependent slice position. This artifact is called Chemical Shift Displacement Error (CSDE) and is calculated using eq. 1.7, in which BW is the RF pulse bandwidth and Δf is the frequency difference between the metabolite and RF pulse. At 3T the common volume between two metabolites separated by 3.5 ppm, and an RF bandwidth of 2.3 KHz, is only 65% (Andronesi et al., 2010; Kreis, 2004).

$$CSDE(\Delta f) = \frac{\Delta f}{BW} \tag{1.7}$$

STEAM, like PRESS, uses three orthogonal slice selective RF pulses, but each RF pulse is a 90° excitation. A stimulated echo will be generated in the volume where the three orthogonal planes intersect. All other echoes and FID's generated by the 90° excitations are dephased by gradients applied between them. If t_1 is the time between the first and second RF pulses, and t_2 is the time between the second and third RF pulses (known as the mixing time), then the simulated echo occurs at a time $2t_1 + t_2$.The advantage of using 90° pulses over 180° is that their

University of Cape Town

excitation profile is sharper, and that this sequence enables a shorter TE than PRESS. The shorter TE primarily results from the shorter duration of 90° RF pulses compared to 180° RF pulses. The disadvantage of STEAM is that the amplitude of the stimulated echo is only 50% of that arising from the spin echo in PRESS (de Graaf, 2007), however, the shorter TE's achieve a higher signal that recovers some of this loss. As in PRESS, STEAM also suffers from non perfect slice profiles, but the CSDE of STEAM is less than that of PRESS as 90° RF pulses have a greater bandwidth.

LASER inner volume excitation uses adiabatic RF pulses to overcome the limitations of the standard RF pulses used in STEAM and PRESS. Their higher bandwidth reduces the chemical shift displacement error, such that the common volume for metabolites separated by 3.5 ppm is 81% (Andronesi et al., 2010). Further reduction in the CSDE is achieved with Gradient Offset Independent Adiabacity (GOIA, Tannús and Garwood, 1997) and Frequency Offset Corrected Inversion (FOCI, Kinchesh and Ordidge, 2005) and can increase the common volume of metabolites separated by 3.5 ppm to 96% (Andronesi et al., 2010). The LASER sequence consists of a non selective Adiabatic Half Passage (AHP) excitation followed by three pairs of Adiabatic Full Passage (AFP) pulses, giving a total of 7 RF pulses. AFP pulses are applied in pairs in order to recover the phase dispersion generated from a single AFP. The other advantage of adiabatic RF pulses is an improved slice profile which reduces the signal observed from outside the volume of interest.

University of Cape Town

1.2.5 Single voxel spectroscopy and spectroscopic imaging

Single Voxel Spectroscopy (SVS) and MRS Imaging (MRSI) employ two different mechanisms of spatial localisation. SVS uses inner volume excitation (as discussed above) to ensure that for every measurement the spectrum originates from a single voxel. Typical voxel sizes range from $(15\ \text{mm})^3$ to $(20\ \text{mm})^3$. The measurement is repeated 64 or more times and averaged to produce an adequate SNR. In order to allow sufficient time for T1 recovery between measurements, TR should be 1.5 s or greater. The advantage of a small SVS VOI is that both B0 (discussed in section 1.3) and B1 can be highly optimised. Spurious echoes, generated from the

intersections at the boundaries of multiple non-ideal RF pulses, are also minimised through the use of phase cycling (Hennig, 1992; Sison et al., 2007).

MRSI localises spectra using 2D or 3D k-space phase encoding. Each acquisition or TR now acquires data at a single point in k-space. In this manner MRSI acquires a matrix / grid of spectra across a large VOI. It also uses inner volume excitation to prevent the excitation of subcutaneous fat and reduce the volume over which B0 and B1 need to be optimised. Although inner volume excitation is used, the within slice Field of View (FOV), or encoded volume, is usually chosen to cover the entire head slice in order to prevent the contamination of the VOI with signal bleed from outside the VOI. Typically, the k-space FOV is divided into a grid that can vary in size from 8 x 8 up to 32 x 32, and requires 64 to 1024 acquisitions to completely sample k-space. This large number of acquisitions demands a long scan time. The spectral SNR is, however, proportional to the number of acquisitions and the voxel volume. An elliptical k-space, which is a form of partial Fourier, can reduce the number of acquisitions required, while having a minimal effect on the point spread function. The chemical shift displacement error (CSDE) that arises from the inner volume excitation is proportional to the VOI and is therefore significant in MRSI. Lastly, outer volume suppression is required for inner volume excitation methods that have bad CSDE and poor slice profiles, such as PRESS and STEAM.

University of Cape Town

1.2.6 Metabolite quantification and data pre-processing

Metabolite quantification is a complex process requiring data pre-processing and metabolite fitting. Data pre-processing involves several steps. In SVS both phase and frequency correction can be applied to improve the coherence of the measurements prior to averaging. These methods are presented in further detail in section 1.4.2. Line shape distortions resulting from non-linearity induced in the gradients by eddy currents produce line shapes that deviate from the expected Lorentzian. A water signal spectrum, acquired with the same measurement parameters (without averaging) can be used to measure and correct for these line shape distortions. This water spectrum can further be used as a reference for absolute metabolite quantification. In MRSI, the low sampling of k-space pro-

duces a non ideal spatial point spread function, containing large side bands. To improve the spatial point spread function a k-space filter can be applied. One such k-space filter is the Hanning filter.

The quantification of metabolites in a spectrum relies on the prior knowledge of metabolite signatures and the expected line shape. A collection of expected metabolite signatures, measured by a specific MRS sequence, is known as a basis set. A popular quantification method is to find the linear combination of the basis set that best fits the measured spectrum (De Graaf and Bovée, 1990). With this method the line shape (linewidth and phasing) of the basis set must be matched to the spectrum. The software LCModel (Provencher, 1993) has popularised this approach and additionally uses a water sample spectrum to correct for experimental line shape variations.

Poor spectral quality, including broad linewidths, low SNR, and spectral artifacts, will reduce the accuracy of the quantification. For this reason both quantitative and qualitative measures must be defined to discard spectra that may lead to erroneous quantification. The qualitative observation of artifacts in the spectrum is not straightforward and requires experience. In a recent review paper, Kreis (2004) discusses artifacts that are typically observed in spectroscopy. For spectra that do not have clear artifacts or distortions, the linewidth and signal to noise ratio (SNR) should be used as quantitative measures to assess spectral quality. Broad linewidths lead to poor specificity and may produce meaningless results (Kreis, 2004). Likewise a low SNR will produce fitting errors.

One tool that provides a measure of the uncertainty of the quantification is the Cramer-Rao Minimum Variance Bounds (CRMVB, Cavassila et al., 2001). This is a stochastic measure of the minimum variance of a single measurement given a model and known SNR. However, CRMVB do not include systematic errors such as deviations in T1, T2, and line shape from those used in the model. This should be considered particularly when examining pathology. Kreis (2004) constructed the following criteria for the rejection of data based on theory, literature, and an opinion poll:

1. FWHM of metabolites $>$ 0.07-0.1 ppm;

2. CRMVB $>$ 50%;

University of Cape Town

3. Unexplained features in residuals: reject if artifact; or expand model if unexpected metabolite;

4. Split peaks, or patient moved;

5. Line shape strongly asymmetric after eddy correction;

6. Outer volume ghosts or other artifacts present (at least exclude metabolites overlaid with artifact).

1.3 B0 magnetic field effects and optimisation

1.3.1 Effects of an inhomogeneous B0 on spectroscopy and degrees of optimisation

Spatial and temporal variations in the B0 magnetic field are reflected as frequency variations (eq. 1.1) that impact on several aspects of the spectroscopy acquisition. Frequency offsets shift the water suppression band, thus reducing its effectiveness, and additionally may interfere with the spectrum of interest. In SVS a temporal frequency shift will cause both split peaks and line broadening, while higher order frequency spatial variations result in line broadening (increased FWHM) and reduced peak amplitude (SNR). In MRSI spatial and temporal frequency variations will produce the same effects, however, temporal variations in the spatial frequencies will additionally generate voxel to voxel frequency differences and shifts. An optimal B0 is thus important for good quality spectroscopy.

Temporal B0 inhomogeneity potentially compromises spectral integrity due to the formation of split peaks. In SVS it is possible to remove a limited range of frequency shifts through data pre-processing (see section 1.4.2). However, in MRSI this generally is not possible due to each measurement having a different k-space encoding. Temporal changes in B0 occur due to the heating of gradient elements, movement of the subject, or movement of objects near the scanner.

University of Cape Town

1.3.2 B0 shimming

Spatial B0 inhomogeneity can be minimised through B0 shimming. Both static and dynamic mechanisms are employed to optimise the magnetic field. Static shimming is performed during commissioning of a scanner using a set of ferromagnetic elements strategically placed around the bore of the scanner. Dynamic shimming enables a subject and VOI specific B0 optimisation and typically includes the use of a frequency offset (zero-order), three linear gradient offsets (first-order), and five second-order shim coils, and in some specialised high field scanners, third- or higher-order shim coils. A frequency offset is achieved by RF frequency adjustment and analogue to digital converter (ADC) frequency (demodulation frequency) adjustment. First-order adjustment is achieved by setting a constant offset to the linear spatial encoding gradients. The second-order shims are set using a set of second-order shim coils, each producing a magnetic profile of, XZ, YZ, XY, X^2 - Y^2 and Z^2, respectively. This combination, however, does not allow the decoupling of X^2 and Y^2 elements. These shim coils and offsets can be set dynamically, typically prior to the start of each scan. On the scanners used in this study, the second-order shim gradients did not have eddy current compensation and as a result settling time must be considered after manipulating them.

The magnitude of each shim coil and frequency offset can either be calculated using B0 field sensitive measurements or interactively by the operator. A technique proposed by Gruetter (1993) called "a Fast Automatic Shimming Technique by Mapping Along Projections" (FASTMAP) acquires a minimal number of spatial projections to fit zero-, first-, and second-order shim terms. A more popular automated technique is to acquire a phase difference image known as a field map. A field map is constructed from the complex division of two images with differing echo times where the difference in echo times (ΔTE) is chosen to maintain fat in phase with water between the two images. At 3T, ΔTE = 2.2 to 2.5 ms. From the field map, linear regression can be used to fit the spatial shim terms to the B0 field. Reese et al. (1995) demonstrated this field map based shimming using a rapid Echo Planar Imaging (EPI) sequence to measure the field map. They also demonstrated different cost functions used in the regression and found that

University of Cape Town

a simple minimum square error was sufficient for such B0 optimisation.

Further to automated shimming, manual or interactive shimming is usually performed in spectroscopy. This process is based on the minimisation of the water FWHM and maximisation of T2*. In spectroscopy, a narrow linewidth is the ultimate goal and thus this technique provides operators with a measure of spectral quality prior to the start of the scan. With all shim adjustment techniques, it should be noted that first- and second-order shim fields are applied about the isocenter of the scanner, which usually does not coincide with the centre of the VOI. This means that all second-order shim adjustments will affect the first- and zero-order shim, and likewise all first-order shim adjustments will affect the zero-order shim.

1.4 Effects of subject movement in the scanner

1.4.1 Movement induced artifacts in spectroscopy

Motion causes spectral artifacts due to shifting anatomy, changes in the B0 magnetic field, velocity related dephasing, and coil proximity related dephasing. A shift in anatomy will only be detected in both SVS and MRSI if unexpected resonances are introduced into the spectra, such as the introduction of subcutaneous fat into the VOI. This type of artifact will otherwise go completely unnoticed. Current methods to measure and correct head movement in the scanner are presented in section 1.4.3. Changes in the B0 magnetic field are, however, observable in the spectrum. Zero-order changes will shift the frequency of the measurement and manifest as a split peak and sub-optimal water suppression in both SVS and MRSI. The split peak spectrum will no longer represent a Lorentzian line shape, resulting in inaccurate metabolite quantification. First- and second-order perturbations manifest within a voxel as line broadening. This line broadening is quantified in chapter 2. In MRSI first- and second-order perturbations result in spatially dependent frequency changes of each voxel, leading to split peaks and uneven water suppression. Section 1.4.2 presents the current methods for zero-order B0 correction.

Dephasing in a spectrum results from velocity during the volume selective gra-

University of Cape Town

dients of PRESS, STEAM, and LASER. These changes in head position result in unbalanced refocusing gradients causing accumulation of phase. Current methods to correct for this dephasing are presented in section 1.4.2. Lastly, in multi channel studies, a change in the VOIs proximity to the receiver coils will alter the phase of the measurements in each coil, leading to destructive recombination of the measurements.

1.4.2 Correction of motion induced artifacts in spectroscopy

Several prospective and retrospective artifact correction techniques have been demonstrated in SVS, some of which can also be applied to MRSI. The first group of techniques deal with both zero-order B0 (frequency) correction and removal of measurement to measurement dephasing. In SVS, frequency shifts, and dephasing can be corrected retrospectively. The retrospective frequency correction is, however, limited by the resultant shift of the water suppression band. If large enough, the water suppression will be ineffective and potentially suppress the spectrum of interest. The frequency and phase of each SVS measurement can be measured directly from its spectrum. Ernst and Li (2009); Star-Lack et al. (2000); and Helms and Piringer (2001) used an under suppressed residual water signal as a frequency and phase marker. In this manner a high SNR frequency and phase measurement can be achieved. This is, however, at the expense of introducing water signal into the spectrum. Gabr et al. (2006), and Waddell et al. (2007) used a number of data points from a "high SNR" metabolite peak to form a water independent frequency and phase measure. When using a "high SNR" metabolite peak the noise level must be taken into account by taking the average of several points (Gabr et al., 2006). Posse et al. (1993) applied the residual water method to MRSI by initializing the FID readout prior to the k-space phase encoding gradients. In a similar manner Kim et al. (2004) used spiral readout gradient MRSI encoding to acquire the center of K-space on each measurement for use in phase correction.

An alternative approach to frequency correction is to acquire a separate water measurement as a navigator each TR, interleaved with the spectroscopy measurements/encodings. Henry et al. (1999) used a non selective 5° excitation

University of Cape Town

to measure the frequency shift of the system, however, this only corrects for system related frequency drifts and not motion related frequency drifts. Thiel et al. (2002) used a PRESS inner volume excitation with an initial 20° flip angle to obtain a motion sensitive frequency navigator. The advantage of frequency navigators is that they seamlessly extend to MRSI, however, they are unable to measure velocity-induced dephasing as the instantaneous velocity cannot be considered constant between the spectroscopy measurement and the navigator. While all of the frequency correction techniques can be applied prospectively or retrospectively, phase correction can only be performed retrospectively in data pre-processing. Such steps are critical in maintaining suitable data quality; however, without anatomical specificity such artifacts should raise concern about the validity of spectral localisation.

We can correct the location of the VOI for anatomical shifts by appropriately adjusting the frequency of the RF pulses and reorienting the axes of the gradient system. In SVS, Keating et al. (2010) used a navigator based technique called PROspective Motion (PROMO) correction, while Zaitsev et al. (2010b) used a camera based optical tracking device to correct for anatomical changes. These and other head pose tracking techniques are described in section 1.4.3. While Keating et al. (2010) have used the PROMO technique to quantify first-order B0 shim changes of a phantom in SVS, it has not been demonstrated *in vivo*, and cannot be transferred to MRSI due to the limited field of view of the navigator.

University of Cape Town

1.4.3 Subject pose measurement and correction in the scanner

The animate nature of people in NMR examinations has given rise to the development of several techniques capable of measuring and maintaining varying degrees of a subject specific frame of reference during a scan. These techniques are based on various media, such as, NMR interleaved navigators, the MRI acquisition itself, external optical tracking devices, and micro coils. The concept of a navigator was first proposed by Ehman and Felmlee (Ehman and Felmlee, 1989), who proposed the use of an interleaved excitation to acquire a 1D projection of a plane. An image space cross-correlation or k-space phase roll is then

used to determine the 1D displacement along the readout direction. This type of 1D measurement is popular in cardiothoracic imaging.

Orbital navigators were subsequently developed (Fu et al., 1995) to sample a circle of k-space at a prescribed radius and plane. Using Fourier Transform theory, a rigid body rotation in image space is equivalent to a rotation in k-space. Thus a rotation about the prescribed axis can be measured using cross-correlation between two navigator acquisitions. This method is limited by the fact that any out of plane rotation will invalidate the procedure. The cloverleaf navigator (Van der Kouwe et al., 2006) combines these two principles into an elegant 3D k-space traversal, measuring three orthogonal arcs, and three orthogonal lines through the centre of k-space. The registration of these cloverleaf navigators to a reference map fully resolves the six degrees of freedom in a rigid body transformation. A different approach to measuring all six degrees of freedom is to completely sample a sphere of k-space (Welch et al., 2002), where the rotations are estimated from sphere to sphere registration, and translation from the linear phase roll between each navigator acquisition.

The nature and timing of pulse sequences vary depending on the intended contrast. A number of pulse sequences have magnetisation recovery or magnetisation preparation times on the order of 500 ms to 1 s or greater. This is the case in both spectroscopy and Magnetisation Prepared Rapid Gradient Echo (MPRAGE, Mugler and Brookeman, 1990) sequences. The magnetisation recovery/preparation time can be used to generate a complete image or set of images using a sufficiently small flip angle. A small flip angle avoids interference with the magnetisation relaxation process. In this manner, PROMO (White et al., 2010) employs spiral imaging for the acquisition of three orthogonal images and co-registers them to a map of such spiral images. They use a flip angle of 8°. To achieve sufficient accuracy and stability they acquire a set of five such navigators every 100 ms in imaging applications or every 300 ms in SVS, totalling 500 ms or 1 500 ms duration, respectivly, for the complete PROMO block. An advantage of image based motion navigation is that an anatomical mask can be employed.

Another approach to motion correction is to use information inherent in the MRI acquisition to calculate motion correction parameters. The 2D Periodically Rotated Overlapping ParallEL Lines with Enhanced Reconstruction (PRO-

University of Cape Town

PELLER) pulse sequence (Pipe, 1999) was designed to acquire data in concentric rectangular strips. In this manner the centre portion of k-space, which is acquired on each strip, can be used to calculate 1D rotation and 2D translation (both within the 2D plane). Thesen et al. (2000) developed a Prospective Acquisition CorrEction (PACE) technique for functional MRI (fMRI). In fMRI multiple complete image volumes are acquired in rapid succession, approximately every 1 s to 3 s. Each successive measurement can be registered to the first volume using image volume based registration (Friston et al., 1995).

Optical tracking can be performed using additional equipment, external to the MRI scanner, such as stereo cameras (Qin et al., 2009; Zaitsev et al., 2006) , retrograde reflectors with a single camera (Zaitsev et al., 2010a), or laser positioning of retro reflectors (Eviatar et al., 1999). These systems require the camera(s) or lasers to be rigidly affixed within the MR environment, either onto the head coil (Qin et al., 2009) or outside the scanner bore (Eviatar et al., 1999; Zaitsev et al., 2010a, 2006). They must be in line-of-sight of a specific marker or set of markers that are affixed to the subject's head. The additional hardware required, with the subject wearing additional regalia, makes these systems cumbersome and expensive to set up. The limited space within the MR environment and enclosed head coils limit the field of view available and hamper their practical implementation.

Active markers, known as microcoils or locator coils (Derbyshire et al., 1998; Ooi et al., 2009) determine the position and orientation of the head by affixing three microcoils to the subject's head. These microcoils are tuned to receive the NMR response of a water filled bead within the coil. The position of the bead is then determined using a specific gradient waveform to form a spatially dependent phase encode and frequency of each bead.

1.5 Echo planar strategies for rapid image acquisition

Rapid acquisition of imaging navigators can be achieved by sampling 2D k-space after a single excitation. There are two popular echo planar readout trajectories,

University of Cape Town

the Cartesian trajectory of Echo Planar Imaging (EPI), and a non-Cartesian spiral trajectory. Each of these trajectories introduce artifacts with varying severity, as described below.

1.5.1 Echo planar imaging - Cartesian

In a Cartesian EPI readout trajectory, k-space is sampled line by line, with each line alternating in direction and a phase encode gradient between each line. A 3D acquisition can be achieved using multi-shot EPI, where each partition (slice of k-space) is acquired following an excitation. Echo planar techniques are acquired using high bandwidths in order to achieve complete 2D k-space coverage within the T2* relaxation window. Due to its Cartesian nature, other MRI acceleration techniques, such as partial Fourier, are easily transferred to EPI.

Echo planar imaging suffers from Nyquist ghost artifacts. These are the formation of an image replica, shifted by half the field of view, known as N/2 ghosts. They appear due to the phase difference and opposite phase roll accumulated in consecutive lines. This phase difference can be corrected with a phase navigator. A phase navigator is a separate acquisition, without phase encoding, that obtains both positive and negative direction readouts. From these readouts the constant phase difference between each line and the linear phase roll along each line, are calculated and the readout lines are adjusted accordingly (Bruder et al., 1992; Jesmanowicz et al., 1993). Nyquist ghosts are also generated from a k-space shift of the readout samples, causing a positive shift for positive lines and negative for negative lines. These result from spatially linear eddy currents, gradient delays, and gradient amplifier hysteresis. In a similar manner k-space shifts in the phase encode direction will also result in ghosts.

Echo planar imaging is sensitive to off resonance effects such as B0 magnetic field inhomogeneities and chemical shifts of tissues such as fat. Off resonance is manifested in the image as a displacement of the affected tissue. This shift is quantified by equation 1.8, in which Δf is the frequency shift, BW_{pe} is the bandwidth along the phase encode direction (inverse of time between each readout

University of Cape Town

line), and L_{pe} is the phase encode FOV.

$$\Delta y = \frac{\Delta f}{BW_{pe}} L_{pe} \tag{1.8}$$

As a result, off resonance effects manifest as image distortions and tissue specific displacements. Such distortions can be measured by a dual echo field map (see section 1.3.2) and the image regridded appropriately. The phase encode bandwidth is roughly equal to the readout bandwidth divided by the number of readout samples, so that the shift in the readout direction is insignificant compared to the phase encode direction.

1.5.2 Spiral echo planar imaging

Spiral trajectories change the manifestation of artifacts in the image and inherently accomplishes flow and motion rephasing. A popular spiral trajectory is the Archimedean spiral, which has equidistant revolutions through k-space. These trajectories are achieved using oscillating gradient wave forms. The spiral k-space sampling is regridded into a Cartesian grid which is then inverse fast Fourier transformed to produce the image.

The primary difference between EPI and spirals is the manifestation of the off resonance effects. In spirals, off resonance results in image blurring which in turn is proportional to the spiral duration. The blurring can be reduced by acquiring multiple interleaved spirals, each of a shorter duration. Deblurring techniques are possible, however, they are computationally expensive and do not lend themselves to real-time applications (Noll et al., 1991).

Spirals do not suffer from Nyqist N/2 ghosts. However, the effects of inaccuracies in the k-space trajectory originating from gradient errors or concomitant fields also result in image blurring (Block and Frahm, 2005). As spiral imaging is demanding on image reconstruction due to regridding and deblurring, it does not lend itself to real-time applications. In motion correction image registration is a critical step, so that the off resonance effects of blurring should be considered in relation to the image distortions of EPI.

University of Cape Town

Chapter 2

Real-time Motion and B0 corrected single voxel spectroscopy using volumetric navigators[1]

Aaron T. Hess[2], M. Dylan Tisdall[3], Ovidiu C. Andronesi[3], Ernesta M. Meintjes[2], and André J.W. van der Kouwe[3]

University of Cape Town

Abstract

In population groups where head pose cannot be assumed to be constant during an MRS examination or in difficult-to-shim regions of the brain, real-time volume of interest (VOI), frequency, and shim optimisation may be necessary. We investigate the effect of pose change on the B0 homogeneity of a (2 cm)^3 volume and observe typical first-order shim changes of 1 μT/m per 1° rotation (chin down to up) in four different VOI's in a single volunteer. An EPI volume navigator (vNav) was constructed to measure and apply in real-time within each TR: VOI positioning, frequency adjustment, and first-order shim adjustment. This vNav is demonstrated in six healthy volunteers and achieved a mean linewidth of 4.4 Hz, similar to that obtained by manual shim adjustment of 4.9 Hz. Furthermore,

[1]Published in Magnetic Resonance In Medicine and reproduced with permission from John Wiley & Sons.

[2]University of Cape Town.

[3]Martinos Center, MGH, Harvard Medical School.

this linewidth is maintained by the vNav at 4.9 Hz in the presence of pose change. By comparison, a mean linewidth of 7.5 Hz was observed when no correction was applied.

2.1 Introduction

Single voxel spectroscopy (SVS) relies on a homogeneous B0, a consistent frequency, and assumes that the localisation remains valid for the duration of the scan. For a restless subject who is unable to maintain a consistent pose during the scan, these do not hold true. We present a method that provides real-time (once every TR) B0 and frequency measurements in addition to real-time correction of the volume of interest (VOI) position. Current motion and artifact correction methods in Magnetic Resonance Spectroscopy (MRS) can be divided into two categories: phase and frequency adjustment, and localisation correction. Phase and frequency adjustment refers to a group of techniques that measure the signal phase and frequency by using either the residual water signal (Ernst and Li, 2009; Helms and Piringer, 2001; Posse et al., 1993; Star-Lack et al., 2000) or a secondary navigator (Henry et al., 1999; Thiel et al., 2002). These methods correct both a velocity-induced phase error and frequency changes that result from either scanner drift or pose change. Phase and frequency adjustment can be applied both retrospectively and prospectively, but only prospective methods are able to correct the change in water saturation frequency.

Localisation correction techniques in MRS have been demonstrated using an optical tracking system (Zaitsev et al., 2010b) and an imaging navigator technique called PROspective MOtion correction (PROMO, Keating et al., 2010). The technique presented by Zaitsev provides both frequency and localisation correction by combining optical tracking with navigator based frequency correction in addition to reacquisition of free induction decays (FID's) with velocity-induced phase errors. The disadvantages of an optical device are that they require additional hardware, a marker to be rigidly affixed to the head, a clear line of sight between camera and marker, and the calibration of a camera to scanner transform.

There are several navigator-based motion tracking methods available that take

University of Cape Town

advantage of the k-space properties of rigid body transforms to subsample k-space in a time efficient manner. These include orbital (Fu et al., 1995), spherical (Welch et al., 2002) and cloverleaf (Van der Kouwe et al., 2006) navigators. While these techniques can be particularly fast, an imaging navigator is better suited to MRS due to its long repetition times (on the order of 1.5 s to 3 s) and lack of anatomical information. One such navigator is PROMO (White et al., 2010), which uses a set of three perpendicular, single slice, low resolution spiral images to register the head position to a reference map. This was demonstrated in MRS by Keating (Keating et al., 2010).

In this work the effect of changing head pose on zero-, first- and second-order B0 homogeneity was investigated in four different VOI's for a single volunteer. The use of an echo planar imaging (EPI) volume navigator (vNav) to correct in real time for both VOI position and zero- to first-order B0 inhomogeneity changes is demonstrated in six healthy volunteers. Finally, we demonstrate that this navigator minimally affects the metabolite signal and maintains spectral quality when a subject moves during the scan.

University of Cape Town

2.2 Background theory

The relationship between linewidth and B0 inhomogeneity can be expressed in terms of first- and second-order B0 changes. The signal from a single substance (n) can be described by Eq. 2.1 (Webb et al., 1992).

$$S_n(t) = a_n exp(\frac{-t}{T2_n^*}) \int_{voxel} exp(j2\pi t[f_n + \Delta f(x,y,z)])dxdydz \qquad (2.1)$$

where a_n is the relative amplitude of the signal, $T2_n^*$ depicts the inherent linewidth and $\Delta f(x,y,z) = \gamma(g_1^f x + g_2^f y + g_3^f z + g_1^s zy + g_2^s zx + g_3^s xy + g_4^s z^2 + g_5^s(x^2 - y^2))$ for a voxel with B0 inhomogeneity expressed as the magnitude of first- (g_1^f to g_3^f) and second-order (g_1^s to g_5^s) shim correction terms. Figure 2.1 demonstrates the theoretical effect of B0 inhomogeneity on linewidth based on eq. 2.1. Figure 2.1A shows the change in linewidth as a function of a first-order B0 gradient, for which the magnitude ranges from 0 to 20 μT/m, for three

different metabolite linewidths ($T2_n^* = 40$ ms, 80 ms and 160 ms) and a voxel size of $(2\text{ cm})^3$. Figure 2.1B demonstrates how first-order B0 inhomogeneity affects different voxel sizes for a metabolite linewidth of $T2_n^* = 80$ ms. The effect of a second-order inhomogeneity is more complicated as the linewidth and signal amplitude are not proportional to one another. Figure 2.1C plots the linewidth as a function of the magnitude of the five second-order shim currents while fig. 2.1D plots the spectral amplitude for the same relative to its amplitude in a homogeneous VOI.

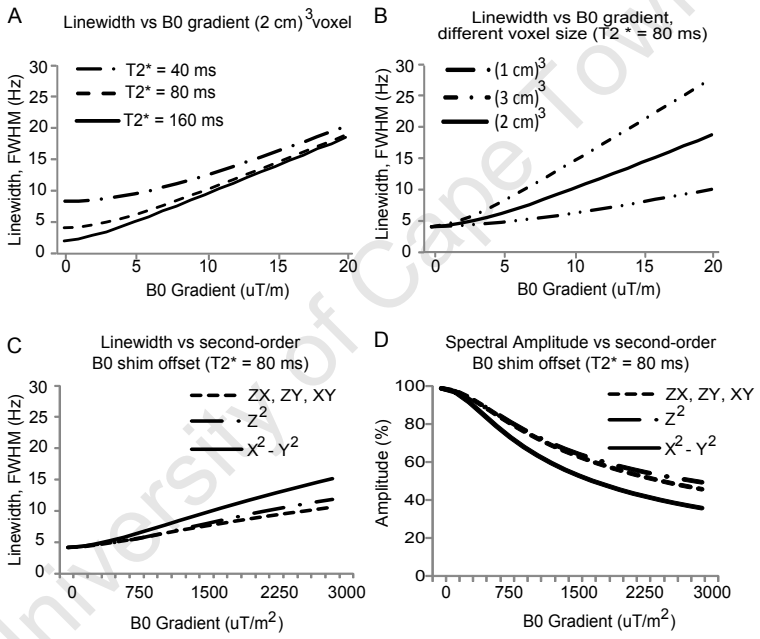

Figure 2.1: A. Change in linewidth as a function of first-order B0 inhomogeneity for 40 ms, 80 ms and 160 ms inherent linewidths in a $(2\text{ cm})^3$ voxel. B. Change in linewidth as a function of first-order B0 inhomogeneity for varying voxel sizes, $(1\text{ cm})^3$, $(2\text{ cm})^3$, and $(3\text{ cm})^3$. C. Change in linewidth against second-order B0 gradient for ZX, ZY, XY, Z^2 and (X^2-Y^2) at an inherent linewidth of 80 ms. D. Spectral amplitude as a function of second-order B0 terms ZX, ZY, XY, Z^2 and (X^2-Y^2), relative to the amplitude in a homogeneous VOI.

A field map can be used to optimise the shim currents of the scanner (Reese et al., 1995). A field map is generated by the complex division of two images with differing echo times. The difference in echo time is typically chosen such that fat

University of Cape Town

and water are in phase. This occurs for a TE difference of roughly 2.2 ms to 2.5 ms for a gradient echo at 3T. The best fit of the shim gradients to the spatially varying B0 field can be determined by minimum square error regression over the volume of interest, taking care to exclude voxels that do not have adequate SNR. Reese et al. (1995) suggest that a least square error cost function in the regression is sufficient for this application. Finally, image distortions resulting from the B0 field variations can be corrected using the known frequency offset of each voxel.

2.3 Materials and methods

All scans were performed on a Siemens Allegra 3T (Siemens Healthcare, Erlangen, Germany) in Cape Town, South Africa according to protocols that had been approved by the Faculty of Health Science Research Ethics Committee of the University of Cape Town.

University of Cape Town

2.3.1 Investigation of the effect of motion on B0

To demonstrate the change in B0 due to pose variations, a single volunteer was scanned. Twelve high-resolution field maps were acquired with the head in different positions. The volunteer moved his head incrementally, first about the X axis (chin-down to chin-up) and then about the Z axis (rotate left-to-right). Six field maps were acquired during the X axis rotation, from 7.2° to −14.4°, and a further 6 field maps for the Z axis rotation, ranging from −19° to 16°. Resultant rotations were assessed offline. The subject was trained prior to scanning as to how much to move his head.

A gradient echo sequence was used for the field map acquisitions with the following parameters, 48 slices, matrix 64 x 64, FOV = 192 x 192 mm^2, slice thickness = 3 mm, TR = 502 ms, TE_1 = 4.59 ms, TE_2 = 7.05 ms, bandwidth = 260 Hz / pixel, and a slice separation of 0.6 mm. No shim adjustment was performed prior to each field map.

Each field map was registered to a reference 3D Multi Echo Magnetization Prepared Rapid Gradient Echo (MEMPR) (Van Der Kouwe et al., 2008) using SPM5 (Ashburner, 2007) and resliced to match the 3D MEMPR resolution of 1.0

x 1.3 x 1.0 mm^3 using linear interpolation. This process facilitated the extraction of a chosen anatomical VOI based on the MEMPR. Four $(2\ cm)^3$ VOI's were selected; one in medial frontal gray matter anterior to the corpus callosum, one in right frontal white matter, another in right central white matter, and lastly, one in the right inferior occipital brain region above the cerebellum. These VOI's are depicted in fig. 2.2. For each VOI and head orientation the zero-, first-, and second-order B0 inhomogeneity in this VOI was calculated by transforming the voxel coordinates into the scanner frame of reference.

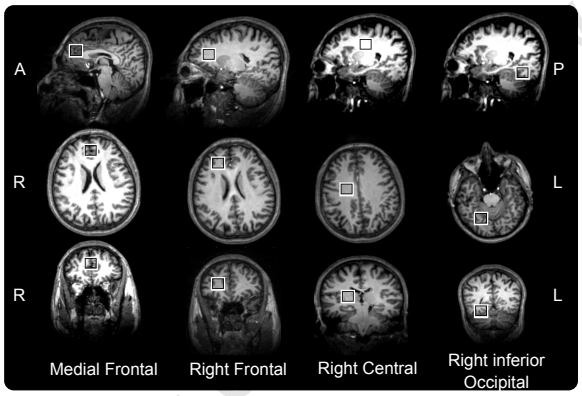

Figure 2.2: VOI's Medial Frontal, Right Frontal, Right Central, and Right inferior Occipital, for which change in B0 shim gradients with respect to movement are demonstrated.

Using the mean frequency, linear B0 gradients, and second-order terms, we investigated the effect of head pose on B0 in the four VOI's in our volunteer. The mean frequency (zero-order shim term) was calculated without fitting the first- and second-order shim terms, and the first-order shim estimates were calculated without fitting the second-order terms.

2.3.2 The EPI vNav

To measure head pose and B0 inhomogeneity in real time we implemented a 3D multishot EPI vNav with a resolution of 8 x 8 x 8 mm^3, an acquisition matrix of 32 x 32 x 28, and 256 x 256 x 224 mm^3 FOV, so as to completely cover the FOV of the Siemens 3T Allegra scanner used in this study. Two contrasts were acquired

with interleaved partition acquisitions, TE_1 = 6.6 ms and TE_2 = 9.0 ms, TR = 16 ms, and bandwidth 3906 Hz / px. The two contrasts were acquired interleaved in 58 shots, each with 2° flip angle. The first two shots collect a navigator used in N/2 ghost reduction for each contrast and the remaining 56 acquire 28 partition encodes (k-space slices), interleaved, for each contrast giving a total navigator duration of 928 ms.

The navigator sequence is highly customizable on the scanner console allowing for navigators to be tailored to a subject, sequence, and VOI. For example, the number of partitions could be reduced to 16 and still cover the full brain (128 mm), reducing scan time to only 544 ms. This would, however, require the operator to position the navigator to ensure that it overlaps with the brain. As the SVS sequence used in this study has a sufficiently long magnetisation (M0) recovery period, a navigator covering the complete FOV was chosen.

The vNavs are reconstructed immediately online to create a field map and two magnitude volume images. Pose estimation is performed using a single vNav contrast (TE_1) by co-registering subsequent vNav's to the first vNav after the preparation (dummy) TR's. This registration is performed using an optimised Prospective Acquisition CorEction (PACE, Thesen et al., 2000) algorithm that is an established method for registering whole-head EPI. The image reconstruction and PACE registration is performed online immediately after the navigator block in under 80 ms.

Field map phase unwrapping is performed online using Phase Region Expanding Labeller for Unwrapping Discrete Estimates (PRELUDE, Jenkinson, 2003) with a mask created by including all voxels with a magnitude greater than max(|all voxels|)/15 that form part of the largest connected region of such voxels. This threshold was chosen as it ensured the inclusion of all voxels with sufficient SNR . The connected regions are found using routines in the PRELUDE package, with the largest such region selected as the mask. Two frequency and first-order shim estimates are calculated online, one for the selected SVS VOI and one for the navigator FOV. The shim estimate for the navigator FOV is calculated using an unweighted least squares regression while the shim estimate for the chosen VOI uses a weighted least squares regression, where the weighting of each navigator voxel is according to its intersection with the SVS VOI. The final two adjust-

University of Cape Town

ments performed during shim estimation are to correct for B0 distortion of each voxel (Reese et al., 1995) and to shift the VOI position according to the motion estimate for the current TR thus ensuring that the voxel coordinates are mapped to the scanner coordinates taking into account the current pose. This ensures that the SVS shim is calculated over the correct anatomical region. Hence shim estimation can only be performed after completion of PACE.

The complete online block, including transmission of the current estimates back to the sequence, occurs in under 170 ms, enabling the sequence to update the spectroscopy VOI according to current pose and apply the appropriate shim estimate to that VOI within the same TR. Figure 2.3 summarises the flow and operation of the vNav block.

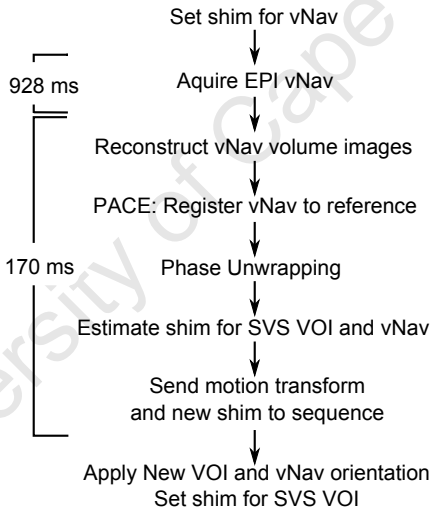

University of Cape Town

Figure 2.3: Work flow of vNav block, sequence and online processing.

2.3.3 Insertion into single voxel spectroscopy PRESS sequence

The navigator block was inserted prior to water suppression in a SVS Point REsolved SpectroScopy (PRESS, Bottomley, 1987) sequence, occupying a portion of the TR used for M0 relaxation. The timing is illustrated in fig. 2.4. As the

navigator has a flip angle of 2°, we hypothesised that it would minimally affect the M0 relaxation process. This was explored in the *in vivo* experiments described below. The navigator real-time shim estimates were applied from the first preparation or dummy TR while the pose estimates were calculated and applied from the second TR after preparation to allow the vNav shim time to stabilise. These estimates were applied synchronously immediately following the vNav block and prior to the water suppression.

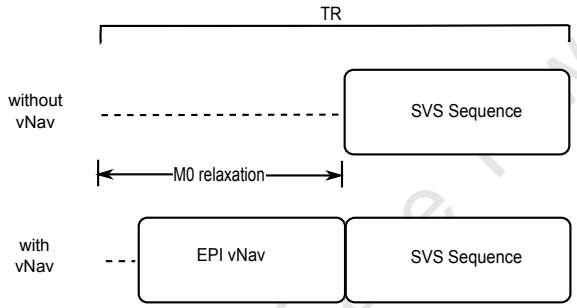

Figure 2.4: A typical SVS PRESS sequence and our navigated SVS PRESS with vNav inserted into the M0 relaxation period.

University of Cape Town

2.3.4 *In vivo* validation

Six SVS PRESS scans were acquired with different protocols for each of six healthy volunteers. The aim was: (i) to investigate the impact of the navigator on the M0 relaxation process, (ii) to compare the navigated real-time shim to that of a manually optimised shim, (iii) to investigate the impact of shim and motion correction in the presence of pose changes, and (iv) to decouple the effects of motion correction, frequency correction and shim correction. A VOI was chosen in the right central white matter as this region is expected to have minimal interaction between pose change and second-order B0 inhomogeneities. Of the six SVS PRESS acquisitions, the first three were baseline scans without movement and included the original Siemens sequence, a sequence with our navigator but no feedback, and a fully shim- and motion-navigated (ShMoCo) sequence. These were acquired in random order. For the remaining three SVS PRESS acquisi-

Table 2.1: Summary of the six SVS protocols acquired for each volunteer in the right central white matter.

	Sequence	Subject Movement	Real-time shim update	Motion correction
1	SVS PRESS			
2	SVS PRESS with vNav			
3	SVS PRESS with vNav (ShMoCo)		√	√
4	SVS PRESS with vNav (ShMoCo)	√	√	√
5	SVS PRESS with vNav (MoCo)	√		√
6	SVS PRESS with vNav (NoCo)	√		

University of Cape Town

tions, the volunteers had been trained to lift their chin by approximately 8° upon receiving a cue at 20 s, to drop it to its rest position and rotate their head left by approximately 10° at a cue 48 s later, and finally return to their rest position a further 52 s later. In order to avoid spectral dephasing, volunteers were instructed to pace each movement to occur slowly and smoothly over a two to three TR window . The first of the SVS PRESS sequences with motion was fully shim- and motion-navigated (ShMoCo), the second was only motion-navigated (MoCo), and the third had no navigator feedback applied (NoCo). For all of the above acquisitions the shim was optimised first using the scanners automatic advanced shim adjustment and then further manually adjusted to acquire a T2* >= 43 ms and a water linewidth < 8.5 Hz . These six SVS acquisitions are summarised in Table 2.1.

The VOI was positioned using an MEMPR. The SVS PRESS voxel was (2 cm)^3 with a TR of 2 s, TE of 30 ms, 512 readout (ADC) sample points, bandwidth 1000 Hz, frequency offset -2.6 ppm, water suppression bandwidth 35 Hz, 64 averages in addition to 4 dummy or preparation acquisitions. For each volunteer a water reference FID with the same parameters, apart from TR = 4 s and a single average, was acquired using the manually optimised shim for further

processing in LCModel (Provencher, 1993). The LCModel measures of linewidth and signal to noise (SNR), as well as the spectra themselves, were compared for spectra acquired with the different protocols.

In order to demonstrate the versatility of the vNav and its use in a VOI with higher B0 inhomogeneity, three additional SVS PRESS scans were acquired in volunteer 5. The VOI chosen was the medial frontal grey matter, as depicted in fig. 2.2. The vNav protocol was changed prior to the first scan in this VOI using a 1 s set scan. This set scan sets the new EPI protocol to be used by the vNav and sets the vNav position over the subject's brain. This protocol had an increased resolution of 5 x 5 x 5 mm^3, reduced FOV of 220 x 200 x 110 mm^3, matrix 44 x 40, 22 partitions, TE's of 8 ms and 12.8 ms, TR of 21 ms, and a bandwidth of 3906 Hz. The three scans had the same SVS parameters as above and varied as follows: i) stationary baseline scan, without any correction, ii) shim and motion corrected scan (ShMoCo) with movement, iii) only motion corrected (MoCo) scan with movement. The subject was asked to move in the same manner as described above.

University of Cape Town

2.4 Results

2.4.1 Investigation of the effect of motion on B0

Figure 2.5 shows the effects of motion on B0 homogeneity in four VOIs for a single volunteer. Figure 2.5A shows the volunteer's motion about the scanner's iso centre for the relevant axes for both the chin down - up and left - right trajectories. Field maps were acquired at six different head poses along each trajectory. Figure 2.5B shows the mean frequency change in each VOI as the head moves. To ease comparison the plots were offset to cross zero at the neutral head pose (pose 3 of chin up - down) by 17.1 Hz, 45.4 Hz, 37.8 Hz, and -90.7 Hz for the medial frontal, right frontal, right central, and lower occipital regions, respectively. Figure 2.5C shows how the magnitude of the first-order shim estimates change in each VOI. As the second-order shim requirements are the greatest in the frontal lobe, the changes in the five second-order shim estimates for only the medial frontal VOI are plotted in fig. 2.5D. The first- and second-order shim estimates are also offset

to cross zero at the neutral position of the chin down - up trajectory.

The magnitude of the second-order shim terms required in the neutral head position of the chin up - down trajectory are compared for the different VOI's in fig. 2.6. This shows that, for most of the terms, the frontal lobe requires a significantly higher second-order B0 shim compared to the central and inferior occipital regions.

2.4.2 *In vivo* vNav validation

Figure 2.7 is a single navigator volume from a single TR showing the magnitude volume of the first echo and the field map derived from the navigator.

The linewidth and SNR, as measured by LCModel, were compared for the different sequences. The VOI for all the scans was in the right central white matter. Figure 2.8A and B present the mean (+/- one standard deviation) of the SNR and linewidth for each of the different SVS protocols calculated over all the volunteers. There is no loss in SNR due to the navigator and no increase in linewidth when using real-time shim and motion correction (ShMoCo) for both stationary and moving scans. When no shim correction was applied to the scans with movement, the linewidth increased on average by approximately 2 Hz while the variability of linewidths increased dramatically with no motion correction. The SNR is 33% lower (significance $p < 0.05$) when no shim correction is applied to the scans with movement. Figure 2.9 shows the spectra for all the scans acquired with movement (fully shim and motion corrected, motion corrected only, and uncorrected scans) for each of the six volunteers superimposed on top of the respective baseline scan without movement. These plots demonstrate that the spectra are affected by the pose change when no correction and only motion correction are applied .

The motion and shim estimates measured as a function of time by the vNav for one of the acquisitions with motion and motion correction only is presented in fig. 2.10. As no shim correction was applied during the scan, the plotted VOI frequency shift was computed using an offline spectral cross-correlation of each FID acquired in the scan to the first FID. The first-order shim estimates have been offset by their values at data point 3 for ease of comparison. As frequency and

University of Cape Town

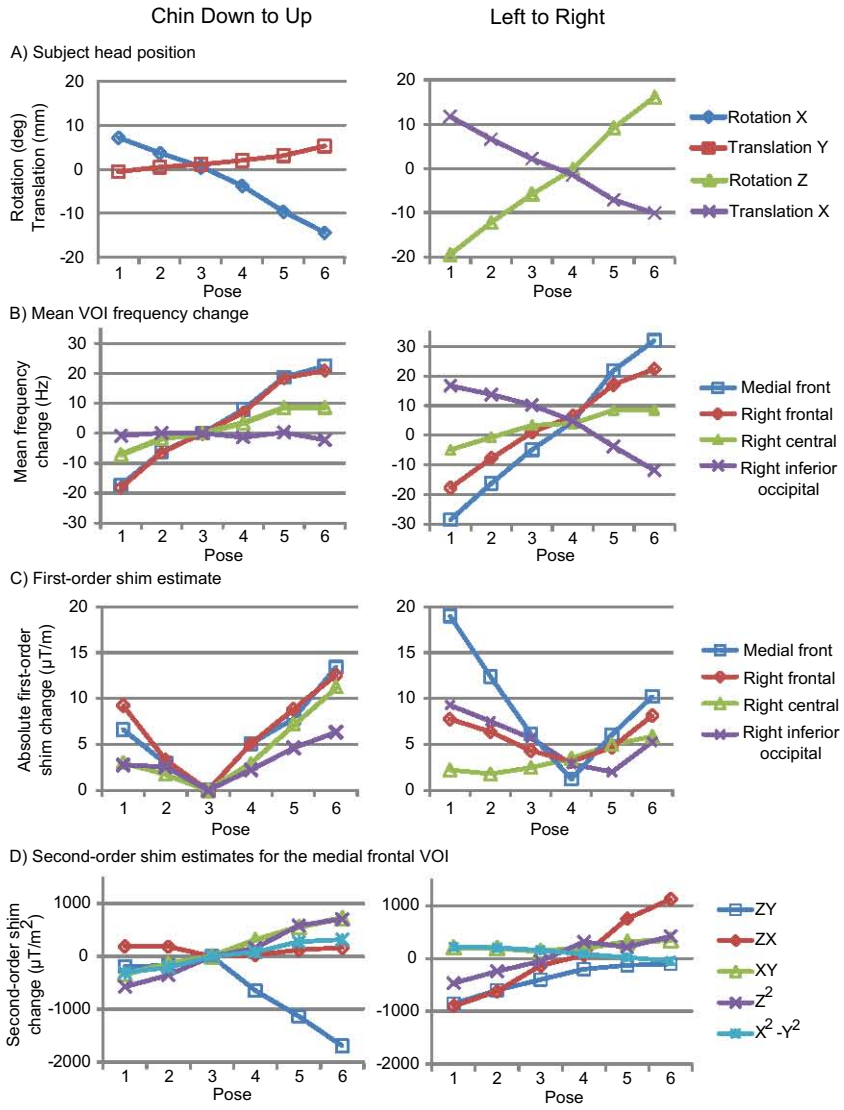

Figure 2.5: B0 changes as a result of chin down - up and left - right motion. A. Motion trajectory, B. Mean VOI frequency change for each VOI, C. Absolute magnitude of first-order B0 shim vector independent of second-order for each VOI, and D. Second-Order B0 shim estimates for the Medial Frontal VOI, offset by the value at rest. X, Y, and Z refer to the scanner axes perpendicular to the sagittal, coronal, and transverse planes and the X axis labels 1 to 6 refer to each of six respective head positions.

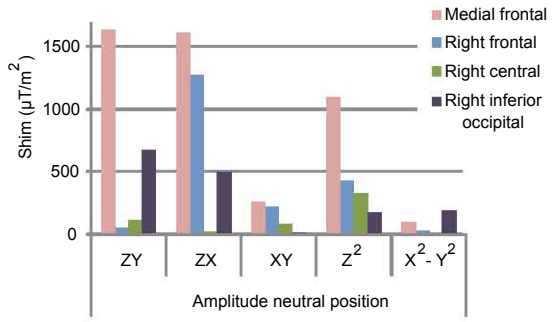

Figure 2.6: Magnitude of the second-order B0 terms in the neutral pose compared for each of the four VOI's demonstrate that the frontal lobe has the highest second-order shim requirements.

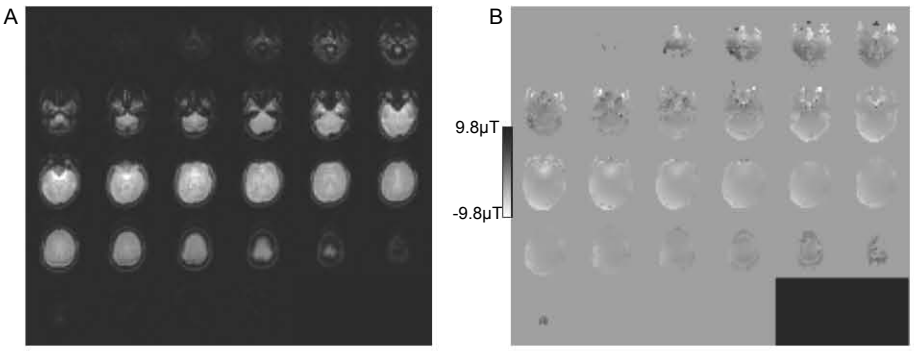

Figure 2.7: Example navigator volumes. A. Magnitude images for first echo, and B. Unwrapped and masked field map with the contrast range doubled (-2π to 2π) due to the phase unwrapping.

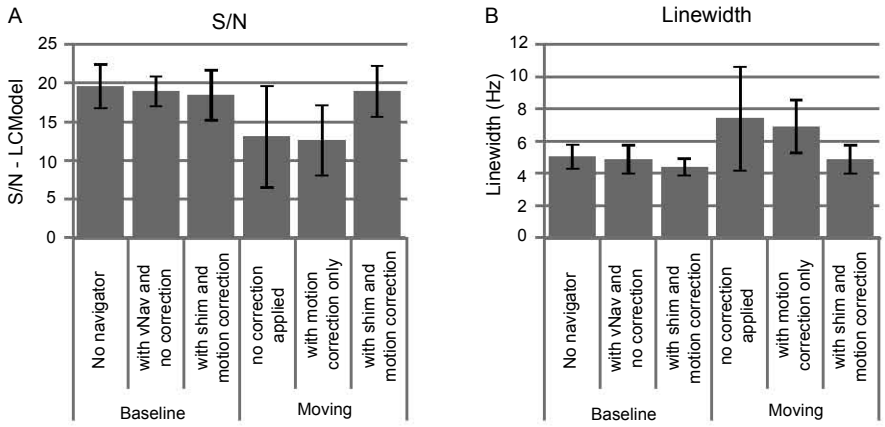

Figure 2.8: A. Bar graph of the mean signal to noise ratio (SNR as calculated by LCModel, +/- one standard deviation). B. Bar graph of the mean linewidth (+/- one standard deviation). Both calculated over the 6 volunteers for each of the three stationary baseline scans and each of the three acquisitions with motion.

shim were measured regardless of whether such feedback was applied, fig. 2.11A and B present scatter plots of the frequency and Y-axis shim change for all three scans with movement in all six volunteers as a function of the angle of rotation about X due to the chin-up movement. The Y shim gradient is plotted here as it was affected most by this movement as seen in fig. 2.10C. These frequency, shim, and head rotations, were measured for the maximum chin-up rotation, averaged over the duration that the subject maintained that pose. These scatter plots demonstrate a correlation of frequency and shim with head pose. For the Y axis shim, the trend is roughly a 1° to 1 μT/m (y = 0.99θ + 0.6) relationship between the head up-down angle and Y shim gradient.

To decouple the effect of frequency shift from first-order shim changes on line broadening, the three scans with movement for three of the volunteers (4, 5, and 6) were processed offline to remove frequency shifts by cross-correlating the spectrum of each FID to that of the first FID and producing a new frequency-coherent average for each scan. These frequency-coherent averages had a mean linewidth (± one standard deviation) averaged across the three volunteers of 4.9 ±0 Hz with shim and motion correction, 6.8 ±0.9 Hz with only motion correction,

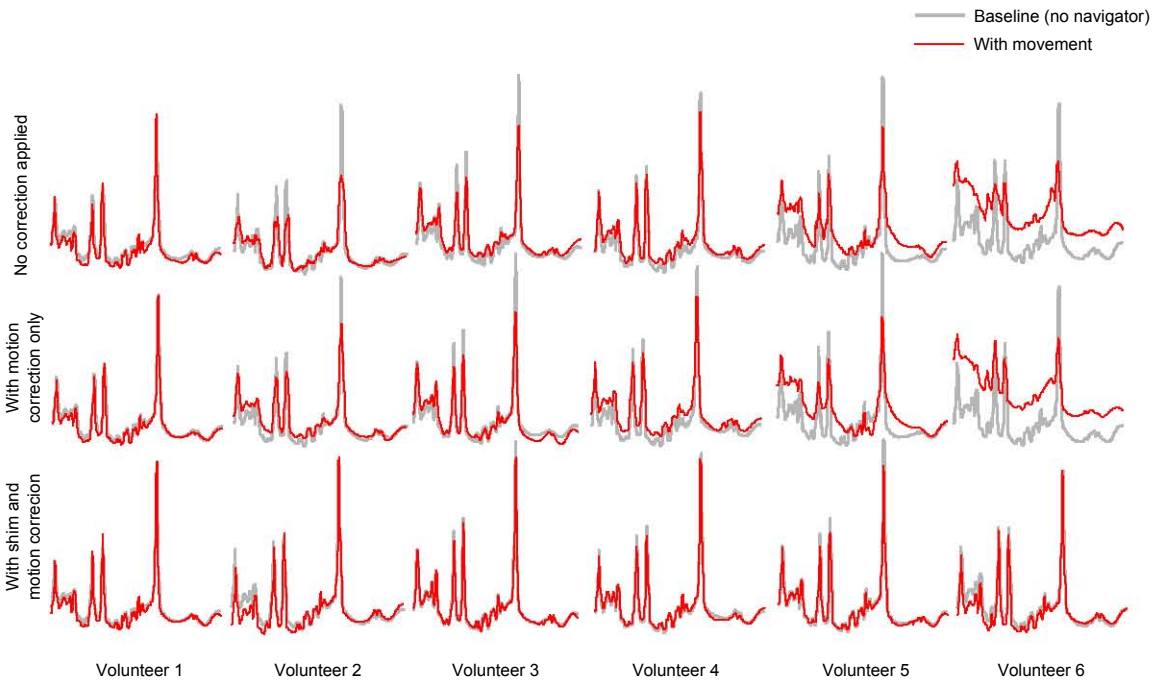

Figure 2.9: Spectra obtained in the right central white matter for the three scans acquired with movement (no correction, with motion correction, and with full shim and motion correction) for all six volunteers superimposed on top of the respective baseline spectra with no navigator. The plots are the spectra as fitted by LCModel.

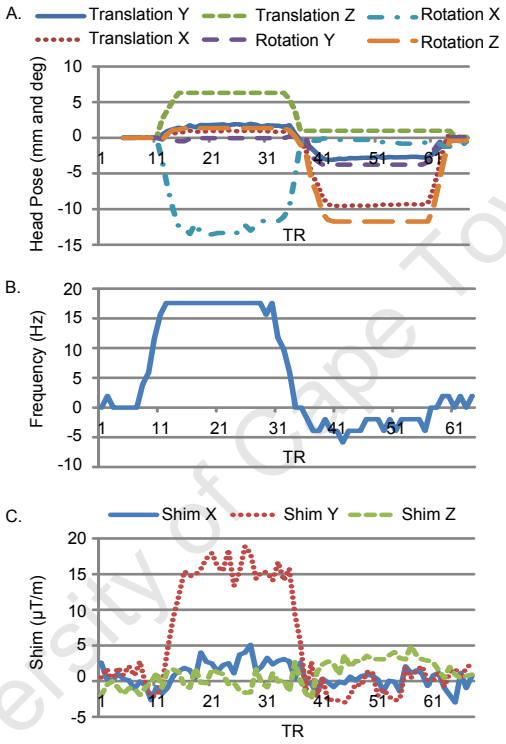

University of Cape Town

Figure 2.10: Navigator output and frequency variation from the motion corrected acquisition of volunteer 6. A. Absolute motion estimate as calculated by the navigator, B. mean VOI frequency as calculated from FID cross-correlation, and C. first-order B0 shim change as calculated by the navigator, all as a function of the TR over the duration of the acquisition. X, Y, and Z refer to the scanner axes perpendicular to the sagittal, coronal, and transverse planes, respectively.

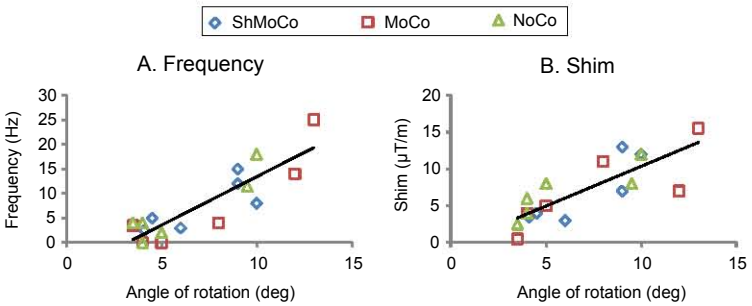

Figure 2.11: A. Scatter plot of change in frequency and B. change in Y shim gradient as a function of the angle of chin-up rotation about X for all three scans with motion from the six volunteers as measured by the vNav. These values were calculated from the maximum chin-up rotation, averaged over the duration that the subject maintained that pose.

and 6.5 ±0.5 Hz when no real time correction is applied. This demonstrates a loss in linewidth purely as a result of first-order shim changes, independent of frequency shifts, of just under 2 Hz when no shim correction is applied.

For the three additional SVS scans acquired in the medial frontal lobe of volunteer 5, the scan with motion and shim with motion correction, had the same linewidth and SNR as the baseline stationary scan, namely 4.9 Hz and 20, respectively. By comparison, the moving scan with only motion correction had a linewidth of 6.8 Hz and SNR of 14. The chin-up rotation produced a shim change in Y of 10 μT/m while the chin-left rotation produced the same shim change in Y of 10 μT/m and additionally a 15 μT/m change in X, both calculated as the mean during the respective pose.

2.5 Discussion

Single voxel spectroscopy is a technique that inherently lacks anatomical information and thus accurate volume localisation cannot be guaranteed. Furthermore, the accuracy of the spectra may be adversely affected by artifacts induced by pose change, including phasing errors, line broadening and frequency drifts over

time that may or may not be observable.

The changes in B0 resulting from changes in pose are dependent on the region of interest. As fig. 2.5 demonstrates, all four VOI's exhibited a frequency and first-order B0 change with both chin-down to chin-up and left-to-right movements, however, first-order B0 changes were not significant in the right central region for left-to-right pose change. The second-order B0 shimming requirements are significant in the frontal lobe and as such the ability to adapt these second-order shim terms in relation to pose changes would be beneficial, although it is not possible on the current hardware.

In this work a vNav capable of measuring head pose and B0 shim correction factors within a single TR was demonstrated. This vNav is ideal for spectroscopy as it provides a series of anatomical images with sufficient resolution to provide online pose estimation and offline registration of the spectra to an anatomical image. The accuracy of the volume-to-volume registration performed by PACE was not scrutinised in this study, however, the baseline fluctuations in position estimates were well below 1 mm and 1°. Two sources of image artifact in the vNav are: the presence of dark bands resulting from the three PRESS slice selection planes, and image distortions due to the use of a spectroscopy-specific shim. The impact of the dark bands is minimised by the use of SVS water suppression; the water suppression perturbs globally the magnetisation of the entire volume thus minimising the dark bands. The second is inherently corrected by the navigator after the first TR by applying the appropriate first-order shim for the vNav as calculated from the vNav itself and thereafter alternately switching the shim between the best calculated values for the navigator and the best values for the spectroscopy VOI.

The first question investigated in this study was whether the navigator impacted the signal of the spectra. SNR measurements in LCModel demonstrated that the vNav had no effect on the SNR compared to acquisitions with no navigator (shown in fig. 2.8). It should be noted that a change in TR from 2 s to 1.5 s would have a noticeable effect on the SNR per shot. The accuracy of the navigator's shim estimate is demonstrated by the linewidth of the baseline acquisitions with real-time shim correction where the mean and standard deviation did not exceed that of the manually optimised shim.

University of Cape Town

This vNav technique provides three real-time adjustments: VOI location, frequency, and first-order shim correction. The benefit of applying all three is clearly demonstrated by the narrow linewidth and high signal to noise in the presence of pose change (fig. 2.8). The effect of shim adjustment and VOI localisation correction was decoupled by acquiring an acquisition with only motion correction. In order to separate the effects of frequency shifts from first-order shim errors on linewidths, offline frequency correction was applied to motion corrected data of 3 subjects. While the linewidth improved with each adjustment, it was only fully regained by applying all three.

In the data presented, each subject's chin was raised for approximately 1/3 of the acquisition and resulted in a mean linewidth increase from 4.9 Hz to 6.8 Hz when offline frequency correction was applied. This is consistent with eq. 2.1 which suggests that for the duration of a 10 μT/m shim change, the linewidth will increase from 5 Hz to 10 Hz. As this only occurred for 1/3 of the acquisition in the present case, the mean linewidth is expected to be 5 Hz + (5 Hz/3) = 6.7 Hz. The use of offline frequency correction demonstrated an improvement in linewidth due solely to shim correction and not due to frequency correction. This is because a single frequency shift, as is present in our data, results in a secondary peak, rather than line broadening.

The real-time shim data and results presented here are the raw estimates from a single navigator. One could further increase the stability of the navigator by taking into account the large time course of data available. This type of temporal filtering would prove beneficial should an accelerated version of the navigator be implemented.

The three scans in the medial frontal grey matter of volunteer 5 demonstrate the application of the vNav in a region of higher B0 inhomogeneity. In such regions a higher vNav spatial resolution provides the specificity required for first-order shim measurements. This higher resolution vNav protocol has a limited FOV that requires the operator to position the vNav over the subject's brain. This additional step should be taken into account when choosing the appropriate vNav protocol for the VOI. This scan demonstrated significant first-order shim changes for both chin-up and chin-left rotations indicating the importance of this type of navigator in regions of high B0 inhomogeneity.

University of Cape Town

As already discussed, the navigator is dynamically configurable and should a shorter TR be necessary, simply reducing the number of partitions acquired and subsequently manually positioning the navigator over the anatomy of interest enables TRs of 1.5 s to be achieved. Acquiring the complete scanner FOV with the navigator simplifies the user interaction and was achievable with our TR of 2 s. The duration of the complete navigator block presented is approximately 1.1 s and is faster than that achieved using the PROMO technique in SVS (Keating et al., 2010) of 1.5 s. Further navigator optimisation is possible by employing acceleration techniques like parallel imaging.

Finally, this work has not addressed phasing errors brought about by subject movement during the PRESS localising gradients. Reacquisition, as presented by Zaitsev et al. (2010a) would be one possible solution. However, as single voxel spectra are accumulated over repeated measurements it may be more appropriate to provide an offline tool to simply exclude dephased measurements.

University of Cape Town

2.6 Conclusion

Changes in B0 homogeneity were demonstrated in four different SVS VOI's in a single volunteer for different head poses. A volume navigator capable of measuring and adjusting, in real time within each TR, head pose, VOI frequency, and VOI first-order shim has been demonstrated. For restless subjects whose head pose cannot be assumed to be constant, this provides a useful addition to the SVS sequence. The first-order shim estimates calculated by the vNav result in linewidths equal to those achieved with manual first-order shim optimisation and maintain spectral quality in the presence of pose changes.

2.7 Acknowledgements

Several people have provided valuable assistance in this project including, Thomas Benner, Michael Hamm and Charles Harris. Resources necessary in the project were provided by University of Cape Town, Martinos Center, and Cape Universities Brain Imaging Centre. This study was supported by the South African

Research Chairs Initiative of the Department of Science and Technology and National Research Foundation of South Africa, the University of Cape Town, the Medical Research Council of South Africa, NIH grants R21AA017410, R33DA026104, R21EB008547, R01NS055754, P41RR014075, and The Ellison Medical Foundation.

University of Cape Town

Chapter 3

Real-time motion and B0 correction for LASER MRSI using EPI volumetric navigators[1]

Aaron T. Hess[2], Ovidiu C. Andronesi[3], M. Dylan Tisdall[3], A. Gregory Sorensen[3], André J.W. van der Kouwe[3], and Ernesta M. Meintjes[2]

University of Cape Town

Abstract

A method is presented to correct the effects of motion and motion related B0 perturbations on spectroscopic imaging in real time through the use of a volumetric navigator (vNav). It is demonstrated that for an axial slice, lifting the chin significantly disrupts the B0 homogeneity in the zero-order (frequency), first-order Y (coronal) axis, and in the second-order ZY term. This vNav is able to measure and correct in real time both head pose and zero- to first-order B0 inhomogeneities. The vNav has been validated in six volunteers who deliberately lifted and then dropped their chin during the scan. These scans show that motion correction alone is not enough to recover the spectral quality. By applying real-time shim adjustments, spectral quality was fully recovered to linewidths under 0.08 ppm (9.9 Hz) and SNR to within acceptable limits in five out of six subjects. In the sixth subject 86% of the spectra within the VOI were recovered, compared

[1]Chapter under review.

[2]University of Cape Town.
[3]Martinos Center, MGH, Harvard Medical School.

to the worst case non shim-corrected scan where none of the voxels fell within these quality bounds. It is shown that the use of a vNav comes at no additional cost to the scan time or spectral SNR.

3.1 Introduction

Magnetic resonance spectroscopic imaging (MRSI) is a powerful non invasive tool for studying biochemistry *in vivo*. However, it suffers from a lack of anatomical resolution and is sensitive to temporal fluctuations in the B0 magnetic field. By contrast to MR imaging, motion during MRSI does not always cause observable artifacts and image displacement and as such may go completely unnoticed. Some of the more observable motion related artifacts in MRSI include lipid contamination, ghosting, and line broadening. The former occurs when the subject's movement causes the volume of interest (VOI) to intersect with a lipid containing region, potentially rendering a large proportion of the spectra unusable. Free-induction decay (FID) dephasing caused by rapid movements by the subject during application of the outer-volume suppression gradients will manifest as ghosting artifacts and amplitude fluctuations. Split spectral peaks and line broadening result from changes in the B0 field due to the new orientation of susceptibility boundaries. Finally, changes in proximity to various coil elements will cause spatially related phase changes in the received signal.

There are various degrees of B0 adjustment in clinical systems ranging from zero-order (frequency) to second- or even third-order spatial adjustments. Several methods have been proposed to prospectively and retrospectively track the *in vivo* zero-order B0 field. One such method initiates the FID readout prior to the application of phase encoding gradients (Posse et al., 1993). In this manner, the non-encoded portion of the FID can be used for phase and frequency correction. An alternative method uses an interleaved navigator with a 5° excitation followed by an FID readout (Henry et al., 1999) to measure the change of the main magnetic field frequency. Tracking of the mean VOI frequency can be achieved if outer-volume suppression is added (Thiel et al., 2002). None of these methods address first- or higher-order B0 changes.

Several real-time head tracking methods have been used in MRI including

University of Cape Town

optical tracking devices and within-sequence navigator methods. Optical tracking devices (Weinhandl et al., 2010; Zaitsev et al., 2010b) use an externally mounted camera to track the subject's movement. One advantage of such systems is a unified coordinate system for both anatomical imaging and spectroscopic imaging, thus providing confidence in MRSI VOI placement and the fact that sequences do not need to be changed fundamentally. The main disadvantage of such devices is the cumbersome additional hardware in the MR room and additional regalia worn by the subject. Navigator methods, on the other hand, require no additional hardware.

Navigator-based motion tracking can be performed using the properties of rigid body transformations exhibited in rapid k-space trajectories. Examples of these are cloverleaf (Van der Kouwe et al., 2006) and orbital (Fu et al., 1995) navigators that can be executed in under 10 ms. An alternative is to use image based navigator techniques such as the EPI volumetric Navigator (vNav) (Hess et al., 2011; Tisdall et al., 2009). The vNav method employs 3D multi-shot EPI to rapidly generate a low resolution 3D image of the subject and register it to a reference volume. A technique that employs three orthogonal low resolution 2D spiral images and registers these to a map has been proposed (White et al., 2010) and is called PROspective MOtion correction or PROMO. The vNav is particularly suited to MRSI as it performs well in sequences with low temporal resolution (long repetition times) and, with respect to MRSI, is the only technique capable of performing real-time first-order shim correction. In MRSI, TR's are of the order of 1.5 s to 3 s. In addition, the vNav provides a crude anatomical image that has the potential for registration to a structural image. Finally, it can generate spatial parameters such as a 3D B0 field map (Hess et al., 2011) that can be used to measure shim adjustment terms.

The magnitude of B0 homogeneity distortions resulting from motion were quantified in a single volunteer using high resolution B0 field maps for both chin left-to-right and chin down-to-up movements. The results demonstrate the need for real-time shim correction in the presence of motion. A navigated Localized Adiabatic SElective Refocusing (LASER, Andronesi et al., 2010) MRSI sequence is presented. The sequence uses an EPI vNav to measure and correct, in real time, VOI position, frequency and first-order shim changes. Six volunteers were

University of Cape Town

scanned to demonstrate how real-time zero- to first-order B0 correction recovers the spectra in the presence of chin-up or -down rotations. Using the zero- to second-order B0 terms measured by the vNav we plot the B0 changes that accompany this motion for one of the volunteers.

3.2 Materials and methods

Two scanners were used in this study: a 3T Siemens Allegra scanner (Erlangen, Germany) in Cape Town, South Africa using a standard single channel head coil; and a 3T Tim Trio at the Martinos Center, Boston, Massachusetts, with a standard 12 channel head coil. All volunteers were scanned according to the ethical guidelines of the respective institution.

University of Cape Town

3.2.1 Analysis of B0 change with respect to pose

To determine the role of frequency, first-order, and second-order shim correction in motion corrected MRSI, the effect of head movement on B0 homogeneity was investigated. We acquired multiple high-resolution B0 field maps in a single volunteer with the subject's head in various positions. The 3T Allegra scanner was used for the experiment. The volunteer was instructed to move their head incrementally, first about the X axis (chin down-to-up) and then about the Z axis (left-to-right rotation). Six field maps were acquired during the X axis rotation, ranging from 7.2 to -14.4, and 6 field maps for the Z axis rotation, ranging from -19 to 16. Resultant rotations were assessed offline. The subject was trained how much to move his head prior to scanning.

A gradient echo sequence was used to acquire the field maps. The parameters were as follows: 48 slices, matrix 64 x 64, FOV = 192 x 192 mm^2, slice thickness = 3 mm, TR = 502 ms, TE1 = 4.59 ms, TE2 = 7.05 ms, bandwidth = 260 Hz/pixel and a slice separation of 0.6 mm. No shim adjustment was performed prior to each field map acquisition.

Each field map was registered to a reference 3D Multi echo MPRAGE (MEMPR, Van Der Kouwe et al., 2008) using SPM5 (Ashburner, 2007) in order to remove the effect of shifting anatomy, and further resliced to match the 3D MEMPR reso-

lution of 1.0 x 1.3 x 1.0 mm^3 using linear interpolation. An axial VOI was selected superior to the ventricles. For both movement trajectories, one position was taken as the neutral head pose. In the chin down-to-up trajectory, this was the third position and in the chin left-to-right trajectory this was the fourth position. To remove the effect of B0 inhomogeneities that would normally be corrected by the scanner's automated shimming procedure, a VOI-specific second-order shim estimate was calculated for each of the two neutral poses. This shim estimate was then subtracted from each field map in the respective series to emulate the expected B0 field in a shimmed MRSI experiment. Two operations were performed on the acquired field maps. Firstly, a mean frequency was calculated within the VOI. Secondly a 1 x 1 x 1.5 cm^3 kernel was convolved with the field maps to emulate the resolution, and thus mean frequency of an MRSI voxel.

3.2.2 LASER sequence with vNav for real-time shim and motion correction

A dual-contrast multi-shot 3D EPI vNav (Hess et al., 2011; Tisdall et al., 2009) was inserted into a LASER MRSI sequence (Andronesi et al., 2010). The vNav calculates both shim and head pose once per TR and applies the relevant corrections within the same TR. It has been shown previously that this LASER sequence has excellent spatial and chemical shift localisation (Andronesi et al., 2010).

The vNav EPI protocol used is as follows: 32 x 32 matrix, 16 slices, 256 x 256 x 128 mm^3 FOV (8 x 8 x 8 mm^3 isotropic). Two contrasts were generated with interleaved partition acquisitions: $TE_1 = 6.6$ ms and $TE_2 = 9.0$ ms, TR = 16 ms, and bandwidth 3906 Hz/px. The two volumes were acquired interleaved in 34 shots, each with a 2° flip angle. The first two shots acquire the phase correction navigator used for N/2 ghost reduction of the two contrasts and the remaining 32 shots acquire 16 partition encodes, interleaved, for each contrast, giving a total navigator duration of 544 ms. The navigator is positioned over the subject's brain using a "set" sequence that runs a single repetition of the navigator in the chosen position and is completed in under 1 s.

The vNavs are reconstructed immediately online and a field map is generated

University of Cape Town

from the complex division of the two EPI volumes. Pose estimation is performed using a single vNav contrast (TE_1) by co-registering subsequent vNav's to the first vNav after the preparation ("dummy") TR's. This registration is performed using an optimised Prospective Acquisition CorEction (PACE, Thesen et al., 2000) algorithm that is an established method for registering whole-head EPI. The image reconstruction and PACE registration is performed online immediately after the navigator block in under 80 ms.

A mask is created to exclude voxels with an insufficient signal to noise ratio (SNR). The mask is defined as all voxels with a magnitude greater than max(|all voxels|)/15; this mask is fast to calculate and excludes background noise. Field map phase unwrapping is then performed online using PRELUDE (Jenkinson, 2003). Two pairs of frequency and first-order shim estimates are calculated online, one for the required MRSI VOI and one for the navigator FOV. The shim estimates for the navigator FOV are calculated using an unweighted least squares regression while the shim estimate for the chosen VOI uses a weighted least squares regression, where the weighting of each navigator voxel is according to its intersection with the MRSI VOI. The final two adjustments performed during shim estimation are, firstly, to correct for the B0 distortion of each voxel (Reese et al., 1995) and, secondly, to shift the VOI according to the motion estimate for the current TR. This ensures that the voxel coordinates are mapped to the scanner coordinates taking into account the current pose. Hence shim estimation can only be performed after completion of PACE. The complete online block, including transmission of the current estimates back to the sequence, occurs in less than 170 ms, enabling the sequence to update the spectroscopy VOI according to current pose and apply the appropriate shim estimate to that VOI within the same TR. The total navigator block, including sequence (544 ms) and online processing (170 ms) takes 714 ms.

The MRSI LASER sequence was set up with the following parameters: TE = 50 ms, TR = 1.5 s, elliptical phase encoding (16x16 matrix), FOV = 208 x 224 mm^2, Hamming filter width = 50% of the FOV, 1 acquisition, TA = 3 min 50 s , final matrix size 32x32. Offset independent adiabatic pulses (Tp = 4 ms, BW = 6 kHz) based on WURST-8 waveforms (Andronesi et al., 2010; Tannús and Garwood, 1996) were used for selection of VOI (80 x 90 x 15 mm^3, APxRLxFH).

University of Cape Town

Constant gradients were enforced to enable dynamic slice positioning using a frequency offset. Water suppression was realized with a WET scheme (Ogg et al., 1994). Outer volume suppression (OVS) was not necessary due to the sharp LASER excitation profile of the VOI.

The vNav was inserted into the LASER sequence prior to water suppression, occupying a portion of the TR used for M0 relaxation. It has been shown that in SVS the small flip angle of the vNav does not observably affect the M0 relaxation process (Hess et al., 2011). The navigator real-time shim estimates are calculated from the first preparation TR while the pose estimation is initiated on the second TR after preparation. The navigator additionally calculates a VOI specific second-order B0 shim that is not applied, but recorded in a log file.

3.2.3 Validation of navigated LASER sequence

The sequence was validated in six healthy volunteers; two were scanned at the Martinos Center on a 3T Siemens Tim Trio (Erlangen, Germany) using a standard 12 channel head coil, and four at the Cape Universities Brain Imaging Centre on a 3T Siemens Allegra (Erlangen, Germany) using a standard single channel head coil. The protocol consisted of a structural MEMPR used for VOI localisation, followed by five vNav LASER MRSI scans with an 80 x 90 x 15 mm^3 VOI positioned axially above the ventricles. The pre-scan shim was adjusted automatically by the scanner over the MRSI VOI. For scans at the Martinos Center, 256 FID samples were acquired per readout and in Cape Town, 512 FID samples were acquired per readout, both at a bandwidth of 1024 Hz. While the 512 FID samples will provide an increased spectral resolution for the scans in Cape Town, the 12 channel head coil used at the Martinos Center will increase SNR for those scans. These inter site differences will not have an impact on the data as only intra-subject comparisons of scans are presented.

For the first two MRSI scans the volunteers were asked not to move. In the first scan, real-time shim and motion correction (ShMoCo) were applied, and in the second the navigated sequence was used with the feedback disabled i.e. no correction applied (NoCo). For the remaining three scans the volunteers were trained to lift their chin by approximately 5°-10° on a cue presented 1 min into

University of Cape Town

the scan, drop it approximately 5° lower than the neutral position after a further 1 min 15 s, and hold it there for the remainder of the scan (a further 1 min 35 s). After each scan they returned to the neutral position. One scan was acquired with shim and motion correction applied (ShMoCo), one with only motion correction applied (MoCo), and one with no correction applied (NoCo). These scans were executed in random order.

The spectra were processed in LCModel (Provencher, 2001) using standard approaches with a LASER sequence-specific basis set. Two SNR measures were calculated. The first (SNR_{LCM}) is the SNR reported by LCModel. SNR_{LCM} is defined as the spectral maximum divided by two times the RMS of the residual. An additional measure of SNR (SNR_{NAA}) was calculated as the maximum of the N-Acetylaspartate (NAA) peak (between 1.9 and 2.2 ppm) divided by the standard deviation of the signal between 0.5 and 0.2 ppm. When computing SNR_{NAA} we used the raw spectra after LCModel phase and baseline correction.

Two further volunteers were scanned, volunteer 7 and 8, on the Siemens 3T Allegra scanner in Cape Town. Volunteer 7 was scanned to confirm that the vNav has no observable effect on the spectral SNR. This was previously shown in single voxel spectroscopy (Hess et al., 2011). The volunteer was scanned three times while they remained stationary. The first scan was acquired using the standard LASER sequence, while the second and the third were acquired with the navigated LASER sequence. The second was acquired with shim and motion correction applied (ShMoCo) and the third with no correction applied (NoCo). In this manner the effect on spectral quality of the vNav and applying the correction can be determined separately.

Volunteer 8 was scanned in order to investigate the performance of the navigated sequence with pseudo random movements. The subject was scanned three times, first with the standard LASER sequence while the subject remained stationary. In the second and third scans the navigated LASER sequence was used and the subject was asked to perform a random cycle of motions that they could repeat throughout the duration of the scan. The subject moved upon an audible cue every 11 s to 12 s. The first of these two scans with motion was acquired with ShMoCo, while the second was acquired with NoCo. The resultant motion trajectories were assessed offline to ensure that the pattern of motion in these

University of Cape Town

two scans was comparable.

3.3 Results

3.3.1 Analysis of B0 change with respect to pose

The processed field maps acquired in a single volunteer are shown in fig. 3.1. This figure shows i) the pose-to-pose mean VOI-frequency and ii) a frequency map of the higher-order B0 changes after subtracting the mean VOI-frequency. Significant frequency, first- and higher-order changes are evident in the chin-up and down poses. In the chin-left and chin-right poses only small frequency changes are evident. In the two extreme chin-left positions (-12 and -19), non-zero-order effects are evident at the edge of the VOI with roughly a 5 Hz 10 Hz amplitude.

3.3.2 Validation of navigated LASER sequence

Figure 3.2 is an example of the first contrast of a single vNav acquisition and the phase unwrapped field map from both echoes.

The frequency, first-order, and second-order shim was measured by the vNav during each scan acquired with the navigated LASER sequence in the six volunteers who performed a chin-up to chin-down movement. As an example, the motion and shim logged by the vNav for the ShMoCo scan of one of the volunteers are plotted in fig. 3.3. The motion measurements have been transformed into the same coordinate system as the scanner's shim gradients (scanner XYZ coordinate system). In fig. 3.3B we plot the mean frequency within the VOI. The frequency was calculated from the sum of the mean VOI frequency and the frequency offset resulting from the applied first-order shim. Figure 3.3C shows the first-order shim estimate, scaled to Hz/cm. This scale facilitates an interpretation of the expected frequency shifts across the VOI as a result of the change. Figure 3.3D shows the second-order shim change scaled to Hz/cm^2. Figure 3.3 also demonstrates the variance in the vNav measurements. In most of the scans the Z^2 shim estimate was very noisy, varying by as much as 3 Hz / cm^2 in some volunteers. Otherwise, the variance of the motion estimates was consistent be-

University of Cape Town

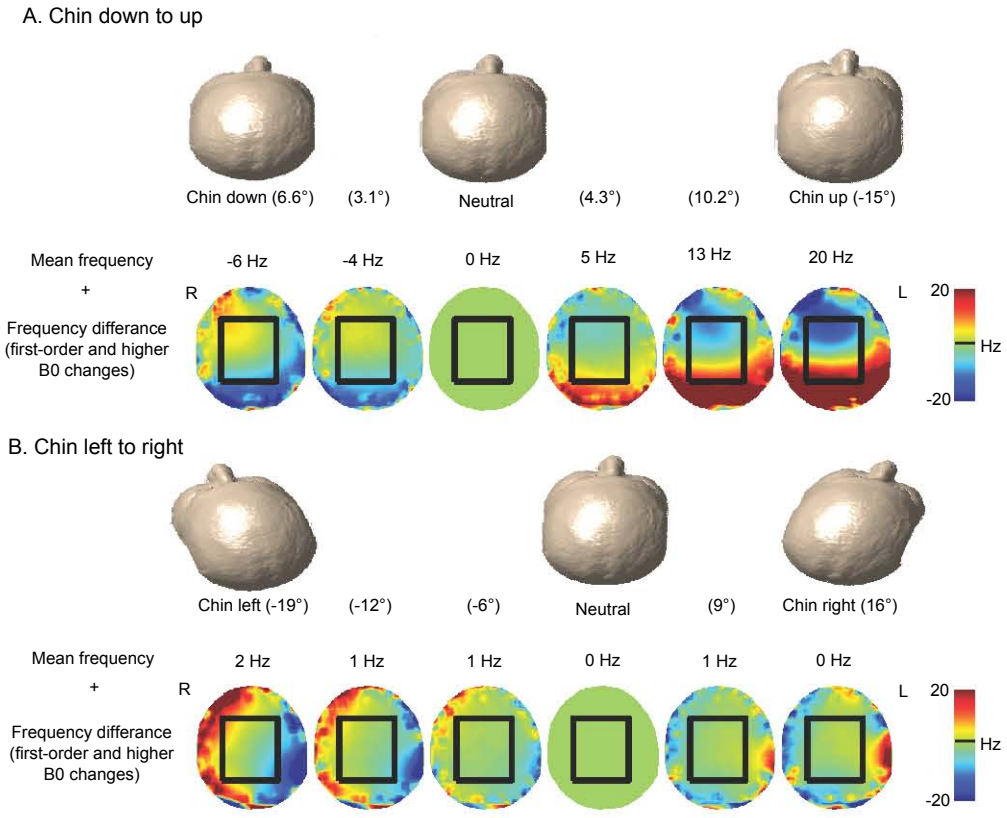

Figure 3.1: A 3D reconstruction of the volunteer's head pose, the mean frequency of the VOI in each pose, and the frequency gradient after mean normalisation that included subtraction of the neutral pose frequency and mean frequency (black box is VOI used). A. Chin-down to -up rotation and B. chin-left to -right rotation.

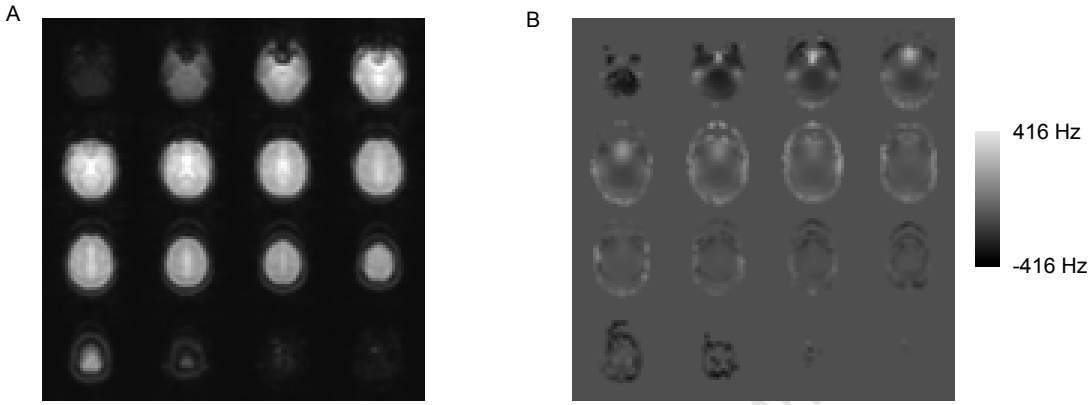

Figure 3.2: Example navigator images. A. Magnitude image for first echo, and B. Unwrapped and masked field map with the contrast range doubled (-2π to 2π) due to the phase unwrapping.

University of Cape Town

tween volunteers with worst case standard deviations during a stationary scan of 0.3 mm and 0.1°.

Figure 3.4 is a series of scatter plots demonstrating intersubject zero- to second-order shim changes, as determined by the vNav, as a function of the angle of rotation of the head about the sagittal (X) axis. For the first-order plots, the X shim was excluded as it did not demonstrate a significant shim change in any of the volunteers. For the same reason, only YZ and Z^2 are plotted for the second-order changes. Only volunteer 4 demonstrated a change in X^2 - Y^2 of 0.17 Hz/cm^2. Data from volunteers 1 and 2 were not included in the second-order scatter plots as second-order shim logs were not recorded during these scans.

Figure 3.5 shows four baseline corrected spectral grids of the central 9 x 9 rows and columns within the VOI for volunteer 2. Shown are spectra acquired without motion using ShMoCo, with motion and NoCo, with motion and MoCo, and with motion and ShMoCo. The spectra plotted are the raw spectra after LCModel phase and baseline correction. The spectra with movement and no shim correction had significant baseline distortions.

In a review by Kreis (2004) it was recommended that suitable exclusion criteria should include a linewidth threshold between 0.07 and 0.1 ppm and an SNR

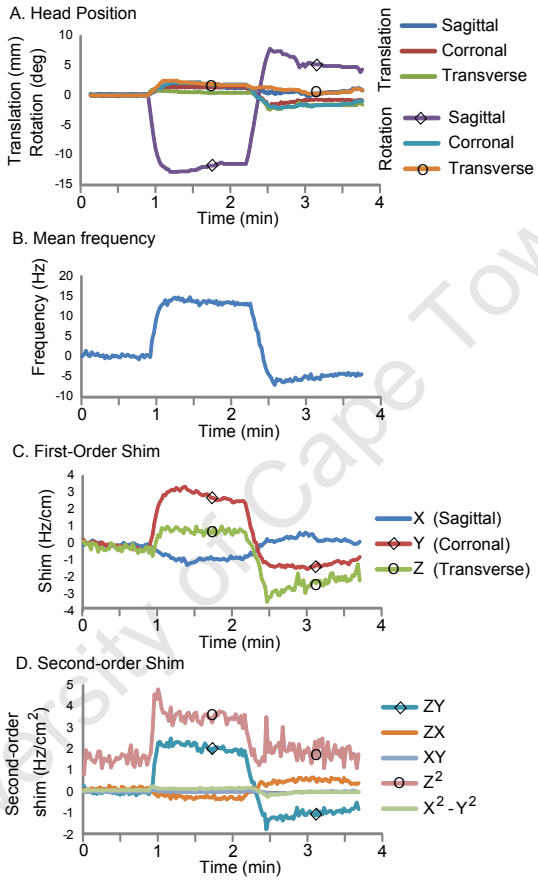

University of Cape Town

Figure 3.3: Motion and shim changes measured by the vNav plotted as a function of time for the ShMoCo scan of volunteer 3. A. Translations and rotations about the scanner's isocenter in scanner XYZ coordinates. B. Changes in mean VOI frequency, measured by the navigator and corrected for real-time first-order gradient changes. C. First-order shim changes within VOI. D. Second-order shim changes measured by vNav.

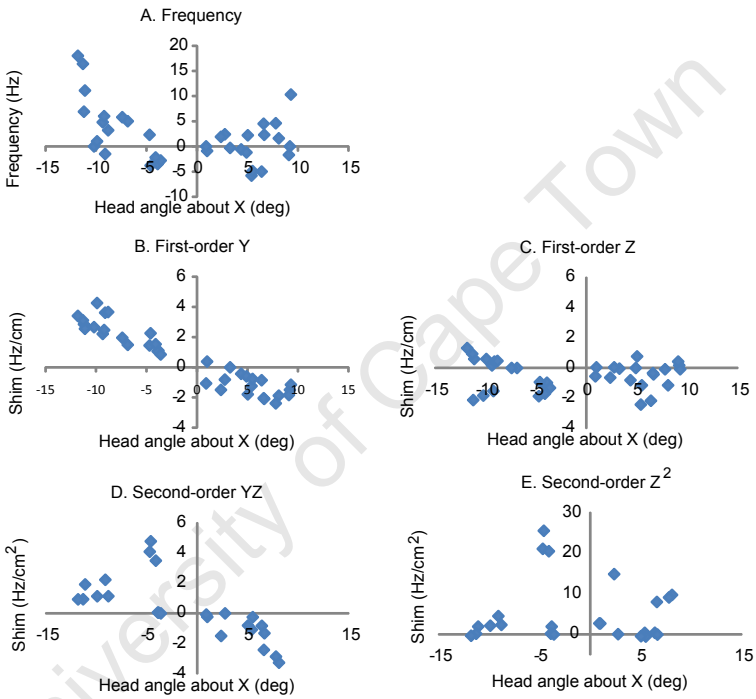

University of Cape Town

Figure 3.4: Shim changes in all volunteers as a function of angle of rotation of the head about the X (Sagittal) axis as measured by the vNav. A. Frequency, B. Y (Coronal) shim, C. Z (Transverse) shim, D. YZ second-order shim, and E. Z^2 second-order shim.

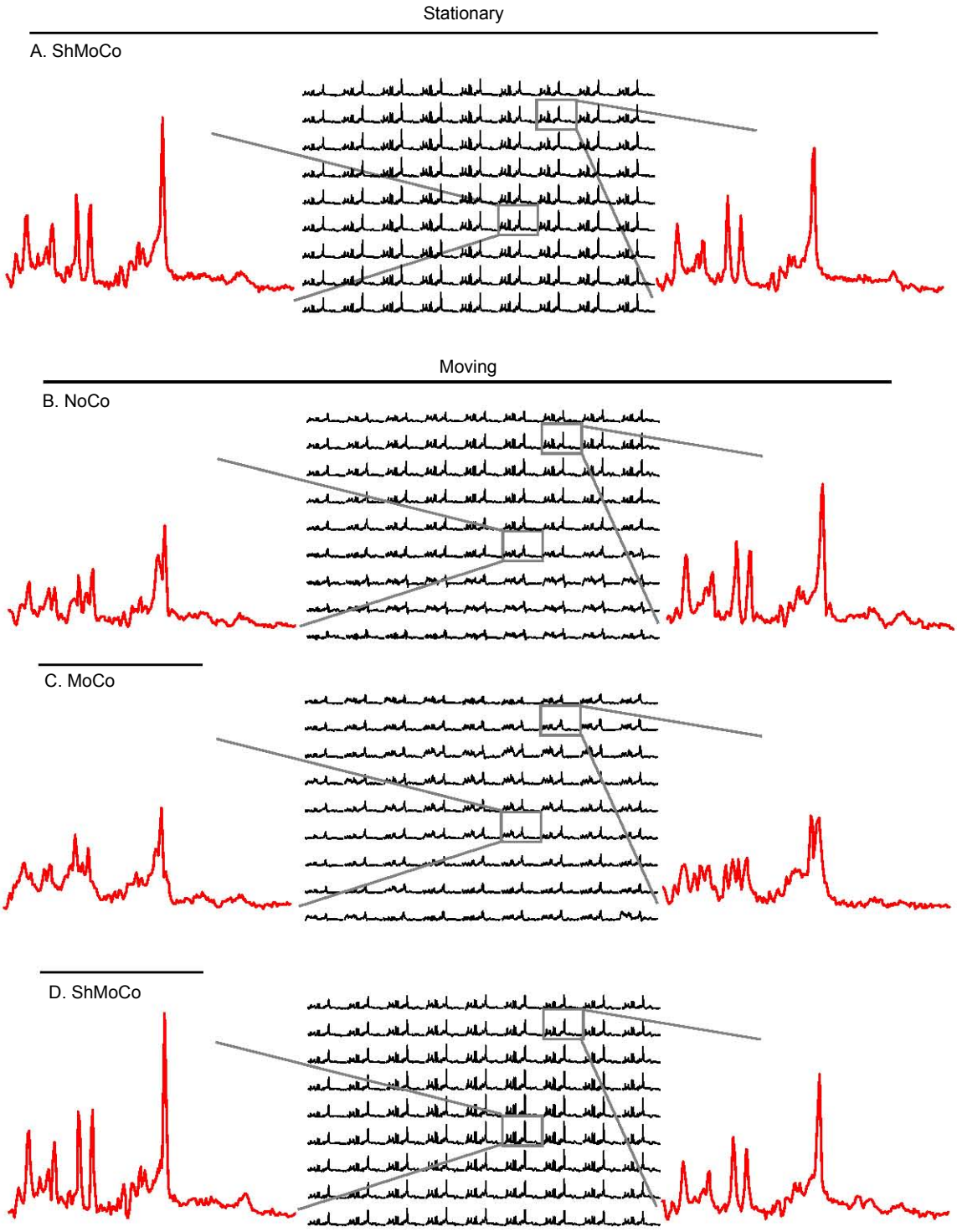

Figure 3.5: Spectra for a single volunteer, from the central 9 x 9 rows and columns. A. Stationary Real-time Shim and Motion Corrected (ShMoCo). B. Moving No Correction (NoCo). C. Moving with motion correction (MoCo) but no shim correction. D. Moving with no ShMoCo. The spectra shown are the raw spectra after baseline and phase correction in LCModel.

threshold below the expected range. Figure 3.6 presents a quality threshold map of the MRSI VOI for each of the scans. Spectra were determined to be within quality bounds if linewidth < 0.08 ppm (9.9 Hz) and $\text{SNR}_{LCM} > 7$. Both measures were calculated by LCModel. Alongside the scans with motion is a bar graph showing the magnitude of head rotation (mean of the absolute rotation in up and down positions) for each scan.

A significant increase in the mean linewidth was observed when there was movement and no ShMoCo. The worst case was the motion corrected (MoCo) scan of volunteer 2 with a 9.8 Hz increase (250%) in the mean spectral linewidth, compared to the worst case increase when using ShMoCo of 1.2 Hz (29%) in volunteer 3. The worst mean SNR_{LCM} loss was in the NoCo scan of volunteer 3, whereas the worst case mean SNR_{LCM} loss in the ShMoCo scans was only 13% in volunteer 5.

Figure 3.7 shows spectral concentration maps for the ratio of NAA to total creatine (tCr) for all the scans. The bar alongside each map demonstrates the magnitude of the movement. Note that LCModel failed to quantify some of the spectra in the uncorrected (NoCo) scan for volunteer 3, so that these are plotted with zero magnitude.

Agreement between ShMoCo and the baseline scan was analyzed with the statistical method of Bland and Altman (1986). Figure 3.8 shows three Bland-Altman diagrams that plot the differences vs. mean of the NAA to tCr ratio for each of the ShMoCo, MoCo, or NoCo scans relative to the baseline scan (no motion, no correction), respectively. This ratio was chosen because NAA, total NAA, and total creatine were the only metabolites that were consistently quantified to within a 20% SD when no shim correction was employed. In these plots, each of the voxels in the central 5 columns and 7 rows were compared to the corresponding voxels in the baseline scan (stationary with NoCo) for all volunteers. All three had a mean difference of 0.0. The confidence interval with NoCo was 0.45 to 0.44 (31% of mean), with MoCo it was -0.71 to 0.72 (50%), and with ShMoCo it was -0.22 to 0.21 (15%).

The second SNR_{NAA} measure was calculated for comparison to SNR_{LCM}. In the stationary NoCo scans it was 107, 101, 52, 46, 54, and 64 in volunteers 1 to 6, respectively. Figure 3.9 shows the effect of motion on the SNR_{NAA} for each

University of Cape Town

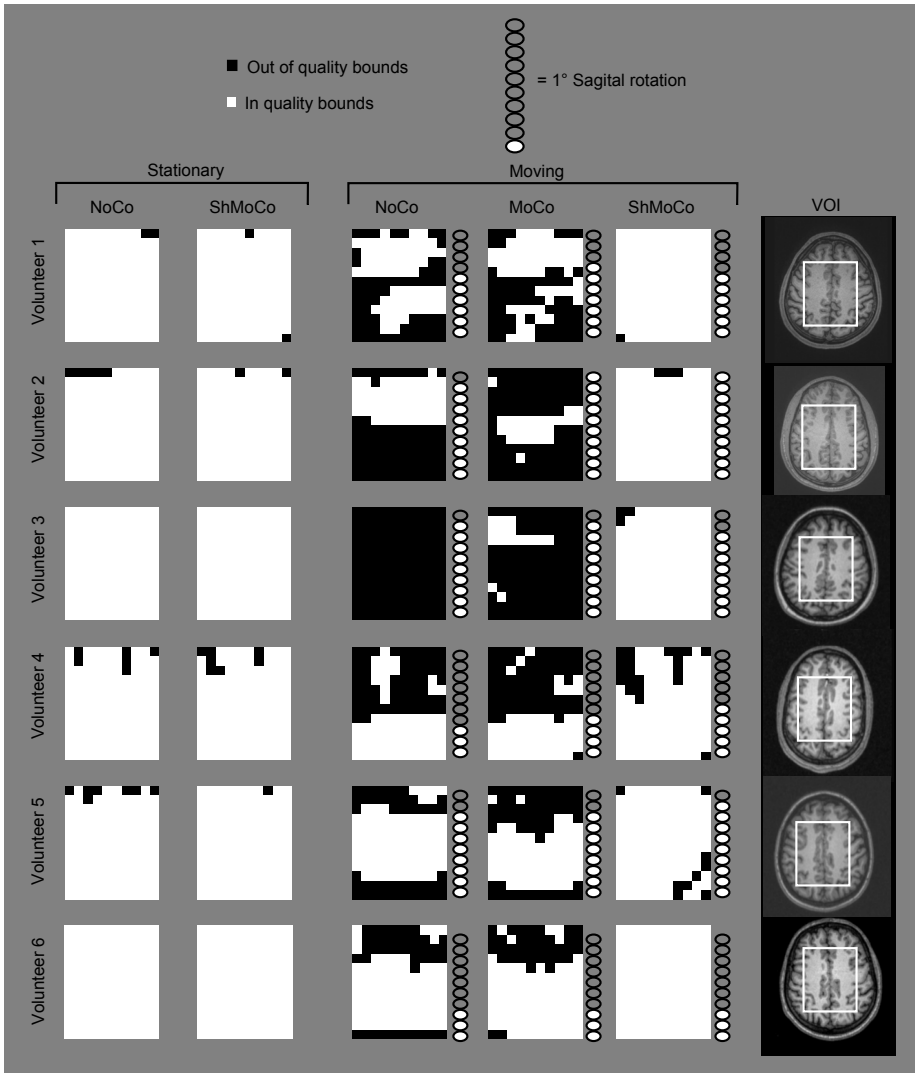

Figure 3.6: Map of voxels with acceptable spectral quality (linewidth < 0.08 ppm or 9.9 Hz and SNR > 7) for each scan for each volunteer. The scans where the subject moved have a bar graph displaying the mean absolute angle of the chin up and chin down rotation, each bar represents 1° rotation.

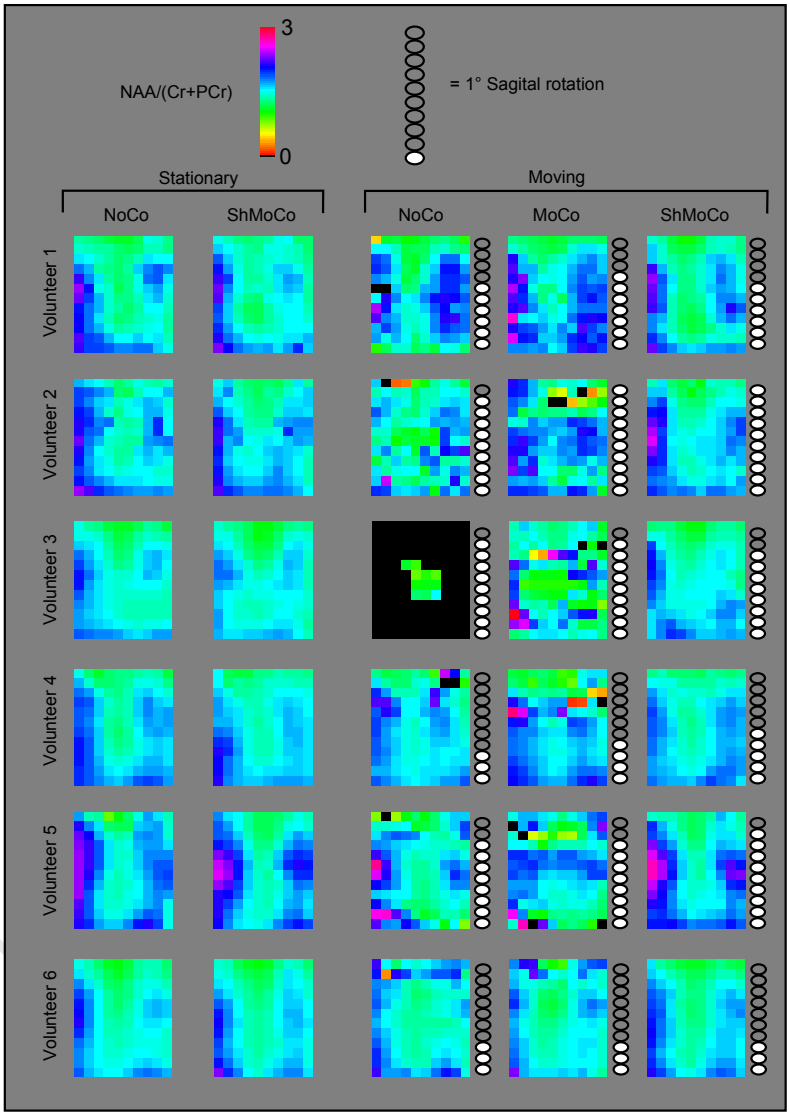

Figure 3.7: Map of relative concentration of NAA to total creatine within the VOI for all scans. The bar graph alongside each image with motion indicates the mean absolute angle through which the head was rotated.

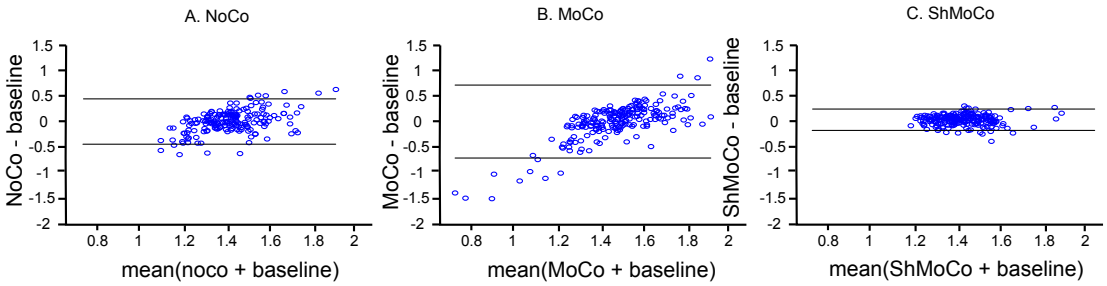

Figure 3.8: Bland-Altman plots of the difference vs. mean for the NAA to total creatine for the NoCo, MoCo, or ShMoCo scans relative to the baseline scan (no motion, no correction). A. Scans with motion and no correction (NoCo), B. Motion corrected (MoCo) scans with movement, and C. Real-time shim and motion corrected (ShMoCo) scans with movement.

University of Cape Town

of the different scans by plotting the ratio of the mean SNR_{NAA} within the VOI for the relevant scan to the mean SNR_{NAA} of the stationary NoCo scan. This simplifies comparison of the data acquired with two different scanners. The plot demonstrates that for all the scans with motion there was a loss in SNR_{NAA}. The biggest loss in SNR_{NAA} in a ShMoCo scan with motion was 11%, while the biggest loss for non shim-corrected scans with motion was 40% in the same volunteer.

When comparing the three stationary scans that were acquired in volunteer 7 in order to investigate the effect of the vNav on the SNR, the mean SNR_{NAA} across the VOI were 51, 53, and 53, respectively. The first was acquired with the standard LASER sequence, the second and third with the navigated sequence with ShMoCo and NoCo, respectively. The SNR_{LCM} was 18 for all three scans.

The two motion logs of volunteer 8 who performed pseudo random movements both demonstrated similar patterns of movement with 19 and 20 pose changes in the ShMoCo and NoCo experiments, respectively. No spectra in the ShMoCo scan had observable spectral degradation, while in the NoCo scan several spectra were degraded, particularly the left anterior region of the VOI. The motion log and one spectrum from each scan, voxel 13-13, are plotted in fig. 3.10. The mean SNR_{LCM} across the VOI were 14, 15, and 12 for the stationary, motion with ShMoCo, and motion with NoCo scans, respectively.

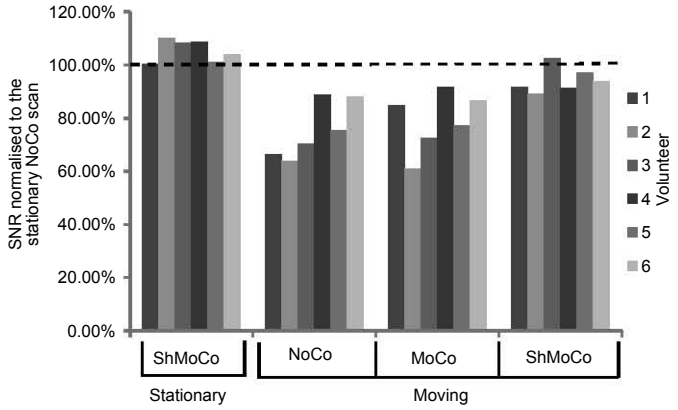

Figure 3.9: Effect of motion on the mean SNR_{NAA} within the VOI for each of the different scanning sequences. SNR_{NAA} is the ratio of the NAA maximum and the standard deviation of the signal between 0.5 and 0.2 ppm. Values plotted are the ratio of the SNR_{NAA} for the relevant scan to the SNR_{NAA} in the stationary uncorrected scan.

3.4 Discussion

3.4.1 Analysis of B0 change with respect to pose

B0 field maps from a single volunteer demonstrate the manner in which head pose affects B0 and thus the mechanism for spectral perturbation. Figure 3.1 shows the effects of lifting the chin compared to a left-to-right rotation. The chin-left to -right rotations demonstrate an almost insignificant change in B0 for rotations less than 12°. In the more extreme rotations (magnitude $\geq$ 12°) first- and higher-order effects are evident. The otherwise insignificant changes resulting from chin-left-to-right are most likely due to the VOI remaining in a similar region relative to the gradient coordinate system. If the VOI were sagittal or coronal, this probably will reorient accordingly. When rotating the chin up and down, significant frequency changes are evident in each pose. Furthermore, after removing the mean frequency the remaining zero- and higher-order changes demonstrate substantial shifts of up to 20 Hz within the VOI for 10° to 15° rotations.

From the vNav output in our six volunteers who performed a chin-up to -

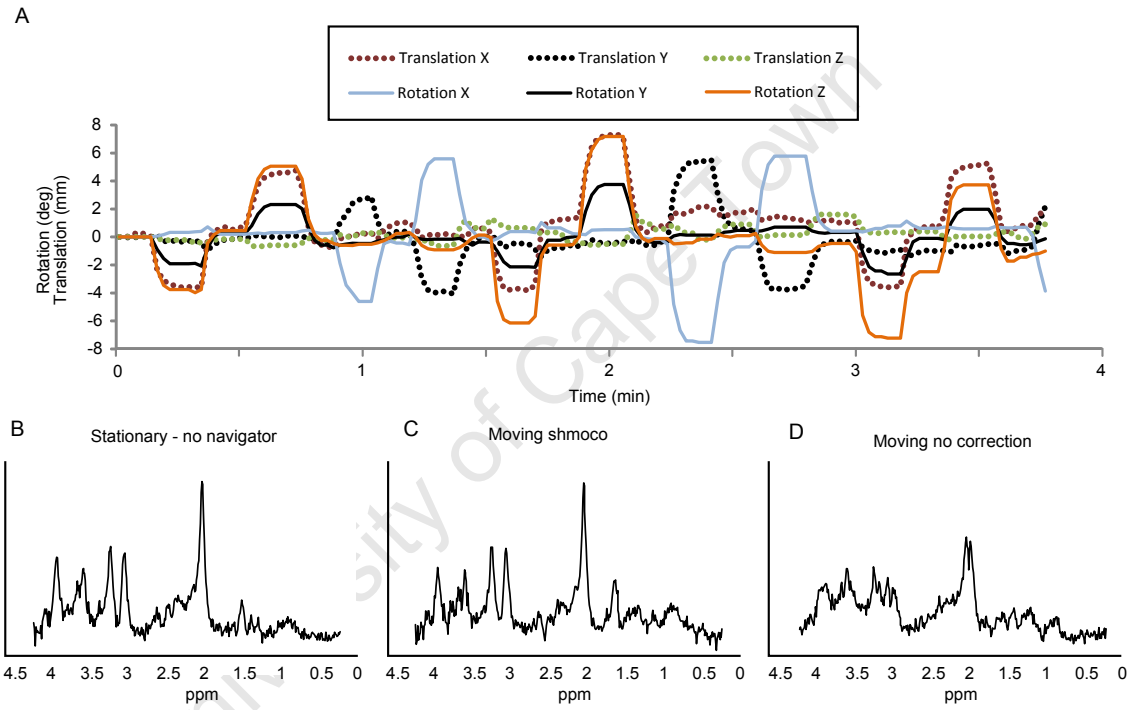

Figure 3.10: A. Motion log for scan with pseudo random movements. B. Spectrum for stationary scan with no navigator, C. spectrum for scan with movement, shim and motion correction (ShMoCo), and D. spectrum from scan without any correction applied (NoCo).

University of Cape Town

down head rotation, significant mean VOI frequency changes are demonstrated in fig. 3.4A for rotations with a magnitude greater than 5°. The most significant first-order shim change was in the Y (coronal) shim resulting from rotations with a magnitude greater than 3°. Figure 3.4B shows how this Y shim varies almost linearly with angle in the chosen VOI. Small shifts in the Z shim were not consistent between volunteers, however this could, however, be related to differences in their particular motion trajectories.

The second-order shim estimates shown in fig. 3.4D and E show changes in YZ of up to 5 Hz/cm^2 and in Z^2 of up to 25 Hz/cm^2. To understand the significance of these second-order shims their origin must be pictured at the centre of the MRSI VOI. This can be done as any offset from this origin simply results in the creation of auxiliary zero- and first-order shim terms that have been calculated and analysed independently. In our axial VOI, shim terms incorporating X and/or Y will have the largest range and result in the most significant effect, while a Z dependence will represent a symmetric frequency spread through the slice. Such a frequency spread will tend to produce spectral broadening as a result of negative frequencies below the centre of the slice and positive above. For this reason the YZ shim change will generate a more significant effect than Z^2. For example, at 45 mm away from the centre of an axial slice, a 2 Hz/cm^2 in YZ shim will correspond to a frequency spread through the slice of -6.75 Hz to 6.75 Hz, and across the VOI of -6.75 Hz to 6.75 Hz. As Z and Y are independent, the frequency spread through the slice will be linear and proportional line broadening will result. The Z^2 shim demonstrated average changes of 9 Hz/cm^2, however, considering that it only manifests in the slice direction, it results in a parabolic frequency spread across the slice ranging from -5.1 Hz to 5.1 Hz. A parabolic frequency distribution will not be linearly proportional to the resultant line broadening. A single volunteer demonstrated a change in X^2 - Y^2 of 0.17 Hz/cm^2. Despite its small magnitude, the VOI is large in X and Y and this change will generate a frequency offset at the corner of the VOI of 3 Hz.

Using both the vNav shim estimate logs and the field map model we have demonstrated that both first-order shim and frequency changes in relation to motion are of equal importance. Frequency changes will cause global split peaks. First-order changes will result in position dependent split peaks and line broad-

University of Cape Town

ening. Second-order changes will generally induce line broadening, but X^2 - Y^2 and XY shim changes will also cause split peaks. Therefore, frequency correction alone is not sufficient to maintain spectral quality in the presence of pose changes.

3.4.2 Validation of navigated LASER sequence

The improvement of spectra when using this vNav system in the presence of motion is evident in the spectral plots of fig. 3.5. Significant spectral and baseline distortions are present in the non shim-corrected scans with motion - these distortions are markedly reduced when using the vNav. The quality threshold maps of fig. 3.6 demonstrate that these distortions are consistent across all the volunteers and again show that unlike the non shim-corrected scans, the ShMoCo scans maintained all spectra within the quality bounds, except for a couple of voxels in the frontal lobe of volunteer 4, accounting for 17% of the VOI. The Bland-Altman plots of fig. 3.8 show that in the presence of motion the relative concentration of NAA to tCr remains within a 16% confidence interval.

The lower spectral quality and increased variance in concentration shown in the MoCo scans compared to the NoCo scans likely results from the VOI in the MoCo scans moving relative to the gradient system. Conversely, in the NoCo scans the VOI remains in the same position relative to the gradients but not always in the same anatomical region. Figure 3.5 demonstrates this behaviour, where the blown up spectra on the right are of good quality in the NoCo scan, but significant split peaks are present in the MoCo scan. It should be noted that the variance in concentration for NoCo scans with movement result from both B0 and anatomical changes.

When using ShMoCo in the presence of motion there was a worst case loss of 13% in mean SNR and 29% increase in mean spectral linewidth, which is small in comparison to the values when not using shim correction. It is believed that this loss in spectral quality is the result of second-order and higher B0 inhomogeneities. These changes can be estimated but not corrected on the hardware used.

The stability of the vNav shim estimates is evident in the quality of spectra obtained (fig. 3.6). Typical frequency and first-order B0 changes are shown in fig. 3.3B and C with the greatest fluctuations, during stationary periods, occurring

University of Cape Town

in the Z shim at insignificant amplitudes. The reduced stability of shim estimates in Z is due to the small number of vNav data points within the VOI in the slice select direction. The effect of the spectroscopy-specific shim used to acquire the vNav is mitigated by applying real-time first-order shim updates specific to the vNav, potentially also mitigating the effect of susceptibility distortions due to motion.

Figure 3.3A demonstrates that the vNav in conjunction with PACE is capable of producing precise and reproducible motion estimates. This article has not addressed the benefits of motion correction alone, but rather the combined benefit of motion correction with B0 correction. The lower quality of motion corrected scans compared to uncorrected scans seen in both fig. 3.6 and fig. 3.8 does not demonstrate that motion correction reduces the data quality in general, as in this experiment the type of motion used was chosen to emphasise changes in the B0 field.

This work has demonstrated the application of the vNav in an axial slice superior to the ventricles, which is a relatively easy to shim region. When scanning in regions with greater B0 inhomogeneity, such as regions lower down in the brain, it is likely that movement will have a greater effect on B0 perturbation, particularly for left-to-right rotations. In our experience the SNR of the navigator is sufficient to provide stable shim estimates in such regions. However, the navigator FOV may need to be increased in order to cover the intended region.

Although the ability of the vNav to measure second-order changes in B0 homogeneity has been demonstrated, our current hardware does not allow these to be adjusted in real time. The only second-order term the navigator was not able to reliably estimate was Z^2 due to there being only two vNav voxels within the thickness of the VOI (along the Z axis). To reliably fit a second-order term, three data points are needed. This problem may be overcome by increasing the thickness of the chosen volume over which the shim adjustment is performed.

Least squares regression was used to estimate shims - we have not examined how appropriate this is. For MRSI, this approach may result in an inhomogeneous region being neglected in favour of an improvement in another region. A system that minimises the maximum off resonance (Lee et al., 2009) regions may prove beneficial when the region of interest is in an area with high B0 inhomogeneity. A

University of Cape Town

technique such as this should be considered to produce uniform spectral quality throughout the VOI.

The proposed sequence does not address subject motion that may occur between the anatomical localiser and the start of the motion tracking procedure, since the tracking reference is created at the beginning of the MRSI scan. This introduces uncertainty in the VOI location and potentially lipid contamination may result. A solution to this could involve online registration of the tracking vNav volume to a structural image. This would provide confidence in the VOI placement and remove the problems of lipid contamination. Alternatively, a technique such as auto-align (Van der Kouwe et al., 2003) can ensure a patient specific reference frame before the start of the MRSI acquisition.

In this work, six volunteers deliberately performed mean rotations ranging from 3° to 10° for 2/3 of the scan and one volunteer performed pseudo random head movements. The range of realistic head movements that may be expected during routine MRSI is not documented. Further understanding of the manner in which various population groups move in the scanner would be beneficial to interpreting the practical use of this technique.

The vNav technique corrects for repetition to repetition changes. It does not, however, address intra repetition effects of motion. This may result in dephasing and residual B0 changes. One approach to mitigate such artifacts is to reacquire FIDs that are likely to contain such artifacts. A method has previously been presented (Hess et al., 2010) where FID's are reacquired when a pose change is detected between two navigators. In our experience, these dephasing and residual effects are difficult to demonstrate in the LASER sequence and require fast and repeated subject movements. Figure 3.10 demonstrates no observable loss in spectral quality with the subject performing 20 movements during the scan (every 11 to 12 sec). These movements were not timed to avoid the acquisition window. However, if they were performed at a faster rate it is possible that the temporal resolution of the vNav system will be too low, resulting in spectral artifacts. This is a limitation of this method compared to optical tracking devices that typically have a higher temporal resolution and could potentially detect the rate of motion during the spectroscopy part of the acquisition cycle.

The vNav has no observable effect on the spectral SNR or acquisition time.

University of Cape Town

The 714 ms duration of the vNav enabled a TR of 1.5 s to be retained. In the 7th volunteer there was no degrading in the spectral SNR when the vNav was inserted into the sequence compared to the standard LASER sequence. This corroborates the same finding in a single voxel spectroscopy PRESS sequence (Hess et al., 2011).

3.5 Conclusion

Spectral quality in an axial VOI is significantly affected by B0 inhomogeneities resulting from chin up-to-down head rotations. Significant zero- and first-order inhomogeneities were demonstrated with pose changes, particularly in the Y (coronal) direction. The addition of a vNav to the LASER MRSI sequence required no increase in TR or loss in SNR and provided real-time zero- to first-order B0 and motion correction. We have demonstrated that this vNav mitigates motion and B0-related spectral distortions.

University of Cape Town

3.6 Acknowledgements

Several people have provided valuable assistance in this project, including Thomas Benner, Michael Hamm and Charles Harris. We thank Dr. Marjanska Malgorzata from the Center for Magnetic Resonance Research, University of Minnesota, for help with building the LCModel basis set for the LASER sequence. Resources necessary in the project were provided by the University of Cape Town, the Athinoula A. Martinos Center for Biomedical Imaging, and the Cape Universities Brain Imaging Centre. This study was supported by the South African Research Chairs Initiative of the Department of Science and Technology and National Research Foundation of South Africa, the University of Cape Town, the Medical Research Council of South Africa, NIH grants R21AA017410, R33DA026104, R21EB008547, R01NS055754, P41RR014075, and The Ellison Medical Foundation.

Chapter 4

The application of an EPI navigated PRESS sequence in studies with 5- and 10-year old children[1]

Aaron T. Hess[2], Sandra W. Jacobson[3], Joseph L. Jacobson[3], Christopher D. Molteno[2], Barbara Laughton[4], André J.W. van der Kouwe[5], and Ernesta M. Meintjes[2]

University of Cape Town

Abstract

We investigate the use of an EPI volume navigated (vNav) single voxel spectroscopy (SVS) PRESS sequence in two groups of children. This sequence applies real-time head pose (location and orientation), frequency, and first-order B0 shim adjustments. A water independent pre-processing algorithm is presented to remove residual frequency and phase shifts that result from within TR movements. The benefits of this sequence are demonstrated in two paediatric studies where sedation was not used. One study allowed a comparison of the results obained a year earlier with the standard PRESS sequence to the vNav PRESS sequence,

[1]Chapter written as an article intended for review and publication.
[2]University of Cape Town.
[3]Wayne State University School of Medicine.
[4]Stellenbosch University and Tygerberg Hospital.
[5]Martinos Center, MGH, Harvard Medical School.

used in combination with the pre-processing software. The study consisted of a cohort of 56 children between 9 and 10 years of age. SVS data were acquired in the deep cerebellar nuclei, initially with the standard PRESS sequence. 52 of the children were re-scanned 1 year later with the vNav PRESS sequence. Good quality data were acquired in 73% of the children using the vNav PRESS sequence compared to only 50% when using the standard PRESS sequence. Additionally, tighter linewidths and smaller variances in the measured concentrations were observed. In the second study, we demonstrate the use of the vNav PRESS sequence in 46 scans acquired in multiple volumes of interest in 17 children who were 5 years of age. There were 7 scans that demonstrated intra scan voxel displacements greater than 3 mm. Despite these movements, all the scans in the 5-year old children had linewidths less than or equal to 5 Hz.

University of Cape Town

4.1 Introduction

Single voxel spectroscopy (SVS) provides useful information of metabolite concentrations. However, this requires the spectra to be acquired within the intended anatomy at a constant frequency and optimal main magnetic field (B0). Subjects must remain stationary during the scanning session as several minutes of signal averaging are required. SVS may not be feasible for restless or uncomfortable subjects and sedation would otherwise be required. In this article we demonstrate the benefits and limitations of using an echo planar imaging (EPI) volume navigated (vNav) (Hess et al., 2011) Point Resolved Spectroscopy (PRESS) sequence in two independent paediatric studies conducted at 5 years of age and 9 to 10 years of age. The vNav is capable of measuring within each TR head pose (location and orientation), zero-order B0 offset (implemented as RF transmit/receive frequency), and spatially higher-order B0 offsets (implemented with shim gradients of which the linear terms are adjustable in real time).

Head pose tracking is important in SVS as there is no way of confirming whether all measurements were acquired from the same volume. This is unlike imaging where blurring of the image occurs in the presence of motion. In SVS, which uses large voxels such as 20 x 20 x 20 mm^3, voxel shifts on the order of 2 to 3 mm may seem inconsequential. However, if the movement is enough to alter

the grey / white matter ratio, mechanisms for partial volume correction will be rendered invalid. By using the vNav to perform head pose correction, one ensures that the measurements are consistently acquired from the same anatomical region.

To date, two head pose tracking systems have been proposed for SVS. The first is based on the prospective motion correction (PROMO) technique (Keating et al., 2010), which performs rigid body head tracking using a set of three orthogonal spiral images. The second employs an optical tracking device to monitor the head pose and prospectively update the sequence (Zaitsev et al., 2010a). This technique additionally performs retrospective frequency correction using an interleaved navigator (Thiel et al., 2002).

While head pose tracking is important, a change in pose is likely to also perturb the B0 field, resulting in frequency shifts and line broadening due to first- or higher-order B0 inhomogeneities. Frequency shifts impact both the acquisition and averaging processes. The acquisition is affected by a relative shift in the water suppression band and produces either suboptimal or non-existent water suppression together with potential interference with the metabolites of interest. A number of methods have been proposed to prospectively track the B0 frequency (Ernst and Li, 2009; Henry et al., 1999) using either a navigator or the residual water signal. By contrast to these methods, the vNav PRESS sequence performs both prospective frequency and first-order B0 shim adjustment, in addition to real-time head pose correction.

While prospective frequency adjustment corrects the system frequency for TR-to-TR changes, pose changes within TR may still result in both residual frequency and phase variations. These phase variations result from the velocity encoding effect of the PRESS (or STEAM) gradients. Detecting the frequency and phase shift of each measurement enables constructive averaging. Methods using the residual water signal within the spectra (Ernst and Li, 2009; Helms and Piringer, 2001; Star-Lack et al., 2000) or a high signal metabolite peak to detect the frequency and phase for each measurement (Gabr et al., 2006; Waddell et al., 2007) have been proposed. In cases where complete water suppression is employed, the frequency and phase of the residual water may be misleading due to the relative shift in the suppression band that causes asymmetric water saturation.

University of Cape Town

A comparison of the results obtained with a standard PRESS and the vNav PRESS sequence is presented. In this comparison, the spectra were obtained in a cerebellar volume of interest (VOI). A cohort of 56 children were initially scanned at 9 years of age using the standard sequence. One year later, 52 of these children again received SVS using the vNav PRESS sequence. Spectral quality when using the vNav sequence is additionally demonstrated in 46 scans acquired in three different VOIs in 17 children at 5 years of age. A pre-processing technique, that is independent of the residual water and uses the spectral range from -3.5 ppm to -1 ppm for both frequency and phase correction is presented. Further, a method to determine inter scan subject movement by registering the first navigator volume in the SVS scan to a reference, acquired immediately prior to the structural scan, is presented.

University of Cape Town

4.2 Methods and applications

4.2.1 Study participants

Two groups of children received SVS in four different VOIs. The first sample consisted of 56 children (27 males/29 females) born in the years 1999-2001 whose mothers were recruited during pregnancy to participate in a longitudinal study of fetal alcohol spectrum disorder (FASD) (Jacobson et al., 2008). The children were examined by two expert dysmorphologists in a diagnostic clinic held in 2005: Eight of the children were diagnosed with fetal alcohol syndrome (FAS), the most severe form of FASD; 17 with partial FAS (pFAS); 14 were nonsyndromal heavily exposed (HE) children; and 17 were healthy controls. SVS data were acquired in the cerebellar deep nuclei (fig. 4.1) in these children in 2009 using the standard PRESS sequence. One year later, the SVS scan was repeated in 52 subjects (7 FAS, 17 pFAS, 14 HE, 14 controls) using the vNav PRESS sequence.

The second group were 5-year old children followed from before 12 weeks of age in two interlinked paediatric HIV studies (Madhi et al., 2010; Violari et al., 2008). SVS data were acquired in 17 of these children (10 males/7 females) in the medial frontal grey matter (mfgm), peritrigonal white matter (ptwm), and the basal ganglia (bg) (fig. 4.1). These children consisted of 6 healthy controls,

Table 4.1: Volumes of Interest scanned and age of children at scan.

Study	Mean Age (years)	Year	Sequence	VOI
1 (scan 1)	9.43 (SD=0.41)	2009	PRESS	Cerebellar deep nuclei
1 (scan 2)	10.39 (SD=0.42)	2010	PRESS vNav	Cerebellar deep nuclei
2	5.25 (SD=0.15)	2010	PRESS vNav	1. Medial Frontal GM (mfgm) 2. Peritrigonal WM (ptwm) 3. Basal ganglia (bg)

9 HIV-exposed, and 2 HIV-infected children on early interrupted or deferred continuous antiretroviral therapy. The scans are summarised in Table 4.1.

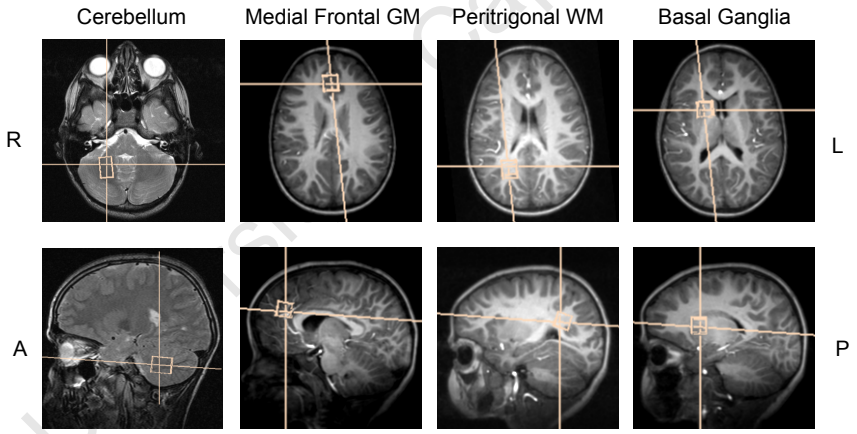

Figure 4.1: Four volumes of interest: cerebellar deep nuclei (9- and 10-year old children); medial frontal grey matter, peritrigonal white matter, and basal ganglia (5-year old children).

4.2.2 MRS protocol

Two sequences were used in the first study: a standard SVS PRESS sequence and an EPI volume navigated (vNav) PRESS sequence (Hess et al., 2011). For the second study, only the vNav PRESS sequence was employed. For all studies,

TE = 30 ms, TR = 2 sec, and bandwidth = 1000 Hz. Vector sizes of 1024 and 512 were used for the standard PRESS and vNav PRESS sequences, respectively. In the cerebellum a voxel size of 20 x 12 x 16 mm^3 with 128 measurements was used. In the other three VOIs a 15 x 15 x 15 mm^3 voxel and 64 measurements were used.

The vNav uses Prospective Acquisition CorrEction (PACE) (Thesen et al., 2000) to register each navigator to the navigator from the first TR (post preparation scans) to correct head pose. In addition, the sequence employs a dual-contrast 3D EPI sequence module to generate within each TR a B0 field map and calculate the absolute frequency and first-order B0 gradient for the intended VOI. In this manner the absolute head position, frequency in the VOI, and first-order shim in the VOI are updated by the navigator each TR. Additionally, a frequency and first-order shim appropriate to the larger field of view of the navigator itself are calculated and applied in each TR.

The vNav protocol was as follows: resolution 5 x 5 x 5 mm^3, FOV 220 x 200 x 110 mm^3, matrix 44 x 40, 22 partitions, TE_1 8 ms, and TE_2 12.8 ms, TR 21 ms, bandwidth 3906 Hz. The orientation was set by the operator and chosen to cover the intended VOIs in addition to maximally covering the brain, as shown in fig. 4.2. The duration of the vNav sequence module was 966 ms and the online processing, including pose, frequency, and shim calculations, took 170 ms per navigator.

University of Cape Town

4.2.3 Offline phase- and frequency-corrected averaging

A method was developed to perform offline frequency-corrected, phase-corrected, and quality-weighted averaging. This method is independent of the residual water in each FID and consists of three steps: i) residual water peak removal, ii) frequency detection by cross-correlation with a simulated spectrum, and iii) complex combination weighting determined by singular value decomposition (SVD). All processing is performed in the spectral domain and upsampled to a frequency resolution of 0.49 Hz. Prior to any processing, a copy of the spectrum acquired in each TR without any water editing is kept for the final averaging. Water peak removal is necessary before pre-processing as it improves the cross-correlation

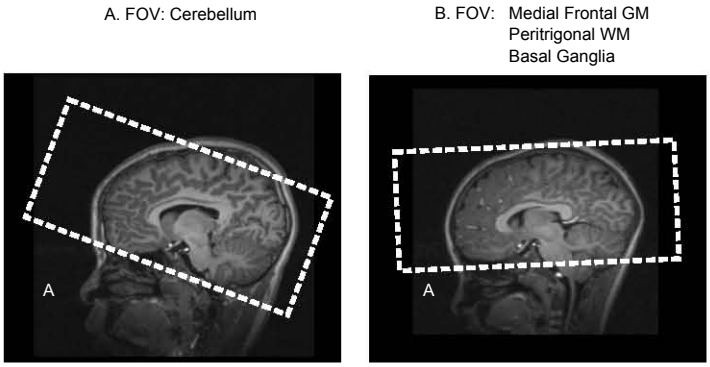

Figure 4.2: Navigator FOV placement for: A. Scans with VOI in the cerebellum, B. Scans with VOI in either the medial frontal grey matter, peritrigonal white matter or basal ganglia.

baseline and more importantly, prevents fluctuations in the water saturation from biasing the SVD. It should be noted that the residual water peak influences the phase of the FID far beyond the water peak, this is rectified through this process. Water peak removal is accomplished by subtracting a scaled water spectrum acquired in the same voxel. The scale and frequency difference between the two is determined by cross-correlating the water spectrum, scaled to unit energy, with the spectrum for each TR. The maximum of these convolutions provides the complex scaling and frequency shift to be applied to the water spectrum in order to remove it. The complex scaling minimizes the phase difference between the residual water and the water sample. If the water frequency shifts ± 25 Hz from its expected frequency, no subtraction is performed as it is assumed to be completely suppressed.

Cross-correlation is a tool used to detect the time of occurrence of an expected pattern in the presence of noise. By performing cross-correlation in the spectral domain, one can determine the frequency shift in the underlying spectrum. For this purpose, a comprehensive model spectrum was simulated using jMRUI NMR Scope (Graveron-Demilly et al., 1993) for the same sequence described above and a linewidth of 2 Hz. The model spectra included choline, creatine, phosphocreatine, phosphocholine, GABA, glutamate, glutamine, myo-inositol, N-acetylaspartate, and N-acetylaspartylglutamate. The range of -3.5

ppm to -1 ppm was cross-correlated with each spectrum to detect its frequency offset and thus re-align both the original (non water-edited) and water-edited spectra appropriately.

The third step utilises SVD to determine a set of complex weightings for each spectrum. If a spectrum does not fit the trend of the data, SVD will generate a reduced weight, and likewise, if there is a phase offset in the data, the weight will reflect the appropriate phase correction. SVD is applied in the range -3.5 ppm to -1 ppm to the water-edited and frequency-adjusted spectra. The output of the SVD operation is the set of matrices **U**, **S**, and **V**, where $\mathbf{USV}^T$ = original set of spectra. The columns of U describe each of the singular components, **S** is the significance of each component, and $\mathbf{V}^T$ describes how to recover the original spectra from **US**. In the ideal case, the first column of **U** is a scaled version of the mean. As we would like to produce a non water-edited spectrum, the following operation is performed on the original, frequency-corrected spectra ($\mathbf{O}_s$) to determine a pseudo **US** matrix: $\mathbf{U}_s\mathbf{S}_s = \mathbf{O}_s inv(\mathbf{V}^T)$, where *inv* denotes the matrix inverse. The first column of $\mathbf{U}_s\mathbf{S}_s$ is the phase independent and weighted combination of the spectra scaled by the mean of the first row of $\mathbf{V}^T$. A summary of these three steps is presented in fig. 4.3.

The pre-processing steps described above could only be applied to the scans that employed the vNav as scans acquired with the standard PRESS sequence unfortunately did not record individual measurements before averaging.

4.2.4 Navigator co-registration for VOI validation

Due to the lack of anatomical information inherent in most spectroscopy scans, it is difficult to gauge the accuracy and consistency of VOI placement. Motion correction with the vNav ensures consistent VOI placement within the scan; however, it does not ensure a consistent patient-specific coordinate system between the planning structural scan and the spectroscopy. In study 2, the spectroscopy was planned using a motion navigated multi echo MPRAGE (MEMPR, Van Der Kouwe et al., 2008). This sequence uses vNavs (Tisdall et al., 2009) to ensure a consistent coordinate system from the start of the MEMPR. It was found that a reliable registration could be obtained between a reference scan with the same

University of Cape Town

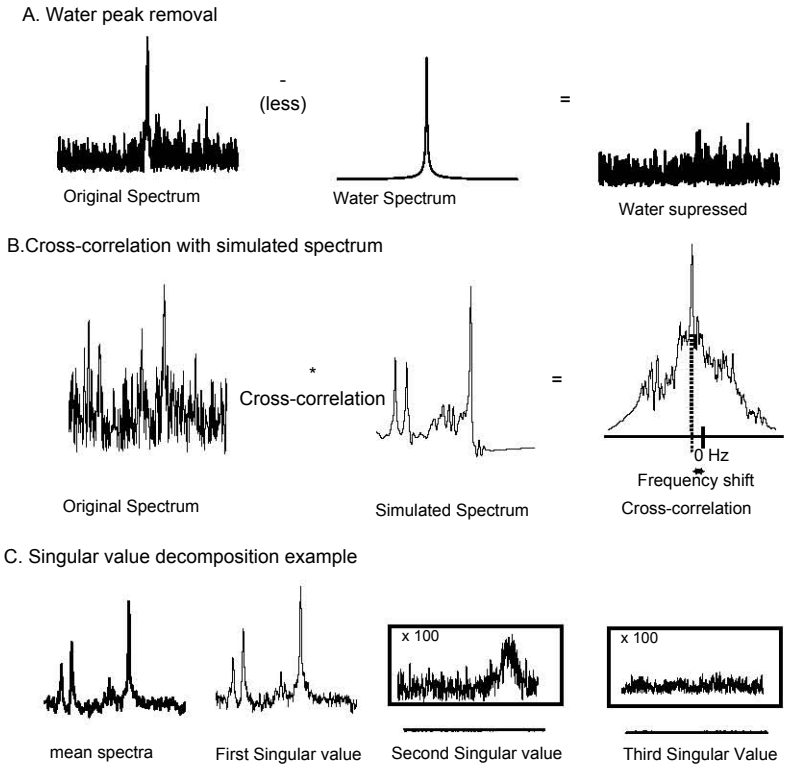

Figure 4.3: Illustration of pre-processing steps: A. Water peak removal by subtracting a scaled water spectrum, B. Cross-correlation of spectrum with simulated spectrum to detect frequency shift, C. Phase independent weighted averaging of spectra using SVD.

protocol as the vNav and the first navigator volume of the spectroscopy scan. This reference scan took 1 s to execute and was acquired immediately prior to the start of the navigated MEMPR.

A Matlab (Mathworks, Natick MA USA) tool was created to allow the user to plot the spectroscopy VOI based on this co-registration. This tool unwarped the B0 distortion inherent in both the vNav and reference EPI volumes using the field maps generated by each. The unwarping procedure used a simple linear interpolation in the phase encoding direction proportional to the voxel frequency. SPM 8 (Ashburner, 2007) was used for the co-registration. After registration, the pose and orientation of the spectroscopy voxel could be displayed on the MEMPR image.

4.2.5 Spectral analysis

The first criterion in determining the success of a technique is how much of the data is usable. We therefore set criteria to exclude data if linewidths are greater than 0.08 ppm (9.9 Hz) or signal-to-noise ratio (SNR) is less than 8. We also performed a visual check of the spectra to ensure they conformed to the expected spectral plot (i.e. no large unknown signals or other type of interference). The excluded data was not included in any further processing.

The vNav records the motion and shim corrections that were applied in a log file. These logs were used to calculate the absolute position of the SVS voxel, as set by the vNav, and thus determine the extent of subject movement during the scan. All metabolite analyses were performed in LCModel (Provencher, 2001). A water reference spectrum was used for water and eddy current correction. The LCModel output includes metabolite concentrations, their percent standard deviation (%SD), linewidth, and signal- to-noise ratio (SNR or SN as reported in LCModel).

4.3 Results

For the first scans of study 1, without vNavs, only 28 of the 56 scans provided spectra of suitable quality (50% success rate); whereas in scan 2, with the vNav,

University of Cape Town

Table 4.2: Technical failures of the vNav.

Number of scans affected	Location affected	Description
6	Cerebellum	A 2π phase offset as a result of the phase unwrapping algorithm. This resulted in a frequency shift of 208 Hz thus rendering the water suppression ineffective.
4	Cerebellum	Ghosting in first vNav EPI volume, rendering the vNav unusable. This results from large shim terms set by the scanner for the voxel.
2	Cerebellum	Water substantially over-suppressed (50% in these cases) as a result of a suboptimal pre-scan shim adjustment and resulting in inappropriate water suppression adjustment.
1	N/A	Movement greater than the limit detectable by PACE (8° or 20 mm).

University of Cape Town

38 of the 41 completed scans provided spectra of suitable quality (93%). Spectra for 11 subjects were not acquired due to various navigator-related failures, giving a 73% success rate of 52 scans. The three reasons for vNav failures in the cerebellum are listed in Table 4.2.

In study 2, all of the spectra were deemed of suitable quality with only one incomplete scan due to subject movement exceeding the limits of the vNav's PACE registration module (20 mm or 8° within a single TR), yielding a 98% success rate. This failure was classified as a technical failure and is included in Table 4.2. A further four intended scans were not acquired in this cohort due to the children requesting to leave the scanner before all three scans were completed. The statistics for studies 1 and 2 are summarised in the pie charts of fig. 4.4.

As an example, the reference vNav volume and associated field map for one of the scans in study 2 is shown in fig. 4.5. To quantify the number of scans affected by motion in the two studies we have plotted the maximum absolute vector displacement of the SVS voxel in fig. 4.6A. This displacement was calculated using the motion transform applied by the vNav and recorded in a log file. This plot shows that 7 out of the 46 scans (15%) in study 2 exhibited voxel displacements during the scan of at least 3 mm; whereas in the second scan of study 1, there

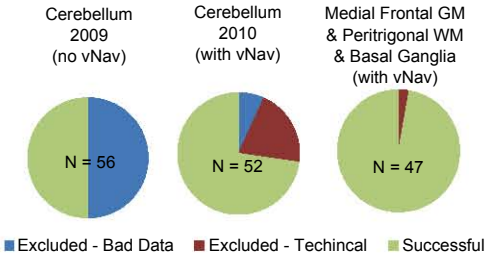

Figure 4.4: Pie charts showing the proportion of data excluded from each of the three data sets due to either bad quality spectra or technical failures of the navigator.

were no scans exhibiting more than 3 mm voxel displacement. Figure 4.6B shows the magnitude of the absolute vector displacement of the VOI for each SVS scan from its position during the reference scan performed prior to the MEMPR. This displacement was calculated by registering this reference scan to the first navigator volume in the scan of interest. Figure 4.7 demonstrates the output from the registration software for a case where there was an absolute displacement of 6 mm between the voxel position at the time of the reference scan and the start of the SVS scan. One scan, for which the time between the reference and the MEMPR was 5 minutes, resulted in a voxel displacement greater than 10 mm.

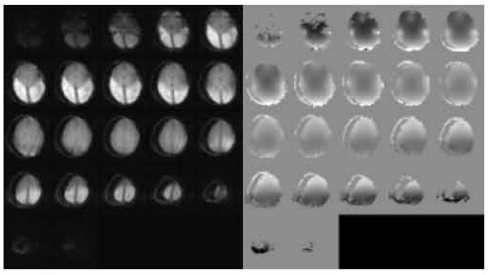

Figure 4.5: Navigator: magnitude of first echo (used for PACE motion estimation) (left) and unwrapped field map (right).

Figure 4.8 compares the mean and standard deviation of the linewidth and SNR acquired in each VOI and, for the cerebellum, using the standard and navigated PRESS sequences. There is a significant improvement in both the mean

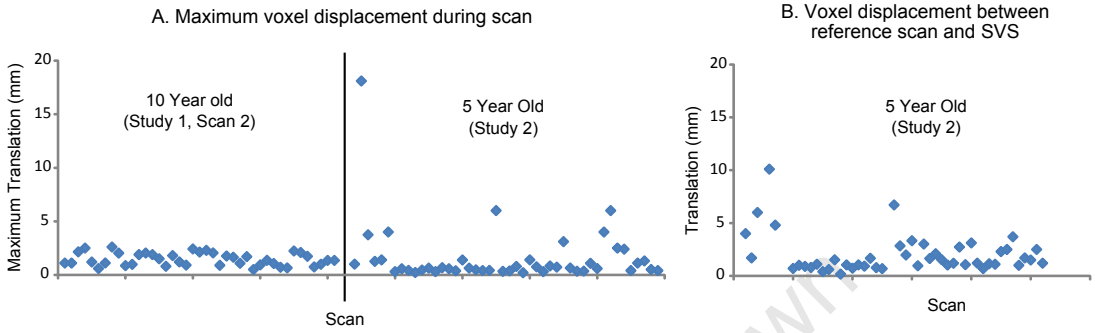

Figure 4.6: A. Scatter plot showing maximum voxel displacement from the reference position during scan. B. Scatter plot showing displacement of voxel between the vNav reference scan and the start of a specific SVS scan.

University of Cape Town

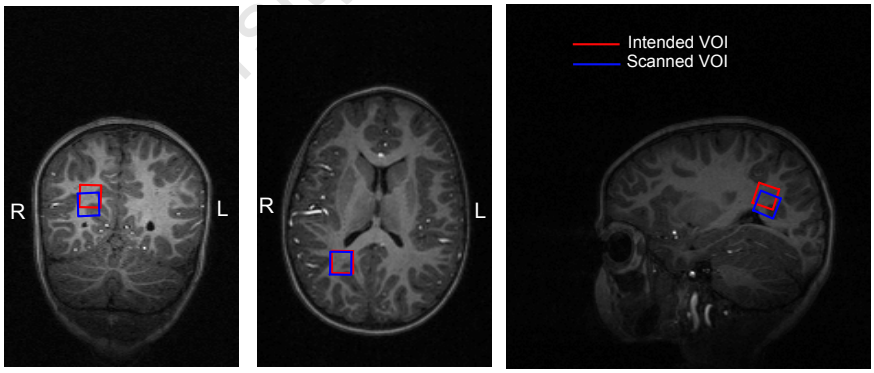

Figure 4.7: Example of location difference between an intended VOI and acquired VOI, as determined using the shift between the reference scan and the first vNav in the acquired scan. This shift represents an absolute voxel shift of 6 mm and has introduced up to 25% additional grey matter into the VOI.

linewidth ($p = 0.03$) and SNR ($p = 0.0001$) between scan 1 and scan 2 in the first study (p-value calculated as a two-tailed paired t-test). For study 2, linewidths range from 2 Hz to 5 Hz and the SNR from 8 to 14.

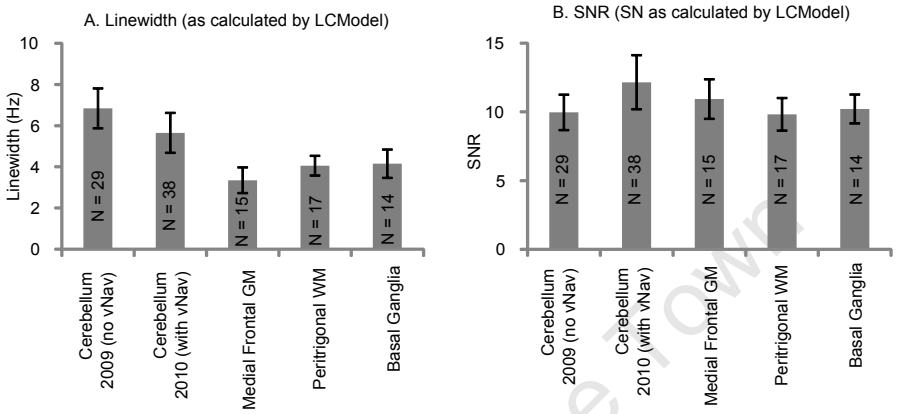

Figure 4.8: Mean linewidths and signal-to-noise ratios (SNR) of all successful scans for the different datasets and volumes of interest.

University of Cape Town

Over and above the quality measures of linewidth and SNR, we wanted to assess the consistency of the measured metabolite concentrations. To compare the variance and range of metabolite concentrations, we have plotted in fig. 4.9 the concentrations in the control children of study 1 for scans 1 and 2, respectively. Data points were excluded from this plot if % SD exceeded 100%. Shown are N-acetylaspartate (NAA), myo-inositol (Ins), creatine (Cr) , N-acetylaspartylglutamate (NAAG), and guanidoacetate (Gua).

To demonstrate the adjustments applied by the vNav, we have plotted in fig. 4.10 data for the two scans with the greatest voxel shifts during the scan. These were from 5-year old children (study 2), one in the peritrigonal white matter and the other in the medial frontal grey matter. In order to demonstrate the change in first-order shim, we subtracted the shim applied in the third TR from the plots. The two movement trajectories demonstrate different patterns. The first, in the peritrigonal white matter, demonstrates a constant restlessness, while the other in the medial frontal grey matter shows a sudden shift starting at TR 31 and returning later to the initial position. For the scan in the peritrigonal white matter, a large frequency shift of 50 Hz occurred.

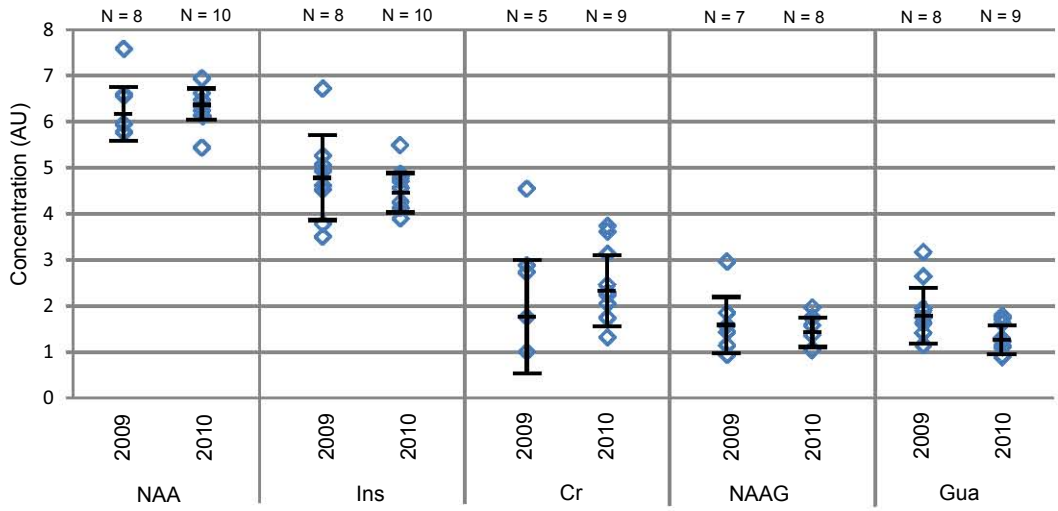

Figure 4.9: Scatter plots comparing the variance and range of metabolite concentrations in control children in the cerebellum for scan 1 (without vNav in 2009) and scan 2 (with vNav in 2010). These data were acquired in the same voxel. Shown is a weighted mean and standard deviation.

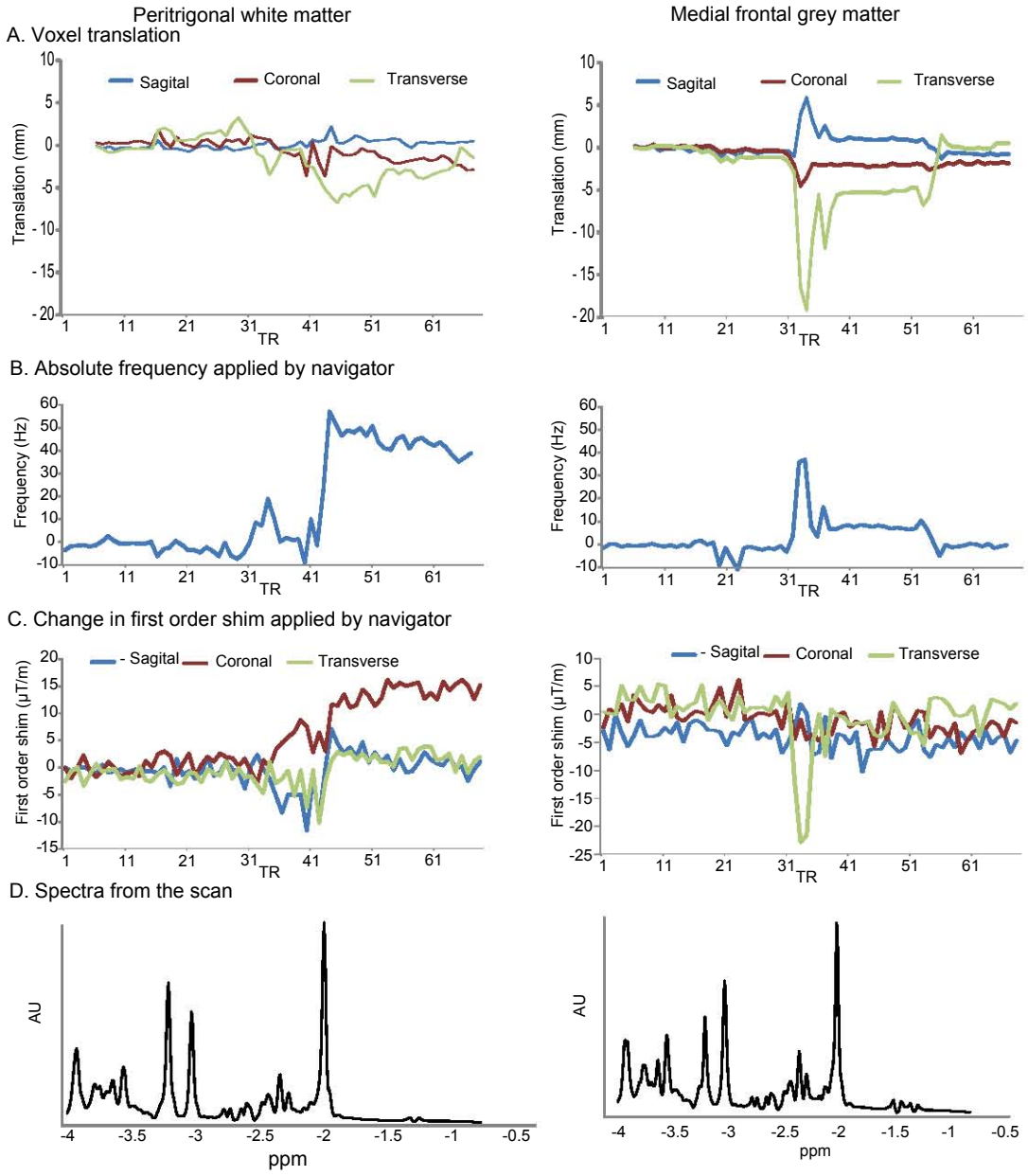

Figure 4.10: vNav output for two scans acquired in 5-year old children that moved. One of the voxels was placed in the peritrigonal white matter and the other in medial frontal grey matter. A. The shift in voxel position during the scan in sagittal, coronal, and transverse directions relative to reference TR. B. Absolute frequency shift in the voxel as measured by the navigator, accounting for first-order shim changes. C. First-order shim changes in sagittal, coronal, and transverse directions. D. Resulting spectra after post processing.

Figure 4.11 demonstrates the corrections applied during the offline pre-processing using the peritrigonal white matter scan from fig. 4.10 where the subject was particularly restless. This figure shows the frequency shift measured by the cross-correlation, the phase of the averaging-weights as calculated by SVD, and the magnitude of the weightings.

4.4 Discussion

For the vNav scans in the cerebellum we encountered three causes of failures. The first and most prevalent was a 2π phase offset that resulted in a 208 Hz shift of the spectrum rendering it unusable. This is the result of the proximity of the cerebellum to the main brain region, in conjunction with large SVS shim gradients, which give rise to a significant frequency offset for the majority of the brain relative to the cerebellum. The phase unwrapping software (Jenkinson, 2003) used in the vNav makes the reasonable assumption that the largest region between two phase wraps is the absolute phase. A simple method to avoid this problem in the future is to use the prior knowledge that at the first TR, before any shim manipulation, the SVS voxel is at the centre frequency, as adjusted by the scanner. For each acquisition after the first TR, the navigator specific shim will ensure that the offset will not occur again.

The second vNav failure was also limited to the cerebellum but is not easily overcome. It arises due to significant ghosting and distortions in the vNav volumes rendering the field map unusable to calculate a vNav-specific shim. All four scans that failed in this manner had at least two second-order shim terms set to values higher than 1000 μT/m^2, which is approaching the shim gradient limit. We believe that these large second-order shim gradients gave rise to the EPI ghosting and distortions. From experience, increasing the volume over which the scanner adjusts these second-order terms will provide more stable and less extreme values. In the future, if such high second-order values are expected, it is recommened to manually check them and set them to a lower magnitude where appropriate.

The third failure resulted from substantial water over-suppression, causing a water saturated spectrum. Over-suppression was identified because the residual water had a phase shift from the water sample spectrum of the same voxel. The

University of Cape Town

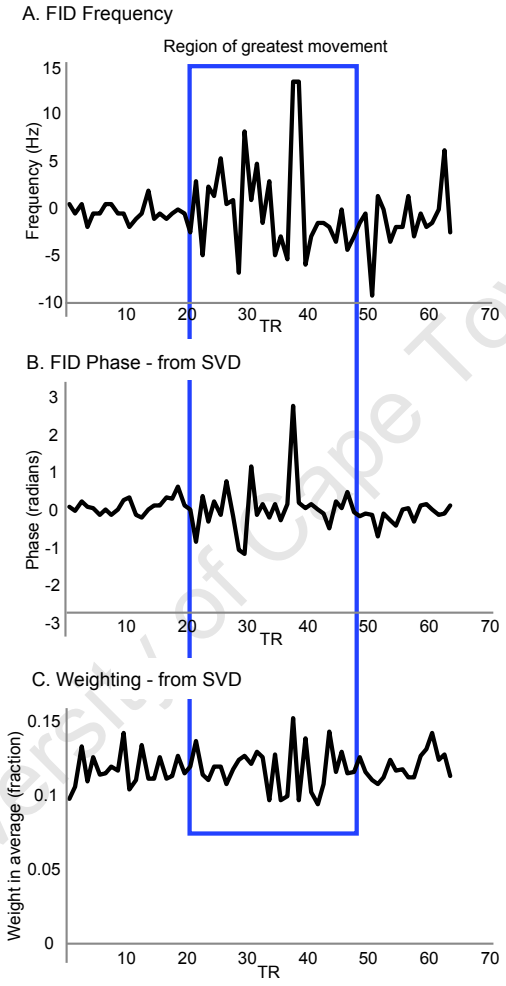

University of Cape Town

Figure 4.11: Corrections performed during offline pre-processing of one of the spectra shown in fig. 4.10 (peritrigonal white matter). A. Frequency shift of each acquisition. B. Phase shift of each acquisition as measured by SVD. C. Weighting applied to each acquisition when performing weighted averaging. The acquisitions/period of greatest subject movement is highlighted.

navigator estimated a shim magnitude that was 350 μT/m different from that set by the scanner. It is possible that the subject was in a different pose or moving during the scanner's shim and water suppression optimisation process, leading to a substantially different optimal shim to that at the start of the SVS scan.

The navigator tracks a subject's movement and maintains a subject-specific coordinate system during the scan defined by the reference vNav. As expected, more of the scans from the 5-year old children exhibited motion. In 7 of these 46 scans, voxel shifts greater than 3 mm occurred, and in a single case exceeded the TR-to-TR limit detectable by PACE. Apart from these cases, the 5-year old children remained surprisingly still, possibly having fallen asleep during the scan. None of the 10-year old children moved so as to cause a voxel shift greater than 3 mm during the scan. They did, however, exhibit small movements as shown in fig. 4.6A. These were generally within a single TR similar to what might be expected from swallowing or coughing. From analysing the movement logs, it is our opinion that motion estimates from the oblique vNav applied in the cerebellum, were of lower quality than those not angled (in the cerebrum). For future scans we recommend increasing the vNav FOV in the slice direction by increasing the number of partition encodes so as to fully cover both the brain and cerebellum.

In the study with the 5-year old children, we retrospectively calculated the shift in the subject's pose between the reference scan acquired prior to the MEMPR and the start of each SVS scan. As this reference scan was acquired within 40 s of the start of the navigated MEMPR scan (except in one subject), this registration closely approximates the subject's pose at the start of the reference volume used in the MEMPR navigation. Nine of these scans demonstrated a voxel shift of more than 3 mm between the reference scan and the start of a particular SVS acquisition. The Matlab software reconstructed both the intended VOI and the scanned VOI. For two of these 9 scans, the VOI was substantially different from that intended; an example of one such case is shown in fig. 4.7. This information is useful, as scans acquired from an incorrect anatomical region can then be excluded from further analyses of the metabolite concentrations. Ideally, if the MEMPR ran a navigator with the same protocol as that used in the SVS scans, the structural and SVS vNavs could potentially use the same refer-

University of Cape Town

ence volume for registration and thus provide a unified subject specific frame of reference. An alternative approach would be to use a tool such as auto-align (Van der Kouwe et al., 2003) to maintain a patient-specific coordinate system.

In the first scan from study 1, without the vNav, only 50 % of the spectra were usable. As no motion tracking was performed, we can only speculate as to the reason for these failures. We suspect that the main problem was poor shimming in the cerebellar VOI. In the follow up scan performed one year later with the vNav, although no significant motion correction was applied, 73% of subjects scanned yielded good data. There are at least two possible reasons for this improvement. Firstly, the increased maturity of the subjects (1 year) and their past experience in the scanner may have made them less restless. Secondly, the combination of vNav shimming with offline frequency and phase correction is likely to have generated higher quality spectra. The scans within quality bounds saw a mean linewidth reduction of 1.2 Hz and an SNR improvement of 2.5 (from 9.6 to 12.1) when using the vNav and offline pre-processing. The effect of this improvement in spectral quality is evident in the reduced range and variance of several metabolites, as shown in fig. 4.9. The quality of the spectra obtained in study 2 with 5-year old children is reflected by optimal linewidths with a range of 2 to 5 Hz, demonstrating the accuracy of the vNav shim.

The benefits of real-time first-order shim adjustment are apparent in fig. 4.10, where a 15 μT/m shim change was observed two thirds of the way through the scan performed in the peritrigonal white matter. This shim change would likely have increased the linewidth for those measurements performed after the change by up to 10 Hz. Other scans (such as that shown in the medial frontal grey matter in fig. 4.10) saw significant shim changes, but often only lasted for a couple of TRs.

The offline correction software presented here has been found to be simple and robust, requiring no user monitoring. The advantage of cross-correlating a spectral range with a simulated spectrum is that it combines the contributions from several metabolites to find the frequency, thus making it robust to noise and variations in the residual water. The choice of SVD to calculate weights for weighted averaging enables the effective minimisation of spectra that do not fit the spectral trend, such as those perturbed by rapid movement. Further, as the SVD

University of Cape Town

operation is performed on complex data, the weights generated are inherently complex, enabling phase-coherent averaging. Figure 4.11 shows how the phase of some measurements changed for a particularly restless subject, almost as much as π radians in one particular instance. The residual frequency shift after vNav correction was almost 15 Hz for two TRs, which fortunately is not enough to shift the water suppression band significantly.

4.5 Conclusions

We have demonstrated the successful application of a vNav PRESS sequence in two separate studies performed in 5- and 10-year old children. The vNav provides a consistent within scan VOI location while maintaining an optimal B0. We have demonstrated improved spectral quality when using the vNav in conjunction with offline pre-processing software as well as a reduced range and variance of metabolite concentrations. These benefits come at no extra scanning time, no technical cost when scanning in standard brain regions, and avoid the risks of sedation in children.

University of Cape Town

4.6 Acknowledgements

The South African Research Chairs Initiative of the Department of Science and Technology and National Research Foundation of South Africa, Medical Research Council of South Africa, NIH grants R21AA017410, R01AA016781, R21EB008547, R21DA026104, R33DA026104, R01NS055754, P41RR014075, and U19A153217 through the Comprehensive International Program of Research on AIDS (CIPRA) network; the Ellison Medical Foundation, the Harry Crossley Foundation, and the University of Cape Town. We thank radiographers Marie-Louise de Villiers and Nailah Maroof, Lindie du Plessis for assistance with LCModel analyses, Mathematician/Physicist M. Dylan Tisdall, Mark F Cotton for advice on the study, Shabir A Madhi for facilitating the study, research assistants Nicolette Hamman, Mariska Pienaar, Maggie September, Emma Makin, and Lungiswa Rosy Khethelo.

Chapter 5

Discussion

5.1 Comparison of the vNav to current techniques

In this work we have presented a motion correction technique for spectroscopy that incorporates frequency, first-order shim, and spectral localisation correction in one solution. In combination with offline residual frequency and phase correction for SVS, a complete motion correction solution is presented. Techniques currently available either perform: online frequency correction, offline frequency and phase correction, or are a hybrid of prospective localisation and frequency correction solutions. To date, no other system has demonstrated *in vivo* first-order shim correction in both SVS and MRSI.

Historically, motion correction techniques in spectroscopy have only addressed frequency shifts and phase artifacts. Without localisation correction these techniques cannot provide any confidence regarding the correct localisation of the VOI. The PROMO technique (Keating et al., 2010) for localisation correction is similar to the vNav as it employs an image based navigator. It is, however, a hybrid solution employing a water cycling mechanism (Ernst and Li, 2009) to perform real-time frequency tracking and offline phase correction. The main difference between PROMO and the vNav is that PROMO utilises five consecutive acquisition and registration blocks of 300 ms each in order to arrive at a stable head pose estimate, whereas the vNav utilises a single acquisition and reg-

University of Cape Town

istration. The advantage of a single acquisition is that it optimises the spatial information acquired with respect to the time used in the sequence. The vNav, when simultaneously performing motion and shim correction, can be completed in 714 ms (see chapter 3), in contrast to the 1.5 s required by PROMO for motion correction only.

An alternative hybrid solution that provides prospective localisation and frequency correction uses stereophotogrammetric cameras (Zaitsev et al., 2010b). This solution incorporates a frequency navigator (Thiel et al., 2002). However, unlike the vNav and PROMO, additional hardware is required in the scanner room and the subject needs to wear specialised and sometimes cumbersome regalia.

The data pre-processing method presented in chapter 4 performs frequency correction using a water independent spectral cross-correlation. The water independent frequency correction is robust against the potentially asymmetric nature of the residual water, which occurs when the water frequency is shifted beyond the linear pass band of the suppression pulses. This is an advantage over residual water based techniques. Phase coherent recombination is achieved independently of the residual water, using the statistical approach of Singular Value Decomposition (SVD). By reducing the weighting of measurements that do not conform to the trends in the data, SVD ensures a consistent spectral amplitude, which otherwise may be inconsistent due to movement within acquisitions. This data pre-processing solution is fully automated and does not depend on a high SNR from one metabolite.

University of Cape Town

5.2 Effects of motion related B0 changes on spectroscopy

In chapters 2 and 3 the effect of various head rotations on the *in vivo* B0 magnetic field was investigated. In both SVS and MRSI, chin up or down rotations by as little as 3° caused frequency shifts of the order of 2.5 Hz. Chin left to right rotations in SVS can be expected to produce similar frequency shifts in three of the four VOIs investigated. A 2 Hz shift would cause an observable split peak

for an underlying linewidth of 5 Hz. This may, however, not be significant within a 10 Hz linewidth. This type of split peak will both alter the magnitude of the spectrum and cause the line shape to deviate from a Lorentzian. In SVS, unlike MRSI, the effect of small frequency shifts can be removed with data pre-processing.

In the volunteer experiments, a 10° or 12° rotation in SVS and MRSI, respectively, caused frequency shifts of 15 Hz. Such frequency shifts are sufficient to render the water suppression ineffective and cause it to interfere with the spectrum. An acquisition in which a frequency shift of this magnitude is present can only be corrected using real-time prospective frequency tracking as with our vNav technique. Large frequency shifts of this nature were observed in two 5-year old paediatric scans. The one child demonstrated a 50 Hz frequency shift, while the other had a frequency shift of 35 Hz. Of interest was that the 50 Hz frequency shift was uncorrelated to the subject's movement at the time, while the 35 Hz shift was correlated with a Z translation.

In chapter 3 it was shown that a chin up or down rotation of 3° causes a 1.8 μT/m (0.8 Hz/cm) Y axis (coronal) gradient in an axial MRSI slice. Similarly, in chapter 2 it was shown that a 3 μT/m change occurs in various SVS voxels for the same rotation. This B0 gradient in MRSI produces a 2 Hz frequency change in voxels that are located 2.5 cm from the centre of the slice, enough to cause a noticeable split peak. This demonstrates the necessity for real-time first-order shim correction in motion corrected MRSI. In SVS the effect of such a first-order B0 change is less drastic. According to eq. 2.1, a first-order change of 5 μT/m is required to increase the spectral linewidth in a 20 x 20 x 20 mm^3 voxel by 1 Hz. The resultant effect will be proportional to the number of measurements affected by the change. For this reason, only fairly large head rotations that are maintained for significant periods during the scan will cause a noticeable loss in linewidth and SNR. However, first-order B0 changes are not limited to such head rotations, as demonstrated by the 15 μT/m shim change that is present for 1/3 of the scan in a 5-year old subject (fig. 4.10). This shim change would have likely resulted from movement near the scanner bore, such as the carer comforting the subject.

Second-order effects on the B0 field were observed in MRSI, with changes as

University of Cape Town

large as 5 Hz/cm^2 occurring in YZ when a subject lifts their chin by 5°. This will effectively induce a ± 11 Hz frequency spread across a 15 mm axial slice, reducing the SNR accordingly. These results demonstrate clearly that zero-, first- and second-order B0 changes occur in the presence of movement and that motion correction techniques used in spectroscopy will be ineffective without employing B0 correction up to first-order.

5.3 Spectral quality of vNav spectroscopy sequences

The aim of a motion correction solution is to ensure optimal spectral quality in both stationary scans and scans in which there is movement. In chapter 2 we hypothesised that the vNav will have no noticeable effect on the spectral signal. This was shown by comparing spectra acquired using two different sequences, one with and one without a vNav, in six stationary healthy adult volunteers. There was no significant difference in SNR between spectra acquired using the two different sequences (fig. 2.8). In a third scan, the real-time shim and motion correction of the vNav was enabled. There was no loss in SNR or linewidth as compared to a manually optimised shim. The same result was shown in a single healthy adult volunteer in MRSI by comparing two scans acquired with the vNav sequence (NoCo and ShMoCo) to one acquired using the standard LASER sequence. Furthermore, the spectral plots in figs. 2.9 and 3.5 demonstrate no loss in spectral specificity.

The spectral quality obtained by the vNav SVS sequence was further demonstrated in 99 scans acquired in 5- and 10-year old children at the Cape Universities Brain Imaging Centre (CUBIC). Of these scans, 52 were follow up scans. In comparison to their initial scan without the vNav, the mean linewidth significantly improved by 1.2 Hz ($p = 0.03$) and mean SNR significantly increased by 22% ($p = 0.0001$), while the number of successful scans increased from 50% to 73%. It should be noted that these figures do not, however, decouple the improvements offered by the data pre-processing from those of the vNav corrections. The remaining 46 vNav SVS scans acquired in the 5-year old children exhibited excellent

University of Cape Town

linewidths of 3.9 Hz on average, with a worst case linewidth of 5.0 Hz, this despite considerable movement in some subjects. These results demonstrate that the vNav causes no degradation of spectral quality while enabling the benefits of motion correction.

The effect of subject movement on SVS and MRSI spectra is striking; unless shim and motion correction is applied, the spectral quality is degraded, rendering some spectra unusable. It was shown in chapter 2 that motion and shim corrected SVS maintains both linewidth and SNR in the presence of motion, while a 2 Hz increase in linewidth and 33% reduction in SNR occurs when no shim correction is applied. Similarly, in MRSI the spectra were maintained within the quality threshold bounds (fig. 3.6, with the exception of a few voxels in the frontal lobe of one subject. This is in contrast to non shim-corrected scans where a significant number of spectra fell below the quality bounds, and in one subject all the spectra from a non shim-corrected scan fell outside of the quality bounds. Shim and motion corrected MRSI scans with movement demonstrated a small loss in spectral quality, with the worst case scan demonstrating a mean increase of 1.5 Hz in linewidth and a 13% reduction in mean SNR when compared to the stationary scan. This signal degradation in MRSI, that we do not observe in SVS, results from the larger VOI which is prone to higher than first-order B0 perturbations.

While spectral quality is key to successful metabolite concentration quantification, the concentration is of interest to the end user. The MRSI concentration maps in fig. 3.7 demonstrate that the concentration patterns are maintained in the presence of motion when shim and motion correction is applied, and how they are significantly perturbed by B0 changes when no shim correction is applied. The Bland and Altman plots of fig. 3.8 demonstrate the accuracy of the concentration measures when using shim and motion correction in the presence of movement. For the ratio of total NAA to total Cr the confidence interval is 15% of the mean concentration for shim and motion corrected MRSI, while this is degraded to 50% and 31%, respectively, with only motion correction and no correction applied. The follow up cerebellar paediatric scans in the healthy control 10-year old children demonstrate a reduced variance and range in several metabolite concentrations when compared to the initial scans acquired one year

University of Cape Town

previously using a standard PRESS sequence (fig. 4.9).

5.4 Accuracy and consistency of motion and shim measures

The excellent spectral quality obtained for numerous scans acquired with the vNav in both SVS and MRSI demonstrates the effectiveness of the technique, the reliability and consistency of the vNav measurements, and provides confidence in the reproducibility of the technique. The first consideration is the variance and range of the applied VOI frequency. The frequency of a VOI is a function of the applied shim gradients and the frequency offset of the RF transmitter and ADC. For this reason the best mechanism of determining the resultant frequency is to use the data pre-processing software presented in chapter 4. Four of the stationary shim and motion corrected scans of chapter 2 were processed using the offline frequency and phase correction software. The worst case frequency standard deviation was 0.9 Hz in volunteer 4 of that study. The frequency measured in each TR for this volunteer is presented in fig. 5.1, demonstrating a range of 3 Hz, of which 1 Hz results from the quantization steps of the scanner's numerically controlled oscillator (NCO) of 1 Hz. The standard deviations of the frequency for the remaining 3 volunteers were 0.7 Hz, 0.5 Hz, and 0.5 Hz, respectively.

University of Cape Town

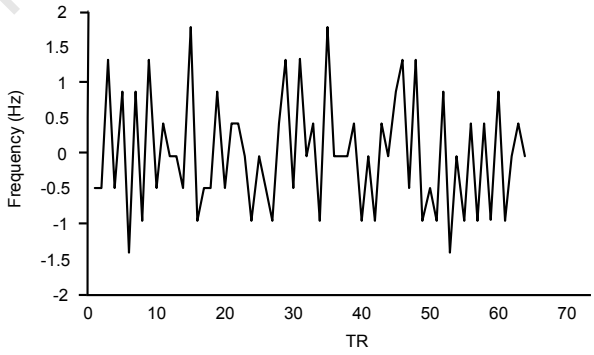

Figure 5.1: Offline frequency correlation, showing variations in the applied frequency for a SVS voxel in volunteer 4.

The variance of the first-order shim estimates depends on the size of the VOI. For the 20 x 20 x 20 mm^3 VOI used in chapter 2, a shim estimate for a scan with movement is shown in fig. 2.10. This volunteer (SVS volunteer 6) had the highest standard deviation for the shim estimates in the baseline shim corrected scan, with a standard deviation in Y shim of 1.7 μT/m. The shim estimates in MRSI are, in general, more stable due to the larger number of voxels available within the VOI to calculate the shim. The standard deviation of shim estimates in MRSI ranged from 0.3 μT/m (0.1 Hz/cm) to 1.3 μT/m (0.6 Hz/cm). Equation 2.1 and fig. 2.1 suggest that a shim perturbation of 3 μT/m in a 20 x 20 x 20 mm^3 voxel will cause an observable effect on the linewidth, so that the variances measured in the first-order shim estimates are unlikely to have an observable effect on the resultant linewidth. The MRSI worst case standard deviation of 0.6 Hz/cm is at the limit of causing observable frequency fluctuations at the edge of a VOI.

In SVS, these variances will become worse for smaller voxel sizes due to a reduction in the number of navigator data points used in the linear regression. For first-order shim estimates this is not a problem as the relationship between linewidth, first-order shim and voxel size is such that the smaller the voxel the greater the tolerance to shim errors (see fig. 2.1B). This tolerance, however, does not extend to frequency variance and care should be taken when using small voxel sizes, below 3.38 ml (15 x 15 x 15 mm^3), as these have not been tested.

In this work we have not scrutinised the accuracy of the image to image registration performed by PACE as it is a well established method. However, the standard deviation of the PACE measurements was calculated in all baseline shim and motion corrected scans of the adult volunteers. The greatest translation variance was in Z, with an average standard deviation of 0.2 mm and a worst case in one volunteer of 0.6 mm standard deviation. The greatest rotation variance was in Y with an average standard deviation of 0.2° and a worst case of 0.6° in one volunteer. These variances demonstrate the stability and reliability with which PACE estimates the rotation and translation parameters in the navigator images.

University of Cape Town

5.5 Observations regarding patterns of movement in 5- and 10-year old children

There is little literature on how much motion can be expected from paediatric subjects and the nature of this movement. Both inter- and intra scan movement is of interest. In this work these were both measured in seventeen 5-year old children. In addition, intra scan movement was measured in 41 10-year old children. The main difference observed between the intra scan movement patterns of these two groups is that the 5-year old children either lay completely still or moved substantially, while the 10-year olds typically displayed small movements throughout the scan.

The extent of each childs movement was quantified as the magnitude of the SVS voxel translation. Seven of the 46 scans (15%) in 5-year olds exhibited substantial intra scan voxel translations that were greater than 3 mm, while none of the 10-year olds presented such translations. The motion of one 5-year old child exceeded the TR to TR limit set by the PACE software of 20 mm translation or 8° rotation, while that of another caused a voxel shift of 18 mm during the scan but returned to their original position a few TRs later.

Inter scan movement was assessed by registering the first navigator volume to a reference scan acquired at the start of the session. This reflects the error in voxel localisation as a result of the subject being in a different position between the anatomical localising scan and the SVS scan. Nine of the 46 scans performed in 5-year old children exhibited substantial inter scan voxel displacements. By examining the resultant position of the SVS VOI on a structural image, two of these 9 scans were determined to no longer represent the intended anatomy. Although the vNav in its current form does not correct for inter scan subject movement, it does provide a method to confirm after the acquisition where the signal was actually acquired from.

These figures provide a motivation for motion and shim corrected SVS in this population. It is important to take into account the subject preparation and scanner setup. The primary mechanisms of motion prevention in the NMR environment should include a good subject preparation technique (Hallowell et al., 2008), a child friendly environment, and a comfortable well fitted patient table.

University of Cape Town

The paediatric subjects examined here were trained prior to the scan in a mock scanner and introduced to the scanner prior to being given the choice to continue with the examination or not. The children were provided with protective head phones in addition to ear plugs. While these head phones provide additional ear protection, they unfortunately leave a lot of room for the children to move around. If close fitting pillows were used the amplitude of movement may be significantly reduced.

5.6 Practical considerations

The vNav software is versatile enabling its application in many different configurations and scenarios. In this section the practicality of various vNav EPI protocols is considered. Considerations take into account the different VOIs, and the practicality of registering the vNav to a reference scan.

5.6.1 vNav Protocol: FOV, Resolution, and speed

When choosing a navigator protocol the user should consider the trade off between navigator speed and accuracy. The advantage of a fast navigator is that a short spectroscopy TR is achievable, leading to a faster spectroscopy scan, although a reduction in vNav information acquired can impact on its accuracy. Increasing the speed of the navigator could involve reducing the resolution, FOV, and/or the use of partial Fourier. When reducing the navigator resolution, there should be at least two, preferably three, navigator voxels across all dimensions of the spectroscopy VOI. If this requirement is not maintained a stable linear regression is not achievable and unstable or inaccurate first-order shims will be generated.

Another mechanism that can be used to speed up the navigator is to reduce its FOV in the slice direction. In this manner the number of partition encodes is reduced and the navigator duration is reduced substantially. This was done in chapter 3 where 16 partitions for each of two contrasts were acquired in 544 ms. The user should consider that two to three partitions at the edges of the slab have a reduced SNR resulting from imperfect slice profiles and should not be used in the VOI shim calculation. When the FOV is reduced, care should be taken to

University of Cape Town

include air superior to the scalp, thus providing PACE with the complete scalp profile as a strong feature for the registration, and to ensure that the spectroscopy VOI is contained within the FOV. It should be noted that the process of placing the navigator is a manual step that introduces possible operator error.

An ideal vNav protocol's FOV will acquire the complete scanner FOV, as demonstrated in chapter 2. This guarantees that every scan will completely cover the brain and that the air-tissue boundary superior to the scalp will be included. The limiting factor of this protocol is its 8 x 8 x 8 mm^3 resolution. Although sufficient for the 20 x 20 x 20 mm^3 SVS voxel in the right central white matter, this navigator resolution is not sufficient when scanning smaller voxels, such as 15 x 15 x 15 mm^3, in less magnetically homogeneous regions, such as the frontal lobe, hippocampus or cerebellum. In such VOIs a navigator resolution of 5 x 5 x 5 mm^3 has been found to work well. Such a resolution is achievable at the expense of a reduced navigator FOV and a reduced navigator SNR.

The shim calculation accuracy is primarily affected by the navigator SNR, more so than the motion estimate. In order to compensate for the reduced SNR when using the higher resolution protocol, the difference in TE between the two contrasts should be doubled (from 2.4 ms to 4.8 ms). By doing so the phase difference is doubled which in turn doubles the phase SNR in the field map. This approach has worked well in the paediatric studies presented in chapter 4. It does, however, place an increased demand on the phase unwrapping software, as the number of phase wraps in the field map doubles. In our experience, phase wraps only occur in the first navigator volume despite a doubled TE difference, after which the navigators self-calculated and applied shim is sufficient to prevent such phase wraps from occurring in subsequent TRs.

University of Cape Town

5.6.2 Effects of large second-order shim gradients on spectroscopy and vNav

When performing SVS in areas of high B0 inhomogeniety, such as the amygdala, hippocampus, and cerebellum, large second-order shim gradients may be necessary. When the shim is calculated using a small VOI, the spatial information is limited and may give rise to extraordinarily large and inappropriate second-order

shim gradients. Large shim gradients will make the spectroscopy acquisition vulnerable to spurious echo artifacts (Kreis, 2004) and additionally render the outer volume water suppression ineffective, potentially introducing further outer volume water artifacts. The vNav can also be adversely affected by large second-order shim gradients, as observed in the cerebellar scans presented in chapter 4. In four of the 52 scans, substantial ghosting rendered the vNav images unusable. This is believed to have resulted from large second-order shim gradients. Non-uniform water suppression will introduce bright areas within the vNav, with the 90° and 180° slice selective pulses forming dark bands within the bright image. Such features are demonstrated in fig. 5.2, and due to their strong contrast may adversely affect the PACE image registration. This problem of non-uniform water suppression does not occur in LASER acquisitions as LASER uses a non selective 90° excitation, thus evenly perturbing the magnetisation throughout.

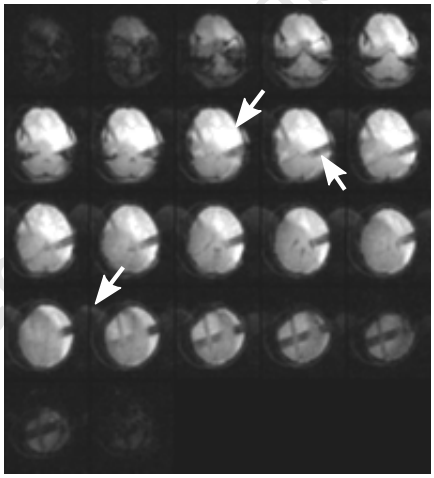

Figure 5.2: Artifacts introduced in vNav images as a result of either poor water suppression or oblique EPI ghosts.

In practice, large second-order shim gradients can be avoided in a two fold approach. Firstly, the volume over which the scanner adjusts the shim settings can be increased (adjustment volume). The larger volume will increase the stability of the scanner's shim optimisation. Secondly, a user can monitor the second-order shims set by the scanner with the "interactive shim" card. This is on the adjustment interface of the Siemens scanners. It is recommended that users look for

second-order gradients that are over 600 μT/m and set them to 600 μT/m. This will ensure that such extreme gradients do not occur. Offsetting the second-order shim gradients will have a substantial impact on the first-order shim settings and frequency. These will, however, automatically be corrected by the vNav.

5.6.3 Other considerations: Nyquist ghosts and inter scan registration

EPI images suffer from a number of different N/2, or Nyquist ghosts. The vNav has a built in navigator to deal with some of these ghosts. However, one such ghost, the oblique Nyquist ghost, arises from gradient delays when combining two gradient systems in the formation of an oblique image. On the Siemens Tim Trio scanner these ghost were not observed. It was, however, observed in the study performed on the Allegra scanner that required an oblique vNav orientation to cover the cerebellum, as shown in fig. 5.2. These ghosts may not have a significant effect on the motion correction. However, if their magnitude is sufficient to include them in the shim calculation mask, they will alter the vNav appropriate shim, which in turn will introduce unwanted image distortions. To prevent these types of ghosts, oblique navigator orientations should be avoided.

The final point to consider is the possibility to measure inter scan movement by registering the first navigator volume to a reference scan. This procedure requires that the reference scan be acquired as soon as possible before the start of the anatomical scan, and that the anatomical scan be motion corrected. This will minimise the likelihood of the subject moving between the reference and the anatomical scan. One procedure to do this would be to set up the reference volume to have the same shim adjustment volume and thus shim settings as the structural scan and ensure that no time is spent shimming between the two scans.

University of Cape Town

5.7 Limitations and recommendations

5.7.1 Shortfalls of the vNav validation

This section discusses some limitations of the sequence validation process. Firstly, the technique has only been validated in six VOIs, each with specific dimensions, namely the right central white matter, cerebellum, medial frontal grey matter, basal ganglia, peritrigonal white matter, and an axial MRSI slice. Each VOI presents different challenges for spectroscopy, including dimension, B0 distortions, and the influences of surrounding tissue. Although this study has validated the vNav technique in several volunteers, subjects, and VOIs, it is necessary to validate the technique in each intended VOI, particularly in areas known to be difficult for spectroscopy, such as the amygdala and hippocampus.

The second limitation is that the technique was not validated for VOIs smaller than 15 x 15 x 15 mm^3. Theoretically a navigator with 5 x 5 x 5 mm^3 resolution should be able to estimate a first-order shim in a 10 x 10 x 10 mm^3 SVS VOI. This should, however, be validated with particular attention to the accuracy of the incidental frequency. If the incidental frequency is unstable in such VOIs, improvements can be sought by temporally filtering the large time course of sampled data.

A third limitation is that the study did not quantify or account for the effects of EPI distortions on the image registration process. EPI images are prone to distortions that include distortion resulting from B0 perturbations that cause displacement in the phase encode direction, and chemical shift artifacts resulting in a shift of the affected tissue. Subcutaneous fat, for example, is displaced by up to four voxels in the navigator images. Although these two types of distortions are expected to remain constant, provided the vNav remains aligned to the anatomy, their effect on the image registration is unknown. In a similar manner the application of inappropriate second-order shim gradients resulting from those set for spectroscopy, generates related B0 distortion. More specifically these second-order shims will induce orientation specific distortions. These distortions possibly cause the real head position to disagree with that measured by registration. The most suitable way to address this problem would be to update the second-order

University of Cape Town

shim in the same manner as the first-order shim, by switching it between an EPI specific shim and a spectroscopy specific shim. This is, however, not possible on the current hardware due to the lack of eddy current compensation. An image registration algorithm that uses a field map to correct for such distortions may be an alternative, but may not be possible in real time.

5.7.2 Future work in SVS

The lack of inter scan motion tracking is the primary and most significant limitation of the vNav system presented. There are several possible ways to overcome this limitation. One obvious solution would be to match the vNav reference volume with that used in a navigated structural scan. In order to use the same reference volume, they need to be acquired with the same vNav protocol, the registration algorithm must be resilient to contrast differences, and the registration algorithm needs to take into account different B0 distortions. The contrast of the vNav in PRESS is complex as it is affected by the global water saturation and VOI localisation. However, LASER does not suffer from this problem as it utilises a non selective 90° adiabatic excitation that ensures a uniformly perturbed magnetisation that in turn generates a predictable, non VOI specific, contrast. Alternatively, a series of reference scans can be acquired at the start of the session, with the different navigated sequences utilising the reference with the appropriate contrast. This, however, would not work for a PRESS sequence as it would require the operator to set the VOI location of the PRESS image to ensure the correct contrast. A simpler solution would be to use a tool such as Auto-Align (Van der Kouwe et al., 2003), which enables a subject specific coordinate system to be set up if it is run prior to the structural image, and then again prior to the navigated spectroscopy. However, thorough testing should be done to ensure no adverse interaction between AutoAlign and the vNav.

A potential limitation of the navigator is its duration when a higher resolution navigator is required. In SVS, the minimum TR achievable is 2.0 s for children and 2.2 s in adults (due to FOV requirements). The navigator acquisition duration can be reduced using parallel imaging, the implementation of which would be straightforward. The time savings achieved with parallel imaging will be in lieu

University of Cape Town

of a reduction in vNav SNR. The considerations for doing this would include analyses of the reconstruction time required for various acceleration factors and the impact of parallel imaging on SNR and B0 shim estimates.

A technical limitation of the implemented system is that the EPI specific frequency updates are disabled after the start of the motion correction. This was necessary in order to avoid an interaction between frequency adjustment and motion correction. By not updating the EPI frequency in real time, the image is displaced in the phase encode direction and the slice select profile will be shifted. A solution to this interaction would be to simply subtract the frequency related phase encode translation estimate from that applied. This would enable frequency and translation estimates to be applied simultaneously to the EPI acquisition.

5.7.3 Future work in MRSI

Real-time shim correction is an important aspect of motion corrected MRSI. While the vNav is capable of measuring second-order shims, their application in real time was not demonstrated in this work. The incorporation of real-time second-order shim correction into the vNav system would require an investigation into the appropriate cost function, mechanisms to limit the maximum shim current, and eddy current correction issues. A least square error cost function minimises the mean square error. The implication of this is that neither the local intra voxel B0 gradient, nor the maximum frequency offset are considered, both of which are important aspects of quality MRSI. An alternative to a least square error cost function would be one that minimises the maximum frequency offset; this is termed a min-max cost function (Lee et al., 2009). The effects of eddy currents could be minimised by adjusting the shim gradients after the spectroscopy, giving them ample time to settle before the next spectroscopy acquisition.

Residual frequency and phase correction was presented in SVS, however, in MRSI no such solution was presented. One option investigated, however, was to reacquire the TRs in which a significant TR to TR pose change occurred. This method was not taken further as we were not able to induce noticeable phase errors in the MRSI spectral grids. While reacquisition is possible it may not be the most optimal solution, primarily because of the long repetition times. Large

University of Cape Town

displacements can occur with slow velocities and not induce a significant frequency or phase offset, while more detrimental effects can occur as a result of short duration, rapid velocities, which do not reflect as gross TR to TR movements. Alternative solutions could utilise pre-phase encoding water samples as done by Posse et al. (1993).

University of Cape Town

Chapter 6

Conclusion

University of Cape Town

A novel technique has been presented that simultaneously performs real-time motion, frequency, and first-order shim correction in magnetic resonance spectroscopy. The technique uses echo planar imaging to rapidly acquire a volumetric navigator (vNav). Registration of successive vNavs to the reference vNav provides robust head position and orientation estimates that are used to update the scanner's current coordinate system once each TR. A dual contrast vNav generates a field map that is used for B0 (frequency, and first-order) correction.

The vNav was incorporated into both single voxel spectroscopy and magnetic resonance spectroscopic imaging sequences with minimal impact on the scan time. The vNav successfully maintains in vivo spectral quality in the presence of both movement and B0 disruption. Both measurements of the changes that occur in the B0 field map of a single moving volunteer and the vNavs own shim estimates demonstrate the need for real-time B0 correction. The vNav shim estimates demonstrated significant movement related B0 disruptions in both axial MRSI and two different SVS VOIs.

An offline data pre-processing software solution was developed to remove residual phase and frequency shifts arising from both physiological and subject movement. The software employs methods that are independent of the residual water signal and that are robust with no user interaction required. The vNav was used to perform inter scan registration between a reference scan acquired prior to the structural scan and the spectroscopy acquisition, which improves confidence in spectroscopic VOI placement.

The vNav was used in combination with the data pre-processing software to acquire SVS data in 99 paediatric subjects. The results from a one year follow up study of 10-year old children showed significant improvements in data quality and a reduction in the number of failed scans. The data acquired in 5-year old children presented excellent spectral quality despite the fact that 15% of the subjects moved significantly in the scanner. In conclusion, a novel spectroscopy and spectroscopic imaging technique that is insensitive to motion has been presented and validated.

University of Cape Town

References

Andronesi, O. C., Ramadan, S., Ratai, E. M., Jennings, D., Mountford, C. E., Sorensen, A. G., 2010. Spectroscopic imaging with improved gradient modulated constant adiabaticity pulses on high-field clinical scanners. Journal of Magnetic Resonance 203 (2), 283–293. 8, 9, 45, 47, 48

Ashburner, J., 2007. A fast diffeomorphic image registration algorithm. Neuroimage 38 (1), 95–113.
URL http://linkinghub.elsevier.com/retrieve/pii/S1053811907005848 25, 46, 77

Bland, J. M., Altman, D. G., 1986. Statistical-Methods for Assessing Agreement between 2 Methods of Clinical Measurement. Lancet (1), 307–310. 57

Block, K. T., Frahm, J., Jun. 2005. Spiral imaging: a critical appraisal. Journal of magnetic resonance imaging : JMRI 21 (6), 657–68.
URL http://www.ncbi.nlm.nih.gov/pubmed/15906329 20

Bottomley, P. A., 1987. Spatial localization in NMR spectroscopy in vivo. Annals of the New York Academy of Sciences 508, 333–318. 7, 28

Bruder, H., Fischer, H., Reinfelder, H.-E., Schmitt, F., Feb. 1992. Image reconstruction for echo planar imaging with nonequidistantk-space sampling. Magnetic Resonance in Medicine 23 (2), 311–323.
URL http://doi.wiley.com/10.1002/mrm.1910230211 19

Cavassila, S., Deval, S., Huegen, C., van Ormondt, D., Graveron-Demilly, D., Jun. 2001. Cramér-Rao bounds: an evaluation tool for quantitation. NMR in

University of Cape Town

biomedicine 14 (4), 278–83.
URL http://www.ncbi.nlm.nih.gov/pubmed/11410946 11

De Graaf, A. A., Bovée, W. M. M. J., Aug. 1990. Improved quantification of in vivo 1H NMR spectra by optimization of signal acquisition and processing and by incorporation of prior knowledge into the spectral fitting. Magnetic Resonance in Medicine 15 (2), 305–319.
URL http://doi.wiley.com/10.1002/mrm.1910150212 11

de Graaf, R. A., Oct. 2007. In Vivo NMR Spectroscopy. John Wiley & Sons, Ltd, Chichester, UK.
URL http://doi.wiley.com/10.1002/9780470512968 9

Derbyshire, J. A., Wright, G. A., Henkelman, R. M., Hinks, R. S., 1998. Dynamic scan-plane tracking using MR position monitoring. Journal of magnetic resonance imaging 8 (4), 924–32.
URL http://www.ncbi.nlm.nih.gov/pubmed/9702895 18

Ehman, R. L., Felmlee, J. P., Oct. 1989. Adaptive technique for high-definition MR imaging of moving structures. Radiology 173 (1), 255–63.
URL http://radiology.rsna.org/content/173/1/255.abstract 16

Ernst, T., Li, J., 2009. Phase Navigators for Localized MR Spectroscopy using Water Suppression Cycling. In: Proceedings of the 17th Annual Meeting of the ISMRM. p. 239. 15, 22, 70, 89

Eviatar, H., Schattka, B., Sharp, J. C., Rendell, J., Alexander, M. E., 1999. Real Time Head Motion Correction for Functional MRI. In: Proceedings of the 7th Annual Meeting of the ISMRM. p. 269. 18

Frahm, J., Bruhn, H., Gyngell, M. L., Merboldt, K. D., Hänicke, W., Sauter, R., Jan. 1989. Localized high-resolution proton NMR spectroscopy using stimulated echoes: initial applications to human brain in vivo. Magnetic Resonance in Medicine 9 (1), 79–93.
URL http://www.ncbi.nlm.nih.gov/pubmed/2540396 8

University of Cape Town

Friston, K. J., Ashburner, J., Frith, C. D., Poline, J.-B., Heather, J. D., Frackowiak, R. S. J., 1995. Spatial registration and normalization of images. Human Brain Mapping 3 (3), 165–189.
URL http://doi.wiley.com/10.1002/hbm.460030303 18

Fu, Z., Wang, Y., Grimm, R., 1995. Orbital navigator echoes for motion measurements in magnetic resonance imaging. Magnetic Resonance in Medicine 34 (5), 746–753.
URL http://onlinelibrary.wiley.com/doi/10.1002/mrm.1910340514/abstract 17, 23, 45

Gabr, R., Sathyanarayana, S., Schär, M., Weiss, R., Bottomley, P., 2006. On restoring motion-induced signal loss in single-voxel magnetic resonance spectra. Magnetic Resonance in Medicine 56 (4), 754–760.
URL http://www3.interscience.wiley.com/journal/112782392/abstract 15, 70

Garwood, M., DelaBarre, L., Dec. 2001. The return of the frequency sweep: designing adiabatic pulses for contemporary NMR. Journal of Magnetic Resonance 153 (2), 155–77.
URL http://www.ncbi.nlm.nih.gov/pubmed/11740891 8

Graveron-Demilly, D., Diop, A., Briguet, A., Fenet, B., 1993. Product-operator algebra for strongly coupled spin systems. Journal of Magnetic Resonance, Series A 101 (3), 233–239.
URL http://linkinghub.elsevier.com/retrieve/pii/S1064185883710387 74

Gruetter, R., Jun. 1993. Automatic, localized in vivo adjustment of all first- and second-order shim coils. Magnetic Resonance in Medicine 29 (6), 804–11.
URL http://www.ncbi.nlm.nih.gov/pubmed/8350724 13

Haase, A., Frahm, J., Hanicke, W., Matthaei, D., 1985. 1 H NMR chemical shift selective (CHESS) imaging. Physics in Medicine and Biology 30 (4), 341.
URL http://stacks.iop.org/0031-9155/30/i=4/a=008 7

University of Cape Town

Hallowell, L. M., Stewart, S. E., de Amorim e Silva, C. T., Ditchfield, M. R., Mar. 2008. Reviewing the process of preparing children for MRI. Pediatric radiology 38 (3), 271–9.
URL http://www.ncbi.nlm.nih.gov/pubmed/18084752 96

Helms, G., Piringer, A., 2001. Restoration of motion-related signal loss and line-shape deterioration of proton MR spectra using the residual water as intrinsic reference. Magnetic Resonance in Medicine 46 (2), 395–400.
URL http://onlinelibrary.wiley.com/doi/10.1002/mrm.1203/full 15, 22, 70

Hennig, J., Jan. 1992. The application of phase rotation for localized in Vivo proton spectroscopy with short echo times. Journal of Magnetic Resonance (1969) 96 (1), 40–49.
URL http://linkinghub.elsevier.com/retrieve/pii/002223649290286G 10

Henry, P., van De Moortele, P., Giacomini, E., Nauerth, A., Bloch, G., 1999. Field-frequency locked in vivo proton MRS on a whole-body spectrometer. Magnetic Resonance in Medicine 42 (4), 636–642.
URL http://www3.interscience.wiley.com/journal/66000374/abstract 15, 22, 44, 70

Hess, A. T., Andronesi, O. C., Tisdall, M. D., Sorensen, A. G., van der Kouwe, A. J. W., Meintjes, E. M., 2010. Motion artefact correction in spectroscopic imaging using an EPI navigator and reacquisition. In: Proceedings of the 18th annual meeting of International Society of Magnetic Resonance in Medicine. p. 3308. 66

Hess, A. T., Tisdall, M. D., Andronesi, O. C., Meintjes, E. M., van der Kouwe, A. J. W., 2011. Real-time Motion and B0 corrected single voxel spectroscopy using volumetric navigators. Magnetic Resonance in Medicine, (In Press). 45, 47, 49, 50, 67, 69, 72

Jacobson, S. W., Stanton, M. E., Molteno, C. D., Burden, M. J., Fuller, D. S., Hoyme, H. E., Robinson, L. K., Khaole, N., Jacobson, J. L., 2008. Impaired eye-

University of Cape Town

blink conditioning in children with fetal alcohol syndrome. Alcoholism: Clinical and Experimental Research 32 (2), 365–372. 71

Jenkinson, M., 2003. Fast, automated, N-dimensional phase-unwrapping algorithm. Magnetic resonance in medicine 49 (1), 193–197.
URL http://onlinelibrary.wiley.com/doi/10.1002/mrm.10354/full 27, 48, 84

Jesmanowicz, A., Wong, E., Hyde, J., 1993. Phase correction for EPI using internal reference lines. In: Proceedings of the 12th Annual Meeting of the Society of Magnetic Resonance in Medicine, New York. p. 1239. 19

Keating, B., Deng, W., Roddey, J., White, N., Dale, A., Stenger, V., Ernst, T., 2010. Prospective motion correction for single-voxel 1H MR spectroscopy. Magnetic Resonance in Medicine 64 (3), 672–679.
URL http://onlinelibrary.wiley.com/doi/10.1002/mrm.22448/full 16, 22, 23, 41, 70, 89

Kim, D., Adalsteinsson, E., Spielman, D., 2004. Spiral readout gradients for the reduction of motion artifacts in chemical shift imaging. Magnetic Resonance in Medicine 51 (3), 458–463.
URL http://onlinelibrary.wiley.com/doi/10.1002/mrm.20004/full 15

Kinchesh, P., Ordidge, R. J., Jul. 2005. Spin-echo MRS in humans at high field: LASER localisation using FOCI pulses. Journal of magnetic resonance (San Diego, Calif. : 1997) 175 (1), 30–43.
URL http://dx.doi.org/10.1016/j.jmr.2005.03.009 9

Kreis, R., 2004. Issues of spectral quality in clinical 1 H-magnetic resonance spectroscopy and a gallery of artifacts. NMR in Biomedicine, 361–381. 8, 11, 53, 99

Lee, J., Lustig, M., Kim, D., Pauly, J., 2009. Improved shim method based on the minimization of the maximum off-resonance frequency for balanced steady-state free precession (bSSFP). Magnetic Resonance in Medicine 61 (6), 1500–1506.

University of Cape Town

URL http://onlinelibrary.wiley.com/doi/10.1002/mrm.21800/full 65, 103

Madhi, S. A., Adrian, P., Cotton, M. F., McIntyre, J. A., Jean-Philippe, P., Meadows, S., Nachman, S., Käyhty, H., Klugman, K. P., Violari, A., 2010. Effect of HIV Infection Status and Anti-Retroviral Treatment on Quantitative and Qualitative Antibody Responses to Pneumococcal Conjugate Vaccine in Infants. The Journal of infectious diseases 202 (3), 355–361. 71

Mescher, M., Tannus, A., Oneil Johnson, M., Garwood, M., Dec. 1996. Solvent Suppression Using Selective Echo Dephasing. Journal of Magnetic Resonance, Series A 123 (2), 226–229.
URL http://dx.doi.org/10.1006/jmra.1996.0242 7

Morris, G., Freeman, R., Mar. 1978. Selective excitation in Fourier transform nuclear magnetic resonance. Journal of Magnetic Resonance 29 (3), 433–462.
URL http://dx.doi.org/10.1016/0022-2364(78)90003-3 7

Mugler, J. P., Brookeman, J. R., Jul. 1990. Three-dimensional magnetization-prepared rapid gradient-echo imaging (3D MP RAGE). Magnetic Resonance in Medicine 15 (1), 152–157.
URL http://doi.wiley.com/10.1002/mrm.1910150117 17

Noll, D. C., Meyer, C. H., Pauly, J. M., Nishimura, D. G., Macovski, A., Jan. 1991. A homogeneity correction method for magnetic resonance imaging with time-varying gradients. IEEE transactions on medical imaging 10 (4), 629–37.
URL http://ieeexplore.ieee.org/xpl/freeabs_all.jsp?arnumber=108599 20

Ogg, R. J., Kingsley, R. B., Taylor, J. S., May 1994. WET, a T1- and B1-Insensitive Water-Suppression Method for in Vivo Localized 1H NMR Spectroscopy. Journal of Magnetic Resonance, Series B 104 (1), 1–10.
URL http://dx.doi.org/10.1006/jmrb.1994.1048 7, 49

Ooi, M. B., Krueger, S., Thomas, W. J., Swaminathan, S. V., Brown, T. R., Oct. 2009. Prospective real-time correction for arbitrary head motion using active

University of Cape Town

markers. Magnetic Resonance in Medicine 62 (4), 943–54.
URL http://www.ncbi.nlm.nih.gov/pubmed/19488989 18

Piotto, M., Saudek, V., Sklená, V., Nov. 1992. Gradient-tailored excitation for single-quantum NMR spectroscopy of aqueous solutions. Journal of Biomolecular NMR 2 (6), 661–665.
URL http://www.springerlink.com/content/ynp48206431x6887/ 7

Pipe, J. G., Nov. 1999. Motion correction with PROPELLER MRI: Application to head motion and free-breathing cardiac imaging. Magnetic Resonance in Medicine 42 (5), 963–969.
URL http://doi.wiley.com/10.1002/(SICI)1522-2594(199911)42:5<963::AID-MRM17>3.0.CO;2-L 18

Posse, S., Cuenod, C., Le Bihan, D., 1993. Motion Artifact Compensation in 1H Spectroscopic Imaging by Signal Tracking. Journal Of Magnetic Resonance Series B 102, 222–222.
URL http://meteoreservice.com/PDFs/Posse93b.pdf 15, 22, 44, 104

Provencher, S. W., 1993. Estimation of metabolite concentrations from localized in vivo proton NMR spectra. Magnetic Resonance in Medicine 30 (6), 672–679. 11, 31

Provencher, S. W., 2001. Automatic quantitation of localized in vivo 1H spectra with LCModel. NMR in biomedicine 14 (4), 260–264. 50, 77

Qin, L., van Gelderen, P., Derbyshire, J. A., Jin, F., Lee, J., de Zwart, J. A., Tao, Y., Duyn, J. H., Oct. 2009. Prospective head-movement correction for high-resolution MRI using an in-bore optical tracking system. Magnetic Resonance in Medicine 62 (4), 924–34.
URL http://www.ncbi.nlm.nih.gov/pubmed/19526503 18

Reese, T. G., Davis, T. L., Weisskoff, R. M., 1995. Automated shimming at 1.5 T using echo-planar image frequency maps. Journal of Magnetic Resonance Imaging 5 (6), 739–745. 13, 24, 25, 28, 48

University of Cape Town

Sison, S., Buonocore, M. H., Maddock, J. R., 2007. Extension of 8 Step Phase Cycling Scheme for improved lipid suppression using four-pulse PRESS MRS Sequences. In: Proceedings of the 16th Annual Meeting of the ISMRM. Vol. 15. p. 1353. 10

Star-Lack, J. M., Adalsteinsson, E., Gold, G. E., Ikeda, D. M., Spielman, D. M., 2000. Motion correction and lipid suppression for 1H magnetic resonance spectroscopy. Magnetic Resonance in Medicine 43 (3), 325–330.
URL http://onlinelibrary.wiley.com/doi/10.1002/(SICI)1522-2594(200003)43:3%3C325::AID-MRM1%3E3.0.CO;2-8/abstract 15, 22, 70

Tannús, A., Garwood, M., 1996. Improved performance of frequency-swept pulses using offset-independent adiabaticity. Journal of Magnetic Resonance, Series A 120 (1), 133–137. 48

Tannús, A., Garwood, M., Dec. 1997. Adiabatic pulses. NMR in Biomedicine 10 (8), 423–434.
URL http://doi.wiley.com/10.1002/(SICI)1099-1492(199712)10:8<423::AID-NBM488>3.0.CO;2-X 9

Thesen, S., Heid, O., Mueller, E., Schad, L. R., 2000. Prospective acquisition correction for head motion with image-based tracking for real-time fMRI. Magnetic Resonance in Medicine 44 (3), 457–465. 18, 27, 48, 73

Thiel, T., Czisch, M., Elbel, G. K., Hennig, J., 2002. Phase coherent averaging in magnetic resonance spectroscopy using interleaved navigator scans: compensation of motion artifacts and magnetic field instabilities. Magnetic Resonance in Medicine 47 (6), 1077–1082. 16, 22, 44, 70, 90

Tisdall, M. D., Hess, A. T., van der Kouwe, A. J. W., 2009. MPRAGE Using EPI Navigators for Prospective Motion Correction. In: Proceedings of the 17th annual meeting of International Society of Magnetic Resonance in Medicine. p. 4656. 45, 47, 75

University of Cape Town

Van der Kouwe, A. J. W., Benner, T., Dale, A. M., 2006. Real-time rigid body motion correction and shimming using cloverleaf navigators. Magnetic Resonance in Medicine 56 (5), 1019–1032. 17, 23, 45

Van Der Kouwe, A. J. W., Benner, T., Salat, D. H., Fischl, B., 2008. Brain morphometry with multiecho MPRAGE. NeuroImage 40 (2), 559–569. 25, 46, 75

Van der Kouwe, A. J. W., Gicquel, S., Chen, G., Schmitt, F., Harder, M., Salat, D., Sorensen, A. G., Fischl, B., Dale, A., 2003. On-line automatic slice positioning and between-scan correction for brain MR protocols. In: Proceedings of the 11th Annual Meeting of ISMRM, Toronto, Canada. 66, 87, 102

Violari, A., Cotton, M. F., Gibb, D. M., Babiker, A. G., Steyn, J., Madhi, S. a., Jean-Philippe, P., McIntyre, J. a., Nov. 2008. Early antiretroviral therapy and mortality among HIV-infected infants. The New England journal of medicine 359 (21), 2233–44.
URL http://www.pubmedcentral.nih.gov/articlerender.fcgi?artid=2950021&tool=pmcentrez&rendertype=abstract 71

Waddell, K. W., Avison, M. J., Joers, J. M., Gore, J. C., 2007. A Practical Guide to Robust Detection of GABA in Human Brain by J-difference Spectroscopy at 3 Tesla Using a Standard Volume Coil. Magnetic resonance imaging 25 (7), 1032. 15, 70

Webb, P., Spielman, D., Macovski, A., 1992. Inhomogeneity correction for in vivo spectroscopy by high-resolution water referencing. Magnetic Resonance in Medicine 23 (1), 1–11. 23

Weinhandl, J. T., Armstrong, B. S. R., Kusik, T. P., Barrows, R. T., OConnor, K. M., 2010. Validation of a single camera three-dimensional motion tracking system. Journal of Biomechanics 43 (7), 1437–1440. 45

Welch, E. B., Manduca, A., Grimm, R. C., Ward, H. A., Jack Jr, C. R., 2002. Spherical navigator echoes for full 3D rigid body motion measurement in MRI. Magnetic Resonance in Medicine 47 (1), 32–41. 17, 23

University of Cape Town

White, N., Roddey, C., Shankaranarayanan, A., Han, E., Rettmann, D., Santos, J., Kuperman, J., Dale, A., 2010. PROMO: Real-time prospective motion correction in MRI using image-based tracking. Magnetic Resonance in Medicine 63 (1), 91–105. 17, 23, 45

Zaitsev, M., Armstrong, B. S. R., Andrews-Shigaki, B., Kusik, T. P., Barrows, R. T., Gumus, K., Kadashevich, I. Y., Prieto, T., Speck, O., Ernst, T. M., 2010a. Prospective Motion Correction for MRI with a Single Retro-Grate Reflector Target and a Single Camera. In: Proceedings of the 18th annual meeting of International Society of Magnetic Resonance in Medicine. Vol. M. p. 5027.
URL http://www.mcw.edu/FileLibrary/Groups/Biophysics/ISMRMAbstracts2010/5027.pdf 18, 41, 70

Zaitsev, M., Dold, C., Sakas, G., Hennig, J., Speck, O., Jul. 2006. Magnetic resonance imaging of freely moving objects: prospective real-time motion correction using an external optical motion tracking system. NeuroImage 31 (3), 1038–50.
URL http://www.ncbi.nlm.nih.gov/pubmed/16600642 18

Zaitsev, M., Speck, O., Hennig, J., Büchert, M., 2010b. Single-voxel MRS with prospective motion correction and retrospective frequency correction. NMR in biomedicine 23 (3), 325–332. 16, 22, 45, 90

University of Cape Town

Appendix A

Phantom Experiments

University of Cape Town

A.1 Aims

- To verify that the spectroscopy voxel is maintained at the intended VOI in:
  - translation.
  - and rotation.
- To verify the navigator shim measurements and that they are correctly applied.

A.2 Apparatus

A.2.1 MRI Scanner

The 3T Siemens Allegra scanner at CUBIC was used for the phantom experiments. The coordinate system of the MRI scanner is defined in fig. A.1.

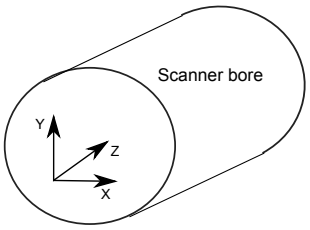

Figure A.1: Coordinate system of MRI scanner

A.2.2 Phantom

A phantom with two compartments was used, namely a main spherical compartment with a 20 x 20 x 20 mm^3 cube (inner dimensions) suspended in the centre of the sphere. The sphere was filled with a choline chloride and magnevist (1 ml magnevist to 1 l of water) solution. The cube was filled with an N-Acetyle-L-aspartic acid and magnevist (0.5 ml magnevist to 1 l of water) solution. The concentrations of choline chloride and N-Acetyle-L-aspartic acid were matched to produce an NMR signal of similar magnitude. This phantom is illustrated in fig. A.2.

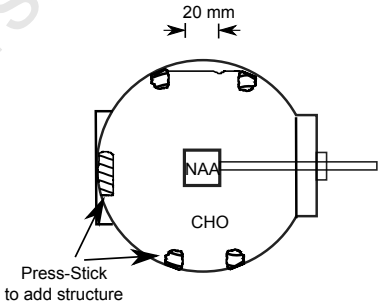

Figure A.2: Spectroscopy phantom, with 20 x 20 x 20 mm^3 cube (inner dimentions) suspended in the cenre

University of Cape Town

A.2.3 Rotation and translation jigs

Three jigs were constructed to produce translations in X, Y, Z, and rotation about Y. The first jig produced X or Y translation depending on its orientation, the second produced Z translation, and the third produced a rotation about Y. Each one was connected via a gearing mechanism to a crank and handle to allow a user to control the motion. The three jigs are shown in fig. A.3.

A.2.4 MR navigator and SVS protocol used

Navigator resolution 5 x 5 x 5 mm^3, FOV 220 x 200 x 140 mm^3, matrix 44 x 40, 28 partitions, TE_1 8 ms, and TE_2 12.8 ms, TR 21 ms, bandwidth 3906 Hz.

SVS PRESS protocol: TE = 30 ms, TR = 2.2 s, Bandwidth = 1000 Hz, Vector size = 512, Voxel size 20 x 20 x 20 mm^3, 32 measurements.

A.3 Methods

A.3.1 Phantom spectra

Two scans were performed with the stationary phantom, one with the voxel positioned over the cube, and one with it positioned outside the cube. These were to measure the NAA and Cho spectra generated from inside and outside the cube, respectively.

A.3.2 Translations and rotations

For the scans with motion, the SVS voxel was positioned inside the cube, fully covering its inner dimensions. Four experiments were performed to test X, Y, Z translations, and rotations about Y, each consisting of the following 6 steps:

1. Multi slice Localizer to show the starting position of cube.
2. Stationary scan with voxel positioned over cube. Shim and motion correction enabled.

University of Cape Town

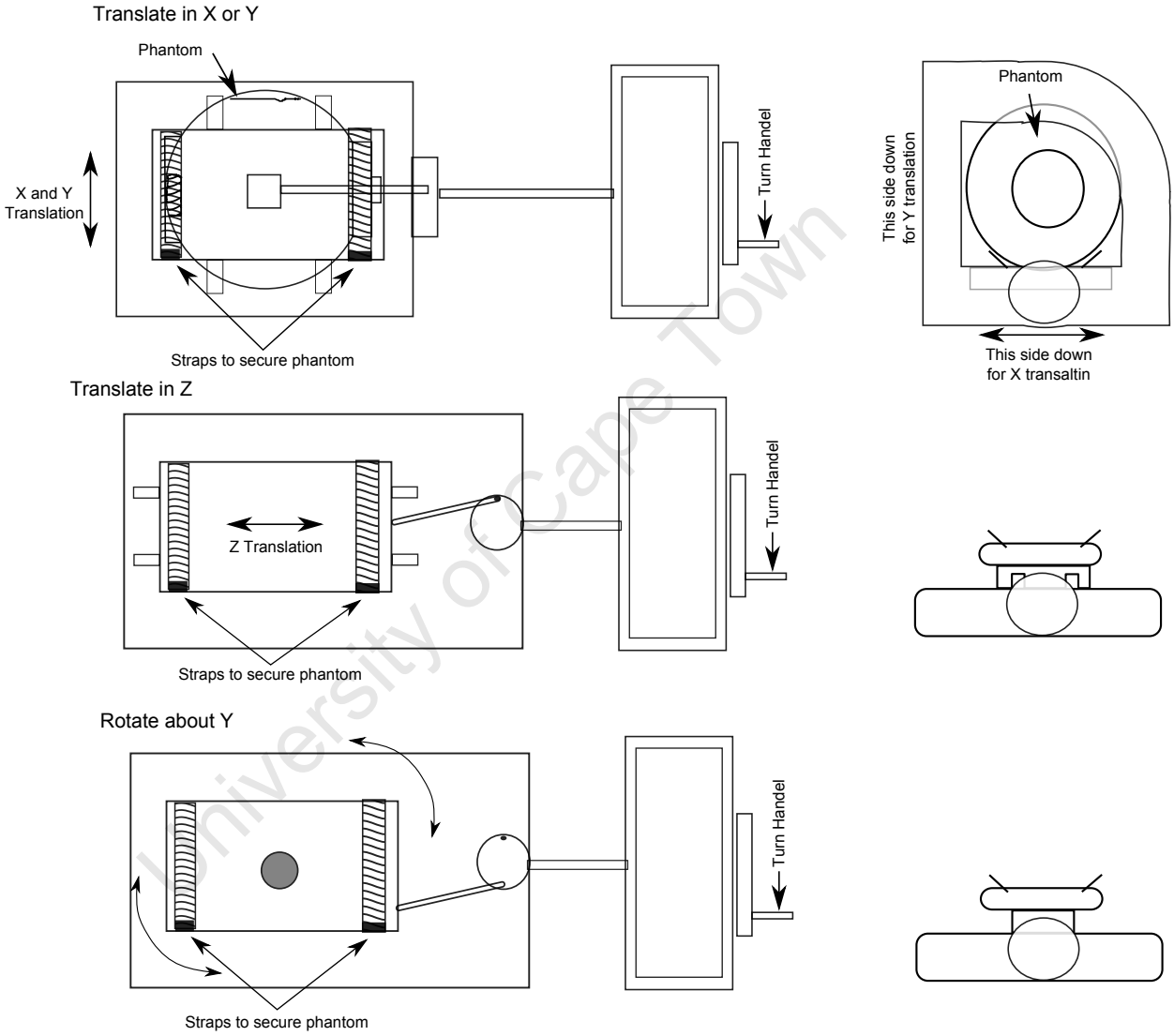

Figure A.3: Movement jigs used. One for translation in X and Y, one for translation in Z, and one for rotation about Y

University of Cape Town

Table A.1: The four experiments performed

	Movement	Magnitude measured on jig
1	Translation X	18 mm
2	Translation Y	13 mm
3	Translation Z	35 mm
4	Rotation about Y	27°

3. Moving Scan with shim and motion correction enabled. Phantom moved over multiple TR's, starting on TR 8, and remaining in the new position for reminder of scan.

4. Localizer to show new position of phantom.

5. Phantom returned to initial position.

6. Moving scan with navigator corrections disabled.

   a. Set scanner's system shim to reflect the same as that applied by navigator in stationary scan. This will ensure a consistent measurement paradigm.

   b. Phantom moved over multiple TR's, starting on TR 8, and remaining in the new position for remainder of scan.

University of Cape Town

The movement performed in each experiment is presented the table A.1. The magnitude of the movement was measured on the jig, using the localizer images, and from the navigator motion estimates.

All SVS acquisitions were processed in LCModel to determine the concentrations of NAA relative to one another.

A.3.3 Shim measurement and adjustment validation

Two scans were performed to validate the shim as measured by the navigator. The first scan measured the difference between the scanners system shim and the

shim set by the navigator. In the second the scanner's system shim was offset 10 μT/m on each of the first-order gradient axes, X, Y, and Z. We hypothesize that the difference in the shim measured by the navigator between the two scans should reflect the 10 μT/m offset.

A.4 Results

A.4.1 Motion estimation

The localizer scans from before and after each of the four motions are shown in fig. A.4. The spectroscopy voxel is overlaid on each to demonstrate the effect of the movement. For the X and Z translations, the voxel was shifted completely outside the cube, whereas in the Y translation the shift was less due to a limited range, and likewise in the Y rotation.

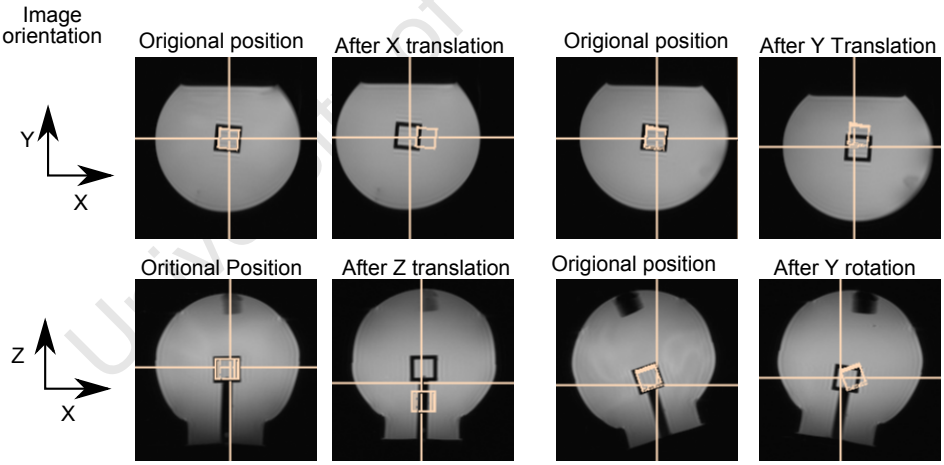

Figure A.4: Localiser images showing Voxel positioning before and after each of the four movements.

The spectra observed, for each scan, are plotted in fig. A.5. In fig. A.5A the stationary scans from inside and outside the voxel are overlaid to show the expected phantom spectra. In fig. A.5B, C, D, and E the spectra from the uncorrected and corrected scans overlaid to facilitate comparison. For the uncorrected

University of Cape Town

Table A.2: Motion performed, as measured on the jig, the localiser images and by the navigator

Experiment	Measured on jig	Measured in localizer images	Measured by navigator	Number of TRs to complete motion
X Translation	X = 18 mm	X = 18 mm	X = 18 mm	3
Y Translation	Y = 13 mm	Y = 14 mm	Y = 14 mm	3
Z Translation	Z = 35 mm	Z = 36 mm	Z = 44 mm, X = 4.5°	5
Y Rotation	Y = 27°	Y = 27°	Y = 24°	6

University of Cape Town

scans a significant reduction in NAA is noticeable, as well as an increase in Cho.

Figure A.6 shows a bar graph of the NAA concentrations measured by LCModel for each of the three different scans in each experiment. A significant reduction in the NAA concentration is observed when no correction is used, noting the spectral distortions prevented any quantification of NAA for the uncorrected scan with Z translation. The uncorrected scans with X translation, Y translations, and Y rotations, included significant contributions from Cho. The NAA concentration in the shim and motion corrected scans was within 5% of the mean NAA concentration (from stationary scans), except for the Z translation which was 23% lower than the mean. Despite the 23% reduction in NAA, Cho was not present in the spectrum (see fig. A.5).

The motion was measured on the jig, by using the localizer images, and by the navigator. For each experiment the respective measurements are compared in table A.2. The measurements of all three were within 1 mm for the X and Y translations, however, there was a discrepancy in both Z translation and Y rotation. The Z translation reported by the navigator was 8 mm greater than that measured both on the jig and using the localizer images (22% difference) with an additional rotation about the X axis of 4.5°. The rotation about Y reported by the navigator was 3° less than that measured on the jig or localizer images.

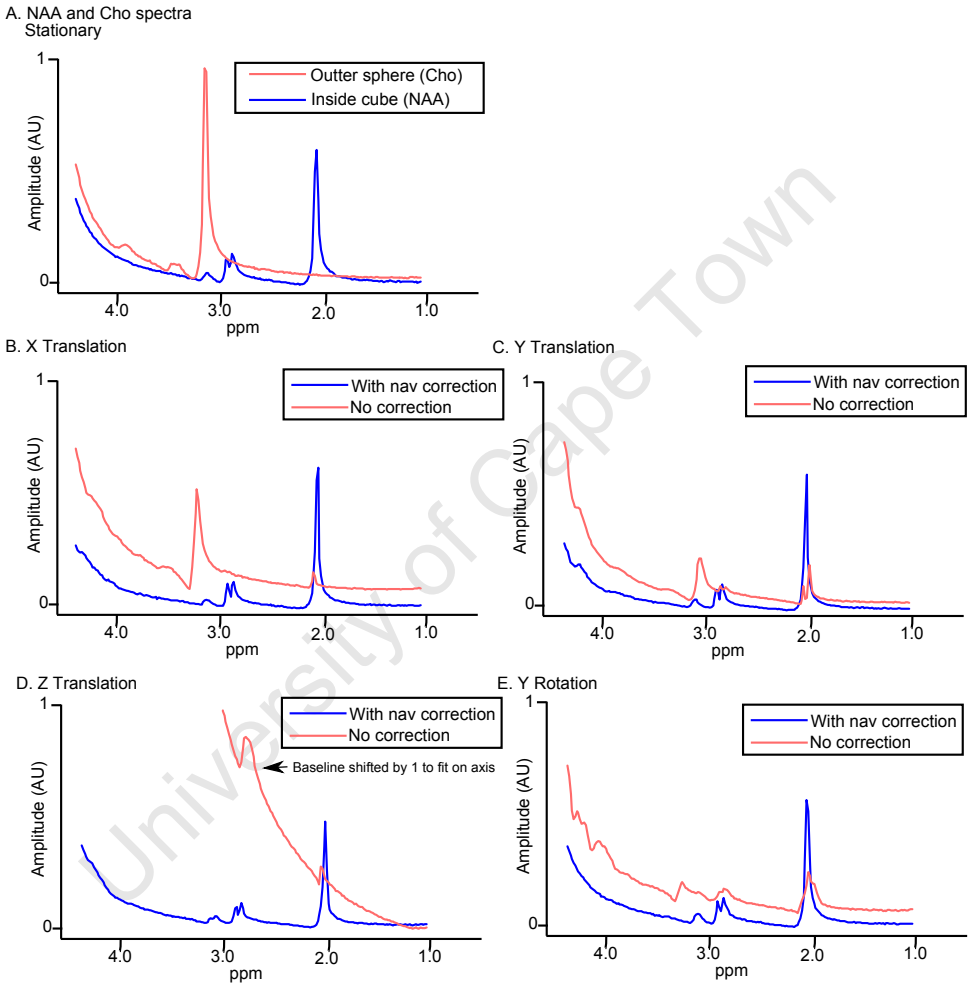

Figure A.5: A. Amplitude of spectra from outside (Cho) and inside the cube (NAA). B, C, D and E: Amplitude of spectra with and without navigator correction for X Translation, Y Translation, Z Translation, and Y rotation

University of Cape Town

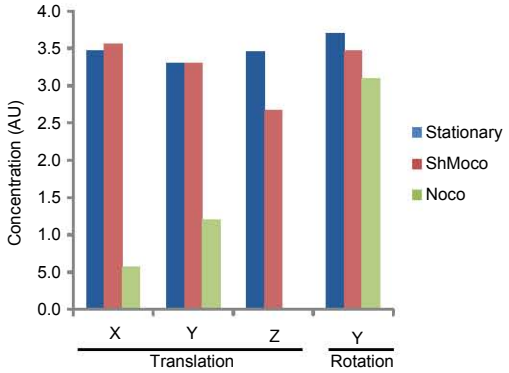

Figure A.6: NAA concentration, measured by LCModel, from the stationary scan, the motion and shim corrected scan (shmoco) and the uncorrected scan (noco).

Table A.3: Shim difference as measured by the navigator, for both navigator FOV and SVS FOV, after a 10 μT/m shim change on all axes

Axis	Navigator shim difference (μT/m)	SVS shim difference (μT/m)
X	10.1	9.6
Y	10.0	9.4
Z	9.2	9.8

A.4.2 Shim measurement and adjustment validation

The absolute shim applied in each TR was calculated for the two acquisitions (with and without an additional 10 μT/m on each axis), as applied for both the navigator and the SVS voxel. The difference between the two absolute shim values was taken for TR 5, which is the first TR after preparation or "dummy" TRs. Figure A.7 shows the two spectra acquired with and without the change in system shim overlaid on each other to demonstrate the navigator correction for the shim offset. Table A.3 shows the difference between the shim measured by the navigator in the acquisition with a 10 μT/m offset and in the acquisition without a 10 μT/m. The table shows the differences calculated for both the navigator FOV and the SVS VOI.

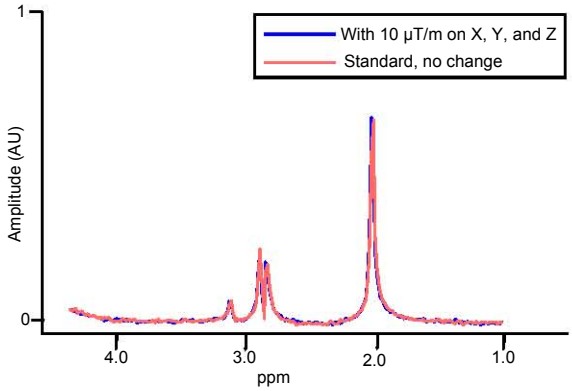

Figure A.7: Spectrum when offsetting system X, Y, and Z shims by 10 μT/m overlaid on spectrum with no offset on system shim.

A.5 Discussion

A limitation of this experiment was that rotation was only tested about the Y axis, not X or Z. However, as a rotation is realised through a gradient axis rotation, this can be extended to the other axes. A second limitation affected the Z translation and Y rotation. These jigs raised the phantom outside the isocenter, such that the magnetic field was no longer homogeneous. This is shown in fig. A.8A where the top of the phantom is distorted and should appear as in fig. A.8B. To reduce the impact of this artifact the navigator FOV was set to exclude this part of the phantom, however, this introduced further complications in the image registration process.

A.5.1 Motion estimation

The translation estimates in X and Y measured by the navigator agreed with that measured on the jig and with the localiser images. The concentrations measured when these motions were performed agreed with the concentrations when no motion was performed, showing that the spectroscopy voxel was maintained over the NAA containing cube throughout the scan. The Z translation was less accurate as is evident in the lower NAA concentration (23% lower) and the over estimation of Z translation (8 mm or 22%) which additionally demonstrated erro-

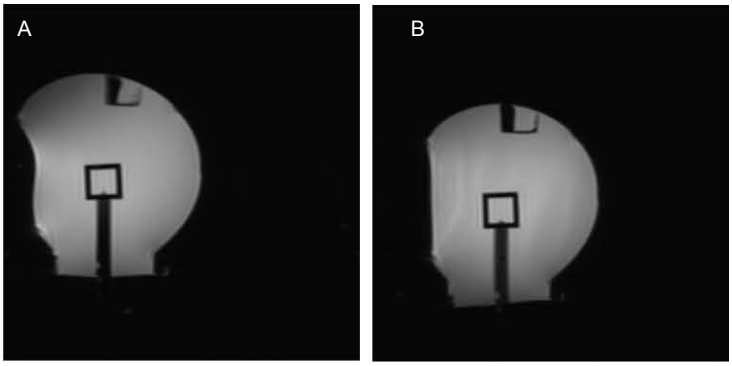

Figure A.8: Distorted phantom due to sitting to high in scanner bore

neous X rotation (4.5°). However, as there was no Cho in the resultant spectrum, the SVS voxel did not leave the NAA containing cube but rather shifted to cover more of the 2 mm perspex enclosing the cube. Although the rotation about the Y axis was under estimated by 3° (11%), the NAA concentration was maintained at the same mean concentration as the stationary scans. It is believed that these motion estimation errors are primarily due to the combination of the out-of-isocentre distortions (see fig. A.8) and the large degree of motion undertaken, 36 mm translation or 27° rotation. This resulted in distortions in the navigator images. Despite these navigator image distortions the motion correction maintained the SVS voxel over the NAA cube.

A.5.2 Shim measurement and adjustment validation

An offset of 10 μT/m in the scanner's, X, Y, and Z shims was reflected in the difference between the navigator estimates in the same TR. The effective application of this shim correction is demonstrated in fig. A.7 where there is no observable difference between the two spectra.

A.6 Conclusion

We have demonstrated that the navigated SVS sequence shifts the SVS voxel to account for rigid body motion of a phantom, maintaining it over a cube of the same inner dimensions as the voxel for three translations and one rotation. Furthermore we have shown that when the scanner's system shim is offset by 10 μT/m, the navigator measures the offset and successfully corrects it.

University of Cape Town